DOCTOR OF PHILOSOPHY

Thesis

Isolation and evaluation of anti-inflammatory constituents from lichen *Dirinaria applanata* and *Lasia spinosa* leaves

NGUYEN QUOC CHAU THANH

Kyoto Institute of Technology

Kyoto, Japan

September 2020

Abstract

Natural products or traditional medicines play essential roles in therapeutic agents as well as a resource for the discovery of new drugs. Lichen *Dirinaria applanata* and *Lasia spinosa* (L.) Thwaites were used as traditional medicines to treat many diseases for centuries. However, chemical components and their effects on inflammatory response are not yet characterized. Thus, the goal of this dissertation is to explore chemical positions and investigate the anti-inflammatory activities of these extracts in lipopolysaccharide (LPS)-induced RAW 264.7 macrophages. Chemical investigation of the lichen *Dirinaria applanata* methanol extract led to isolating two hopane derivatives including 1*β*-acetoxy-21*α*,3*β*-hydroxyhopane-29-oic acid (**1**), hopane-3*β*,6*β*,21*α*-triol (**2**) and a depside namely 2-*O′*-methylnordivaricatic acid (**3**). Their structures were elucidated by spectroscopic data in combination with published literature. Notably, compound **2** was isolated from this lichen species for the first time. Unfortunately, only compound **1** shows the anti-inflammatory effect by reducing nitric oxide (NO) production in LPS-induced inflammation response.

Besides, ethanol extracts of *L. spinosa* leaves showed antioxidant activity due to the presence of high levels of polyphenolic compounds. Therefore, *L. spinosa* leaves may exhibit anti-inflammatory properties. In particular, treatment with the leaf extract significantly repressed the production of inflammatory mediators such as nitric oxide and reactive oxygen species and the expression of pro-inflammatory cytokines in the LPS-stimulated RAW264.7 cells. Moreover, pretreatment of *L. spinosa* leaf extract prevented activation of the nuclear factor-kappa B (NF-κB) pathway by inhibiting nuclear factor of kappa light polypeptide gene enhancer in B-cells inhibitor, alpha (IκBα) degradation. Furthermore, the mitogen-activated kinase (MAPK) and phosphoinositide-3-kinase/protein kinase B (PI3K/Akt) pathways were suppressed upon treatment with the leaf extract. In addition to suppressing inflammatory factors, the extract also promoted the activated nuclear factor erythroid 2-related factor 2/heme-oxygenase-1 (Nrf2/HO-1) pathway. Taken together, the significant findings of these herbs will be highlighted and discussed throughout this dissertation. Result obtained highlights critical findings in assessing the potential of anti-inflammatory constituents. Thereby, we propose to further develop them as novel pharmacological strategies in order to defeat inflammation diseases.

Table of contents

List of Figures

List of Tables

Acknowledgements

Being a Ph.D. student at Kyoto Institute of Technology has been exciting as well as a challenging experience for me in the way I become a scientist. During these years, many people have directly, indirectly, and in different ways, been a part of my journey, and encouraged and supported me along the way.

Foremost, I would like to express my special thanks to my advisor, Associate Prof. Kenji Kanaori; you have been a tremendous mentor for me. I would like to thank you for encouraging me in research and for teaching me how to become a research scientist. Your advice on my research and career development has been invaluable.

Especially, I would also like to express my deepest thanks to Prof. Kaeko Kamei who gave me an opportunity to study in Japan. I highly appreciate your guidance and support throughout my Ph.D. program and my life in Kyoto. The valuable discussion with you has helped me to shape my research trajectory and diversify my way of thinking. Moreover, without your support in my project, I cannot get more knowledge in research and complete my Ph.D. program.

I would especially like to thank my former and current colleagues, my friends, faculties, and staff at Kyoto Institute of Technology to support me through my life in Kyoto. I am also grateful to Dr. Tran Duy Binh and Dr. Tuan L.A Pham who taught me a lot of experience in research as well as big brothers during my life in Kyoto. I am lucky that I have many special people surrounding me and supporting me in all aspects. Thank you for being in my life, making it so meaningful for my Ph.D. life so special. I am grateful to have all of you around.

Most importantly, I would like to express my special thanks to Dr. Nguyen Trong Tuan, head of department of Chemistry at Can Tho University, who supported me through my challenge in research. Especially thank my family, words are not enough to express how grateful I am to you, Dad, Mom and my younger brother, for all of the love that you have for me. Thank you for supporting me, believing in me, and encouraging me on this journey. Finally, I would like to thank all my family members, friends for their support through this program.

Abbreviations

s	*singlet*
d	*doublet*
dd	*double doublet*
t	*triplet*
q	*quartet*
m	*multiplet*
HMBC	Heteronuclear multiple bond correlation
HSQC	Heteronuclear single quantum coherence spectroscopy
NOESY	Nuclear Overhauser enhancement spectroscopy
COSY	Correlated spectroscopy
ELISA	Enzyme-linked immunosorbent assay
PI3K/Akt	Phosphoinositide-3-kinase–protein kinase B/Akt
TRIF	TIR-domain-containing adapter-inducing interferon-β
IRAK	Interleukin-1 (IL-1)-receptor-associated kinase
IRF-3	Interferon regulatory factor-3
PGE2	Prostaglandin E2

Chapter 1 - General introduction

1.1 Potential of traditional medicinal plants

Traditional medicines are of great importance to creating natural products include herbal materials and herbal preparations that contain active ingredients, or other plant materials, or combinations thereof. Known forms of medicine such as traditional Chinese medicine, traditional Korean medicine, Ayurveda have been practiced around the world for a hundred years or even centuries, and they have blossomed into orderly-regulated systems of medicine. Although they may have specific defects in various forms, they are still a valuable repository of human knowledge [1].

The development of new drugs is wholly based on modern technology and is reaching a specific limit. In developing new drugs, the pharmaceutical industry tends to apply high flux synthesis and drug development based on combination chemistry since the 1980s; however, significant efforts made in this direction did not lead to expected productivity. Some major pharmaceutical companies are facing significant challenges in developing new products. Over the years, increasing attention has been paid to natural products from herbal resources in finding new drugs combined with modern technologies [2,3].

Natural products, developed over a million years, have a unique chemical diversity leading to a variety of biological activities and their medicinal properties. Those products have become essential sources for developing new compounds with diverse structures. Natural products will be used continuously to meet the urgent needs of developing drugs and play a leading role in the discovery of drugs to treat human diseases, especially fatal diseases [4].

1.1.1 Role of traditional medicines and natural products in drugs development

Traditional medicines are too valuable to be ignored in the research and development of modern drugs. As we have known, a herb or formula may contain many chemical ingredients, such as alkaloids, terpenoids, flavonoids, etc. In general, these chemicals function alone or in conjunction to create a desired pharmacological effects [5]. It is noteworthy that many traditional medicines derived from drugs have been applied in clinical medicine. Additionally, it has been demonstrated that many herbs desired-drugs have been discovered through their application in traditional medicines.

For instance, Artemisinin and other anti-malarial drugs are examples of modern drugs based on traditional medicines. Artemisinin has been studied for many years and made significant progress, including the synthesis of new analogs and artemisinin derivatives and research efforts biological activity related mechanism. Artemisinin, as well as its effective derivatives, is widely applied worldwide as a new type of anti-malarial drugs [6]. Artemisinin is quite different from the previous medicine, such as chloroquine, which has a unique structure with sesquiterpene lactone carrying a peroxy group and does not contain heterocyclic nitrogen. Compared with previous anti-malarial drugs, Artemisinin is highly effective, quick-acting and low toxicity. It is effective in treating various forms of malaria, such as falciparum and cerebral malaria, resistant to chloroquine, and its mechanism is different from anti-malarial traditional medicine. The discovery of Artemisinin was a great success at a particular time in Chinese history, and it was adopted by the organization of hundreds of researchers. From that breakthrough, scientists have conducted more comprehensive research in areas such as pharmaceuticals chemistry, organic synthetic chemistry, and chemical biology. Through the process of etherification and esterification, they have produced a series of famous new medicines, including Artemether and Artesucky. It has improved efficacy and beneficial solubility for patients given orally or intravenously overcoming high parasite recurrence rates [1]. Most importantly, one of these scientists was awarded the 2015 Nobel Prize in Medicine for her remarkable contribution to discover Artemisinin. Therefore, the discovery of Artemisinin illustrates how traditional medicines form a great knowledge base on the natural product and promise to develop new drugs from this knowledge in the future.

Besides, *Taxus breviolia* was chosen for further research to find cancer drugs from plants that began in 1960 at the National Cancer Institute in the United States. Taxol was isolated as a new compound from *T. breviolia.* It has an unusual chemical structure with a particular mechanism of action and was developed as a novel anti-cancer drug in subsequent decades. However, the drug attracted little attention during its early stages of development because of poor water solubility, low yield from natural products, and other disadvantages. Fortunately, it has been extracted, isolated, and structurally defined; its activity against tumors and its mechanism of action have been established. Finally, it has been developed for clinical practice. Taxol was approved by the US Food and Drug Administration for cancer treatment in 1992 after 21 years. It was used as a primary drug for treating various forms of

cancer diseases and is still developed new synergistic groups of anti-cancer medicines [7]. In addition, Curcumin was extracted from *Curcuma longa* (L.) has been widely used to treat many diseases [8].

From these examples above, many studies find new sources of medicinal herbs and natural compounds to play an essential role in drug development. Generally, the trend of research on natural products is partly based on traditional medicine. From isolated natural compounds, scientists, along with modern technologies, have been creating breakthrough derivatives in the treatment of disease. Besides, some problems need attention in the future. The synergistic effect can exist between compounds that generally occur in natural products; however, the modes and mechanisms of operation are rarely bright. Thus, it needs to make full use of synergistic effects to improve the effectiveness of drugs. It is noted that any side effects of the natural product be controlled appropriately to meet safety standards.

Therefore, the present study focuses on the biological activity as well as the isolation of the main active ingredients of potential herbs in order to find a new drug to support the treatment of diseases.

1.1.2 Dirinaria applanata (Fée) D.D. Awasthi and Lasia spinosa (L.) Thwaites

Dirinaria applanata (Fée) D.D. Awasthi is a lichen commonly found in Asia, especially Vietnam. Lichens are known as nonvascular cryptogams and represent stable, self-supporting symbiotic associations of photobiont (alga or cyanobacterium) and mycobiont (fungus). Lichen can grow in a variety of climatic conditions, including harsh environmental conditions and are considered to be the principal colonies of terrestrial ecosystems. They are used worldwide to treat various diseases such as dyspepsia, bleeding piles, stomach disorders, and many disorders of blood and heart. Lichens produce several secondary metabolites such as depsides, depsones, and dibenzofurans (lichen substances). These compounds are produced mainly by mycobiont and play an essential role in lichen taxonomy. Recently, much attention has been paid to biological activities based on traditional remedies. Lichens extract, and its pure compounds are known to exhibit a range of biological activities such as antioxidant, antifungal, anti-cancer, anti-tumor, analgesic, enzyme inhibitors, wound healing, and other things [9]. A recent report demonstrated that

the ability of *Dirinaria applanata* exhibited a significant antioxidant and considered the most cytotoxic against A549 human lung carcinoma cell line [10].

Besides, *Lasia spinosa* (L.) Thwaites is a stout, intensely prickly marsh plant with a creeping rootstock that is mostly found in Southeast Asia. It is used as a traditional medicine in many formulations and used individually to treat inflammatory diseases. Phytochemical of methanolic extract of *L. spinosa* leaves contains alkaloids, carbohydrates, proteins, saponins, tannins and phenolic compounds.

Dirinaria applanate

Lasia spinosa

Figure 1.1 *Lichen Dirinaria applanata* and *Lasia spinosa*

However, very few studies on the specific composition and biological activity of those plants have been reported in the literature. So, this study was to define the chemical constituents and to evaluate the anti-inflammatory properties to find a possible relationship between these molecules and the biological activities reported for the plant.

1.2 Inflammation

Inflammation is a highly complex biological process, which involves the cascade of events initiated to defend against the foreign challenge or tissue injury [11]. Inflammation is characterized by edema, pain, which is one of the most important elements that protect body from the invading pathogens such as bacteria or viruses [12]. There are two main types of inflammation, depending on the duration of inflammatory response; (i) acute inflammation, lasts for a shorter period, and (ii) chronic inflammation lasts for a more extended period of duration.

Chronic inflammation is characterized by infiltration of lymphocytes and macrophages with angiogenesis, fibrosis and tissue necrosis at sites of inflammation [13]. Inflammatory reactions must be strictly controlled because the inflammatory misregulation has been considered as one of the leading causes of cancer growth in humans. Nitric oxide (NO) and reactive oxygen species (ROS) are the key molecules that play an essential role in the regulation of inflammatory response. Additionally, enzymes, such as inducible nitric

oxide synthase (iNOS), is well known as an index of inflammation. Overproduction of these critical molecules causes excessive inflammatory response [14].

Persistent infections inside the host cause chronic inflammation. DNA damage in the proliferating cells was induced by leukocytes and other phago-cytic cells by the generation of reactive oxygen (ROS) and nitrogen species that are generally produced by these cells in order to fight infection [15]. Chronic inflammation is also linked to the pathogenesis of several chronic diseases, including cardiovascular disease, obesity, diabetes and chronic skin diseases.

1.3 Role of Macrophages in inflammation

Macrophages play an essential role in the inflammation process. During this process, this macrophage is activated and has a destructive effect. Usually, the body protects the penetration of foreign antigens by natural physical barriers such as the skin and mucous membranes of the innate immune response. Besides providing a barrier, the skin contains many immune cells that can be activated by invading pathogens or damaging the skin. Macrophages are one of the most crucial immune cells involved in inflammation and show various immune functions [15]. Macrophages are widely distributed throughout the body, which plays an important role in the pathogenesis of some inflammatory diseases. Therefore, it is necessary to take the necessary steps to develop new methods to reduce activated macrophages and inhibit macrophage products participating in inflammation and various inflammatory diseases. Lipopolysaccharide (LPS) is one of the most activators of macrophages. LPS triggers the activation of macrophages that cause various reactions, including excretion on growth factors, release mediators that cause inflammation, phagocytosis and bone cell rearrangement. The inflammatory response has been extensively studied in RAW macrophage cells 264.7 stimulated by lipopolysaccharides, because this cell line is susceptible to LPS stimulation, providing an excellent model for screening anti-inflammatory drugs and may assess the inhibitors of pathways involved in the production of cytokines and inflammatory enzymes [15]. Moreover, investigating these pathways can help us develop new anti-inflammatory drugs or promote strategies for treating inflammation and inflammatory diseases.

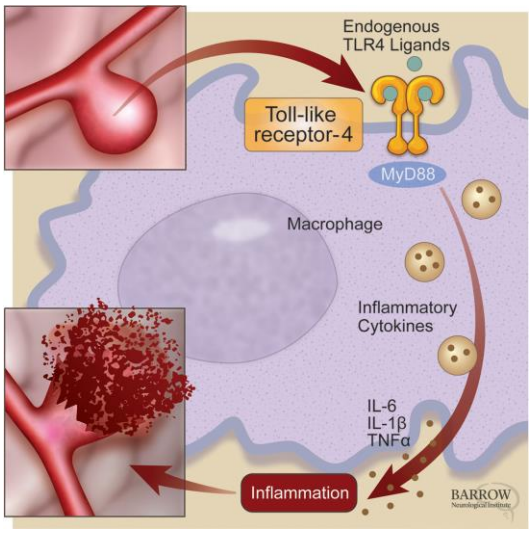

Figure 1.2 Role of macrophages in inflammation

1.4 Oxidative stress and inflammation

Reactive oxygen species (ROS) can be generated by different cell sources and are divided into two main groups, including extracellular and intracellular. In a group, ROS releases as a byproduct or waste in response to various biological processes. In a group, ROS releases as a byproduct or waste in response to various biological processes. In another group, ROS is intentionally created in the form of signaling molecules or as molecules that protect cells, such as in inflammation [16]. Therefore, abnormal accumulation of ROS or failure in antioxidant processes is associated with activation of mitogen-activated protein kinase (MAPKs), inflammatory transcription factors, nuclear factor-kappa B (NF-κB) which play an essential role in regulating cell proliferation, metabolism, survival and cancer development. Macrophages produce and release ROS in response to phagocytes and various stimuli such as activation with LPS. LPS causes excessive production of ROS by macrophages leading to oxidative damage to membrane lipids, DNA, proteins, and lipoproteins. Thus, ROS inhibition is a well-known treatment goal in the treatment of several inflammatory diseases.

Besides, nitric oxide (NO) is considered the focus of research for its role in various biological and pathological processes. NO is an inorganic molecule synthesized from the conversion of L-arginine to L-citrulline through the action of an enzyme, nitric oxide synthetase (NOS). There are three similarities of NOS:

- Neuronal NOS (nNOS or NOS1): mainly expressed by nerve cells in the brain and intestinal nervous system.

- Endothelial NOS (eNOS or NOS3): the expression of this isoform is limited to the

endothelial cells lining the blood vessels. Both eNOS and nNOS enzymes are cytosolic and calcium/calmodulin-dependent and produce NO in low amounts depending on stimulation in a short time. Low amounts of eNOS and nNOS have been considered beneficial for many physiological reactions, including neutral conduction, homeostasis, and host protection [17].

- Inducible NOS (iNOS or NOS2): the third homolog of NOS is calcium-independent and produces NO in a long time. Increasing NO production by iNOS is harmful and is involved in many physiological and pathological processes such as inflammation and tumors. Macrophages exhibit iNOS when activated by cytokine and bacterial factors such as LPS. Inactivated macrophages, iNOS transcribed transcription is responsible for prolonged and profound NO production. Therefore, inhibiting NO production by blocking iNOS expression is known as an essential strategy in the treatment of inflammatory diseases [18].

1.5 Role of signaling pathways in inflammation response and oxidative stress

The nuclear factor kappa-B (NF-κB) was identified as a transcriptional regulator of the immunoglobulin sequence. NF-κB is a vital transcription factor due to its role in inflammatory, immune, including cell proliferation, cell death, and control of genes involved in biological processes [19]. It can be activated in a variety of ways, but the two main signaling pathways that lead to NF-κB activation are canonical and non-canonical pathways. Activation of the canonical NF-κB pathway is due to the stimulation of inflammatory receptors such as the tumor necrosis factor (TNF) receptor, the Toll-like receptor family as (TLRs), and cytokine receptors. This signaling pathway is dependent on the IKK complex (IKK-α and IKK-*β)*, which are catalytic kinases, which acts as a regulatory subunit [20]. This pathway is usually activated lead to the translocation of NF-κB p50/p65 heterodimer, which plays an essential role in inflammation. The non-canonical pathway is primarily stimulated by specific ligation with family members of TNF receptors, including LTβR, CD40, and others, mediated by NF-κB produces kinase (NIK). This pathway is entirely dependent on IKKα, whose phosphorylation activates the p100 process leading to the release of p52 [21]. NF-κB regulates the expression of many genes for various cytokines and enzymes involved in immune and inflammatory reactions such as nitric oxide synthase and cyclooxygenase-2 (COX-2), which increased production

of prostaglandins and thromboxane in inflammation diseases. NF-κB may also be activated in response to pro-inflammatory as interleukin-1β (IL-1β) and TNF-α [20]. Notably, the abnormal activation of NF-κB has been linked to the pathogenesis of inflammatory diseases and also associated with cancer. Thus, NF-κB is a clear target for compounds and drugs with anti-inflammatory activity.

Among NF-κB, mitogen-activated protein kinases (MAPKs) play an important role in intracellular signaling and control of major cellular activities, including cell proliferation, differentiation, death, and transformation. Moreover, activation of MAPKs has been seen in several conditions, including chronic inflammation and cancer [22]. The three main members of the MAPK family are involved in the immune system, namely Extracellular signal-regulated kinase (ERK), p38, and c-Jun N-terminal kinase (JNK). p38 and JNK are known as “stress-induced” MAPK that is triggered in response to physiological stress, LPS, oxidative stress, and cytokines such as TNF-a. The ERK 1/2 pathway is primarily activated in response to stimulation with growth factors (epidermal growth factor, platelet growth factor, etc.); besides, ERK 1/2 is also activated on stimulation of LPS, and adherence monocytes/macrophages [23]. Stimulation of LPS induced an uncontrolled release of inflammatory mediators, such as TNF-α, NO, and ROS. LPS stimulation triggers transcription factors NF-κB and MAPKs, especially ERK 1/2, p38, and JNK. The activation of MAPKs phosphorylated is controlling various critical cellular activities, including gene expression. ERK, p38, and JNK are known to modulate inflammatory and immune responses, which are related to enhancing the expression of COX-2 and iNOS in LPS-induced macrophages. Increased expression of COX-2 and iNOS increased NO, ROS production leading to inflammatory responses.

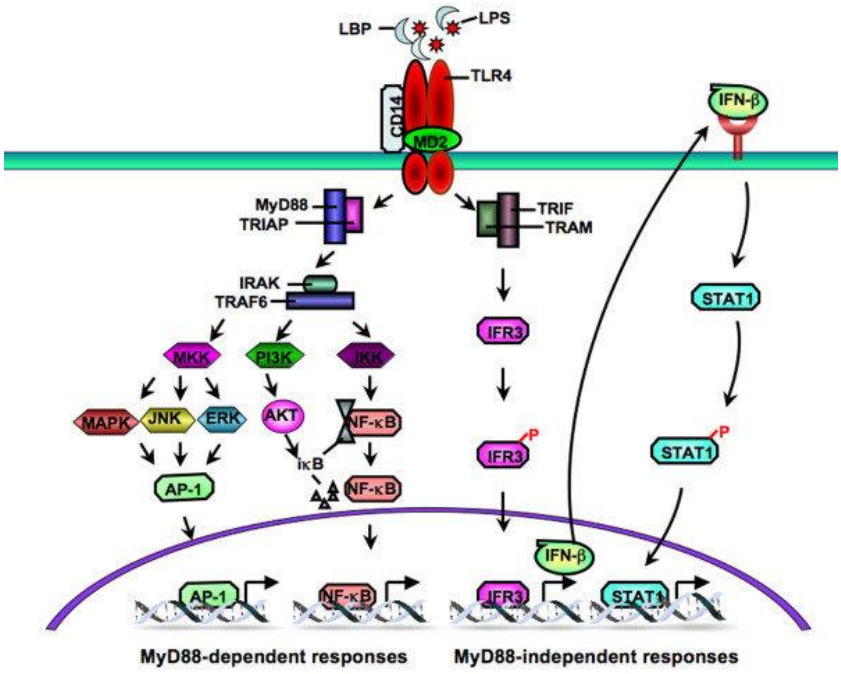

Figure 1.3 Schematic overview of Toll-like receptor (TLR)4 signaling pathway.

Furthermore, the NF-E2-related factor 2 (Nrf2)-mediated signaling pathway provides living organisms an effective and critical defense against environmental impacts and endogenous stressors. Nrf2 combines the primary and inductive expression of antioxidant detoxification and phase II enzymes to adapt to various stress conditions. The stability and cellular distribution of Nrf2 are tightly controlled by a protein-binding protein that binds to Kelch's ECH (Keap1) protein as its an inhibitor. Nrf2 is activated via the Keap1-dependent, evolutionarily conserved, dedepression signaling mechanism, wherein Nrf2 is inhibited under basal conditions through Keap1's ubiquitination-proteasomal degradation and is triggered by oxidizing agents and electrophiles. Activated nrf2 mediates the expression of a range of signaling enzymes and proteins to regulate drug metabolism, antioxidant protection, and oxidative signals, thereby affecting physiological and oxidative pathologies. By adjusting the level of oxidation and signaling, Nrf2 is involved in controlling several programmatic functions, such as autophagy, infrared signaling, UPR, apoptosis, mitochondrial biology, and stem cells regulation. Nrf2 exhibits many protective effects against toxicity and chronic diseases naturally or through pharmacological means, opening new avenues for drug development [24]. Additionally, Nrf2 protects cells from stressors, including endogenous substances, reactive oxygen species, and environmental toxins. Therefore, activating the Nrf2 pathway could be a promising strategy for preventing cancer [25].

Chapter 2

Novel hopanoic acid and depside from lichen *Dirinaria applanata*

2.1 Introduction

Lichens are symbiotic organisms that usually include fungi and photosynthesis organisms (alga or cyanobacteria) [26]. Previous studies on lichens composition unfolded the existence of diverse secondary metabolites, including monocyclic phenols, depsides, depsidones, xanthones and terpenoids [27]. Moreover, the investigation of biological activities indicated that lichens and its composition exhibited a wide range of biological activities such as antioxidant, anticancer, antibacterial, and antifungal, antiviral and enzyme inhibitory [28-30]. *Dirinaria applanata* is a foliose lichen, which widely distributes in tropical areas. Previous chemical investigation showed that *D. applanata* contained antranorin, divaricatinic acid and its ester derivatives, methyl haematommate, methyl *β*-orcinolcarboxylate, ramalinic acid, lichenxanthones, tannins, and terpenes [31-33]. In continuing to explore the chemical composition of *D. applanata*, we herein reported the structural elucidation of two hopane derivatives and a depside.

2.2 Material and methods

2.2.1 General experimental procedures

NMR spectra were acquired on Bruker Advance 500 MHz and Bruker Advance 600 MHz using TMS as an internal standard. FT-IR was conducted using KBr pellet method on Thermo Nicolet 6700. HR-ESI-MS observation was performed on a Bruker MicrOTOF-Q mass spectrometer and a SCIEX X500R-QTOF. The melting point was recorded using glass capillaries without calibration on Stuart Scientific SMP3. The optical rotation instrument was SEPA-200 (Horiba, Japan) with cell length: 50 mm. Silica gel 60 (Merck, 230-400 mesh ASTM) and RP-18 (Sigma-Aldrich) were packed for column chromatography (CC). Precoated silica gel 60 F_{254} plates (Merck) were used for analytical TLC.

2.2.2 Lichen sample

The lichen thallus was collected in Can Tho University campus II, Can Tho city, Vietnam from January to April 2018 by observing thallus morphology and comparing with

the literature [34]. The identification was conducted by Dr. Ngo Thanh Phong, Department of Biology, College of Natural Sciences, Dr. Dang Minh Quan, Department of Biology Education, Can Tho University, and Dr. Vo Thi Phi Giao, Faculty of Biology, HCM University of Science. A voucher specimen was deposited in Laboratory of Plant Biology Department of Biology, Can Tho University, Vietnam under number (Li012018-CT001) and in Herbarium of University of Science, Ho Chi Minh City, Vietnam National University (PHH) with the voucher specimen number PHH0011078. Lichen thallus was kept in paper bags and was naturally dried at room temperature.

2.2.3 Extraction and Isolation

Lichen material was finely powdered (1.28 kg) and extracted with methanol (3 × 5 L) at room temperature. The solvent was evaporated using a rotary evaporator to obtain methanol extract (210 g). The methanol extract was well-mixed with water followed by shaking with hexane and ethyl acetate to give a hexane extract (88 g) and ethyl acetate extract (76 g), respectively. The remaining water layer was condensed to afford water extract (32 g).

The ethyl acetate (30 g) was separated to 10 fractions (**EA1-10**) by flash column chromatography eluted with hexane:EtOAc (5:1 to 0:10) and EtOAc:MeOH (10:1 to 2:1). Fraction **EA3** was applied to column chromatography and was washed with CH_2Cl_2:MeOH (0:10 to 10:0) to afford 8 fractions (**EA3.1-3.8**). Compound **1** (79 mg) was obtained after purifying fraction **EA.3.4** by hexane:CH_2Cl_2 (2:8 to 0:10) and recrystallizing in CH_2Cl_2. Solid residue in fraction **EA.3.3** was washed and repeatedly recrystallized in CH_2Cl_2 to give a white solid named as compound **2** (10.5 mg). The water residue (10 g) was subjected to RP-18 column chromatography and washed with H_2O:MeOH (10:0 to 0:10) to give four fractions (**W1-4**). Repeated purifying fraction **W-3** (0.67 g) by using H_2O:MeOH (3:7) on RP-18 afforded compound **3** (13.5 mg) as a solid.

1β-Acetoxy-3β-hydroxy-21α-hopane-29-oic acid (***1***). White needles, MP. 270-272°C. $[\alpha]_D^{25}$ +12.0 (c = 0.267, $CHCl_3$). HR-ESI-MS *m/z*: $[M-H]^-$ = 515.3734 (calcd. for $C_{32}H_{53}O_5^-$, 515.3736). IR (KBr) ν_{max} (cm^{-1}): = 3418, 2949, 1732, 1716, 1467, 1376, 1248, 1184, 1043, 1019. ^{1}H-NMR and ^{13}CNMR (**Table 2.1**).

21α-Hopane-3β,6β,22-triol (***2***). White solid, MP. 287-289°C. $[\alpha]_D^{25}$ +6.0 (c = 0.2, $CHCl_3$). IR ν_{max} (cm^{-1}): = 3414, 2944, 2851, 1472, 1387, 669. ^{1}H-NMR (600 MHz, $CDCl_3$): *δ* (ppm) = 0.69 (1H, *m*, H-5), 0.77 (3H, *s*, C-28), 0.91 (3H, *s*, C-27), 0.93 (1H, *m*, H-19*α*), 0.97 (1H, *m*, H-19*β*), 1.06 (3H, *s*, H-23), 1.16 (3H, *s*, H-24), 1.18 (3H, *s*, H-29), 1.19 (3H, *s*, H-25), 1.21 (3H, *s*, H-30), 1.24 (1H, *m*, H-15*α*), 1.26 (1H, *m*, H-9), 1.30 (3H, *s*, H-26), 1.44 (1H, *m*, H-15*β*), 1.45 (2H, *m*, H-11), 1.46 (1H, *m*, H-12*α*), 1.46 (1H, *m*, H-17), 1.47 (1H, *m*, H-7*β*), 1.47 (1H, *m*, H-13), 1.50 (1H, *m*, H-20*α*), 1.57 (1H, *m*, H-2*α*), 1.57 (1H, *m*, H-12*β*), 1.55 (1H, *m*, H-19*α*), 1.58 (1H, *m*, H-16*α*), 1.64 (1H, *m*, H-2*β*), 1.67 (1H, *m*, H-1*β*), 1.72 (1H, *m*, H-7*α*), 1.76 (1H, *m*, H-20*β*), 1.94 (1H, *m*, H-16*β*), 2.23 (1H, *dt*, 10.8 & 9.0 Hz, H-21), 3.14 (1H, *m*, H-3), 4.55 (1H, *s*, H-6). ^{13}C-NMR (150 MHz, $CDCl_3$): *δ* (ppm) = 16.3 (C- 28), 16.9 (C-24), 17.0 (C-27), 17.3 (C-26), 17.6 (C-25), 21.1 (C-12), 21.9 (C-16), 24.2 (C-11), 26.6 (C-20), 27.6 (C-2) 27.7 (C-23), 28.8 (C-29), 30.9 (C-30), 34.5 (C-15), 36.7 (C-10), 39.6 (C-4), 40.7 (C-14), 40.8 (C-1), 41.0 (C-7), 41.3 (C-19), 42.0 (C-8), 44.0 (C-18), 48.8 (C-13), 50.9 (C-9), 51.1 (C- 21), 54.0 (C-17), 55.6 (C-5), 69.0 (C-6), 73.9 (C-22), 79.1 (C-3). HR-ESI-MS *m/z*: $[M-H]^-$ =459.3840 (calcd. for $C_{30}H_{51}O_3^-$,459.3843).

2′-O-Methylnordivaricatic acid (***3***). Brownish orange solid, MP. 149-151°C. HR-ESI-MS *m/z*: $[M-H]^-$ = 387.1449 (calcd. for $C_{21}H_{23}O_7^-$, 387.1449). IR ν_{max} (cm^{-1}): = 3408, 2962, 2933, 2873, 1651, 1615, 1586, 1432, 1249, 1206, 1160, 1140, 1043, 956, 826. ^{1}H-NMR and ^{13}C-NMR (**Table 2.2**).

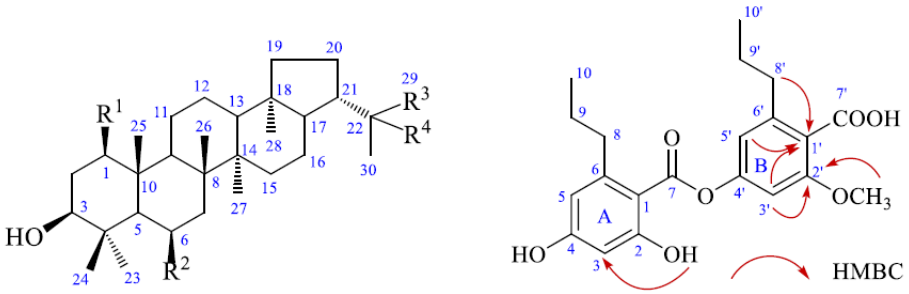

1: R^1 = OAc, R^2 = H, R^3 = COOH, R^4 = H
2: R^1 = H, R^2 = OH, R^3 = CH_3, R^4 = OH

3

Figure 2.1 The structure of compound (**1-3**) and the selected key HMBC correlations of compound **3**

2.2.4 Cell culture and cell viability

RAW 264.7 murine leukemia macrophage cells (ATCC TIB-71^{TM}, USA) were maintained with Dulbecco's modified Eagle's medium (DMEM; FUJIFILM-Wako, Japan) containing 10% fetal bovine serum (FBS; GIBCO BRL, Grand Island, NY, USA) and 1%

penicillin-streptomycin (PS; FUJIFILM-Wako, Japan) in a humidified incubator containing 5% CO_2 at 37 °C.

These compounds were dissolved in 5% (v/v) dimethyl sulfoxide (DMSO; FUJIFILM-Wako, Japan) as a stock. The stock solution was diluted to an appropriate sample concentration with DMEM and then added to the culture medium in 96-well plates that were incubated for 24 h. During treatment, the DMSO concentration was kept at 0.5% (v/v).

Cell viability was measured using the Cell Counting Kit-8 assay (CCK-8; Dojindo Molecular Technologies Inc., Rockville, USA), which is based on the measurement of intracellular dehydrogenase activity. Briefly, the cells were treated with serial concentrations of these compounds (0, 5, 10, 20, 40, and 50 μg/mL) for 24 h in 96 well-plates at a density of 2 x 10^4 cells/well. Then, absorption at 450 nm was read using a SH-1200 microplate reader (CORONA electric, Ibaraki, Japan).

2.2.5 NO production

RAW 264.7 cells were pretreated with the indicated concentration of these compounds dissolved in DMEM for 24 h, the medium was removed, and cells were washed with PBS. Then, cells were stimulated with 1 μg/mL LPS in DMEM for 18 h. To quantify NO, the conditioned medium (0.1 mL) was collected and mixed with an equal volume of Griess reagent (FUJIFILM-Wako) dissolved in water for 10 min at room temperature. The absorbance at 540 nm was measured with a SH-1200 microplate reader, and NO concentration was calculated based on a standard curve generated with sodium nitrite. *N*-Nitro-*L*-arginine methyl ester (L-NAME; FUJIFILM-Wako) (100 μM) was used as a standard iNOS inhibitor (positive control).

2.2.6 Statistical analysis

Experiments were performed at least three times to confirm repeatability, and all data are expressed as means ± S.D. Statistical significance was evaluated using *t*-tests and one-way ANOVAs, where $p < 0.05$ was considered significant.

2.3 Results and discussion

*2.3.1 Structure elucidation of compound **1***

Compound **1** appeared as a white solid. Mass spectra exhibited a pseudo-molecular ion at 515.3734 (calcd. for $C_{32}H_{53}O_5^-$, 515.3736), which corresponded with $C_{32}H_{53}O_5$. The FT-IR spectrum displayed the existence of a hydroxy moiety at 3418 cm^{-1} together with two carbonyl groups at 1732 and 1716 cm^{-1}. The ^{1}H-NMR indicated that there were 7 methyl groups attached to quaternary carbon and one methyl group at δ_H 1.13 (3H, *d*) attached to

methine carbon. Furthermore, two peaks at δ_H 4.59 (1H, *dd*) and 3.31 (1H, *dd*) were deduced for two oxygenated methine carbons. The ^{13}C-NMR and DEPT revealed 32 signals, two of which were oxygenated methine carbons at δ_C 80.9 (C-1) and 75.2 (C-3). Further analysis carbon spectrum showed resonance signals of two carbonyl groups at δ_C 170.5 (C-1′) and 183.6 (C-29) which were well-matched to FT-IR. For these initial analyses, it is proved that compound **1** shared some similarities with 3*β*-hydroxyhopane-29-oic acid [35, 36] except for the presence of an additional acetoxy group.

In HMBC spectrum, proton H-2 exhibited correlations with both oxygenated methine carbons at δ_C 80.9 (C-1) and 75.2 (C-3). Moreover, methine proton at δ_H 4.59 (H-1) interacted with the other oxygenated methine carbon at δ_C 75.2 (C-3) together with C-9,10. Besides, the proton at δ_H 3.31 (H-3) gave cross-signals with two methyl groups C-23 and C-24. These above data evidenced that two oxygenated methine carbons were located at C-1 and C-3. The position of the acetoxy group was confirmed at C-1 as indicated by a cross-peak between H-1 at 4.59 (1H, *dd*) and carbonyl carbon at δ_C 170.5 (C-1′). Further analyzing HMBC indicated that both protons at δ_H 1.13 (H-30) and 2.36 (H-22) showed cross-signals with a carboxyl group at δ_C 183.6 (C-29); therefore, the position of carboxylic acid moiety was logically deduced for attaching to C-22 (Figure 2.2a).

The relative stereochemistry of C-1, C-3 was unambiguously identified by NOESY spectrum (**Figure 2.2b**). Three protons including H-1, H-3, H-5 exhibited pair-to-pair interactions, which can be firmly concluded that these protons were oriented on the same side. In addition, due to the rigidity of pentacyclic skeleton, the H-5 must be downward, and as a result, the conformation of C-1 and C-3 were both *beta*. From all the above data, compound **1** was readily interpreted as 1*β*-acetoxy-3*β*-hydroxy-21*α*-hopane-29-oic acid and this was a new compound.

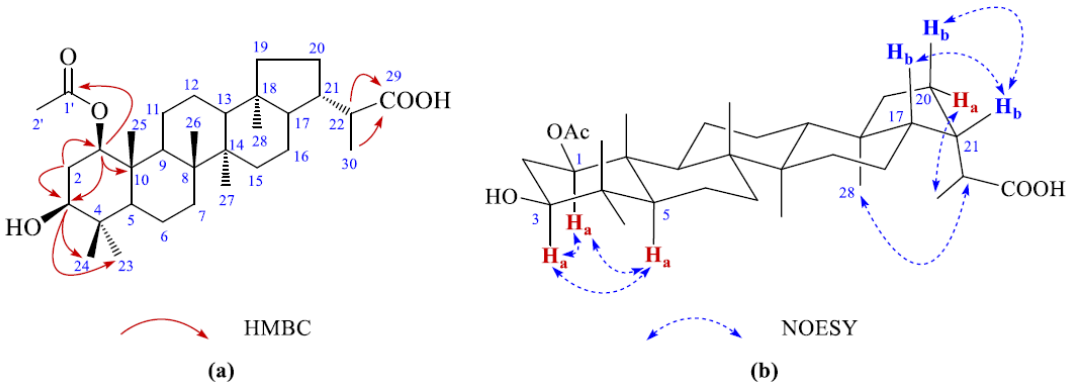

Figure 2.2 The selected key HMBC (*a*) and NOESY (*b*) correlations of compound **1**

Table 2.1 The spectroscopic data of compound 1 ($CDCl_3$, δ in ppm, *J* in Hz)

No.	^{13}C-NMR (150 MHz)	^{1}H-NMR (600 MHz)	HMBC (^{1}H → ^{13}C)	NOESY (^{1}H → ^{1}H)
1	80.9	4.59 (1H, *dd*, 11.34 & 4.62 Hz)	C-2, 3, 9, 10, 25, 1’	2α, 2β, 3, 5, 9, 23
2	33.4	1.91 (1H, *m*, H_α)	C-1, 3, 4, 10	1, 2β, 3
		1.62 (1H, *m*, H_β)	C-1, 3, 4, 10	1, 2α, 24, 32
3	75.2	3.31 (1H, *dd*, 12.24 & 4.26 Hz)	C-1, 2, 4, 5, 23, 24	1, 2α, 5, 23
4	38.8	-		
5	53.0	0.65 (1H, *dd*, 11.58 & 2.04 Hz)	C-1, 3, 4, 6, 7, 9, 10, 23, 24, 25	1, 3, 6α, 9, 23
6	17.9	1.57 (1H, *m*, H_α)		5, 23
		1.49 (1H, *m*, H_β)	C-26	24
7	33.1	1.40 (1H, *m*, H_α)	C-26	7β
		1.21 (1H, *m*, H_β)	C-5, 6, 8, 9, 26	7α, 26
8	42.2	-		
9	50.7	1.45 (1H, *m*)	C-9	1, 5, 23, 27
10	42.2	-		
11	23.0	1.46 (2H, m)		32
12	23.8	1.46 (1H, *m*)	C-13	
		1.32 (1H, *m*)	C-9, 13	
13	48.6	1.32 (1H, *m*)		
14	41.9	-		
15	33.5	1.16 (1H, *m*, H_α)	C-13, 16, 17, 27	15β, 27,16β
		1.32 (1H, *m*, H_β)	C-16	15α, 26
16	19.8	1.28 (1H, *m*, H_α)		
		1.48 (1H, *m*, H_β)	C-14, 15, 17, 18	15α, 21
17	53.6	1.25 (1H, *m*)	C-16, 18, 20, 21, 28	21
18	44.3			
19	40.9	1.51 (1H, *m*, H_α)	C-17, 18, 20, 21, 28	28
		0.90 (1H, *m*, H_β)	C-18	17, 19α, 20β
20	26.6	1.43 (1H, *m*, H_α)		22, 20β, 30
		1.87 (1H, *m*, H_β)	C-17, 18, 19	21, 20α, 19α, 30
21	42.0	2.34 (1H, *m*)	C-17, 18, 20, 22	16β, 17, 20β, 30
22	42.8	2.36 (1H, *m*)	C-21, 29, 30	20α, 28, 30
23	27.9	0.97 (3H, *s*)	C-3, 4, 5, 24	1, 3, 5, 6α, 9, 24
24	15.0	0.77 (3H, *s*)	C-3, 4, 5, 23	2β, 6β, 23
25	12.8	0.98 (3H, *s*)	C-1, 5, 9, 10	
26	16.9	0.94 (3H, *s*)	C-7, 8, 9	7β, 15β
27	16.6	0.91 (3H, *s*)	C-8, 13, 15	9, 15α, 28
28	15.7	0.70 (3H, *s*)	C-13, 17, 18, 19	22, 27, 19α
29	183.6	-		

30	17.6	1.13 (3H, *d*, 6.48 Hz)	C-21, 22, 29	20α, 20β, 21, 22
1′	170.5	-	C-1, 2′	
2′	21.9	1.99 (3H, *s*)	C-1′	2β, 11

3.2. Structure elucidation of compound **3**

Compound **3** was a brownish-orange solid. The negative HR-ESI-MS exhibited a signal at 387.1449 $[M–H]^-$ (calcd. for $C_{21}H_{23}O_7^-$, 387.1449) which was deduced for chemical formula $C_{21}H_{23}O_7$. The ^{1}H-NMR spectrum indicated the presence of two pairs of *meta* coupling at δ_H 6.39 (1H, *d*, 2.5 Hz, C-3); 6.45 (1H, *d*, 2.5 Hz, C-5) and 6.57 (1H, *d*, 2.5Hz, C-3′); 6.50 (1H, *d*, 2.5 Hz, C-5′), suggested for two tetrasubstituted benzene rings. In the upfield region, there were proton signals of two *n*-propyl side chains at δ_H 2.95 (2H, H-8); 1.70 (2H, *m*, H-9); 0.95 (3H, *t*, H-10) and 3.12 (2H, *t*, H-8′); 1.63 (2H, *m*, H-9′); 0.90 (3H, *t*, H-10′). Furthermore, a singlet signal at 3.86 (*s*, 2′–OCH_3) was proposed for a methoxy group. In the downfield of spectra, there were two signals of hydroxy groups, one of which at δ_H 11.17 (1H, *s*, 2-OH) was a chelated hydroxy group, the remaining at δ_H 14.22 (1H, *brs*, -COOH) was assigned for carboxylic acid moiety. Independently, the ^{13}C-NMR and DEPT spectra were also evidenced for two *n*-propyl side chains at δ_C 39.3 (C-8); 25.9 (C-9); 14.4 (C-10) and 38.0 (C-8′); 25.5 (C-9′); 14.4 (C-10′); four unsubstituted aromatic carbon at δ_C 99.8 (C-3), 111.3 (C-5), 114.5 (C-3′), 108.2 (C-5′); and one methoxy carbon at δ_C 55.9 (2′-OCH_3). The other characteristics derived from these spectra were two carbonyl signals at δ_C 170.2 (C-7) and 176.7 (C-7′). In brief, these spectroscopic data indicated key similarity with divaricatic acid, yet compared with published data of divaricatic acid in different solvents, its spectra data showed some minor distinction (**Table A3**) [37, 38]. From the above evidence, the structure of compound **3** was initially interpreted as an isomer of divaricatic acid.

The structure of this compound was not divaricatic acid **3a** as the above discussion. It meant that the methoxy group did not locate at C-4. Thus, two possible isomers were that the methoxy group resided at C-2 in 2-*O*-methylnordivaricatic acid **3b** (**Figure A2**) or at C-2′ in 2′-*O*-methylnordivaricatic acid **3 (Figure 2.1**). In this case, the position of methoxy group could be literally determined by HMBC correlation. Firstly, for a typical depside derivative, the aromatic carbon-bearing ester group C-1 generally shifted to upfield region compared to carboxylic acid moiety at C-1′ as in case of divaricatic acid **3a** (**Table A3**) [37]. The HMBC analysis revealed that three protons including H-3′, 5′, 8′ gave correlated

peaks with nearby C-1′. In addition, both protons of methoxy group and H-3′ correlated with C-2′ (**Table 2.2**). As a result, the methoxy group must reside in B-ring at C-2′. Secondly, the more in-depth analysis HMBC revealed that the 2-OH proton of compound **3** also showed a three-bond correlation with C-3 but not with C-3′. This result confirmed that the 2-OH was located in A ring, and the methoxy group must be bound to C-2′. In brief, the above analysis from HMBC supported the methoxy group located in B-ring and it can be deduced that compound **3** was 2′-*O*-methylnordivaricatic acid, which was a novel compound.

Although the structure of compound **2** has been recorded, the referenced spectroscopic data were not available for comparison. In this study, we fully reported the spectroscopic assignment for this compound (**Table A2**). In addition, this compound was firstly isolated from *D. applanata*. In combination with the previous report [33], we have isolated six phenolic compounds, one depside, two lichenxanthones, and three hopane triterpenoids. They complement to phytochemical database of *D. applanata*. Hopane triterpenoid, especially 3*β*-acetoxyhopane-1*β*,22-diol, was recorded in *Dirinaria* genus [34]. Our results in chemical composition of *D. applanata* have identified three hopane triterpenoids which are hydroxylated at C-3 position whereas the hydroxylation of those hopanes in other lichen genus occurred at C-6 [39, 40]; C-6, 7 [41]; C-6, 15 [42]; C-6, 16 [43]; C-6, 7, 15 [44] or C-6, 7, 16 [45]. This means that 3-hydroxyhopane derivatives could be recognized as a fingerprint for *D. applanata*. In addition, divaricatic acid **3a,** a depside, is recorded in *Dirinaria* genus [34].

Compounds **1** and **3** were chosen to test the anti-inflammatory activity in RAW 264.7 cells. Firstly, the cytotoxicity of these compounds on RAW 264.7 cells growth was assessed using CCK-8 Kit in order to find the optimal concentration with minimum toxicity. The concentration of these compounds up to 10 µg/mL showed no toxicity with cells (**Figure 2.3).**

Table 2.2 The spectroscopic data of compound **3** (Acetone-*d6*, δ in ppm, *J* in Hz)

No.	**^{13}C-NMR** (125 MHz)	**^{1}H-NMR** (500 MHz)	**HMBC** (^{1}H → ^{13}C)
1	105.7	-	
2	166.1	-	
3	99.8	6.39 (1H, *d*, 2.5 Hz)	C-1, 2, 5
4	165.3*	-	

5	111.3	6.45 (1H, *d*, 2.5 Hz)	C-1, 3, 4, 8
6	148.4	-	
7	170.2	-	
8	39.3	2.95 (2H)[#]	C-1, 5, 6, 9, 10
9	25.9	1.70 (2H, *m*)	C-6, 8, 10
10	14.4	0.95 (3H, *t*, 7.0 Hz)	C-8, 9
1′	116.2	-	
2′	165.3*	-	
3′	114.5	6.57 (1H, *d*, 2.5 Hz)	C-1′, 2′, 4′, 5′
4′	152.8	-	
5′	108.2	6.5 (1H, *d*, 2.5 Hz)	C-1′, 3′, 4′, 8′
6′	149.3	-	
7′	176.7	-	
8′	38.0	3.12 (2H, *t*, 7.5 Hz)	C-1′, 5′, 6′, 9′, 10′
9′	25.5	1.63 (2H, *sextet*, 7.5 Hz)	C-6′, 8′, 10′
10′	14.4	0.90 (3H, *t*, 7.0 Hz)	C-8′, 9′
2-OH	-	11.17 (1H, *s*)	C-3
2′-OCH_3	55.9	3.86 (3H, *s*)	C-2′
-COO<u>H</u>	-	14.22 (1H, *brs*)	

* These signals were interchangeable.

This signal was overlapped with acetone-d_6 solvent and was determined by HSQC.

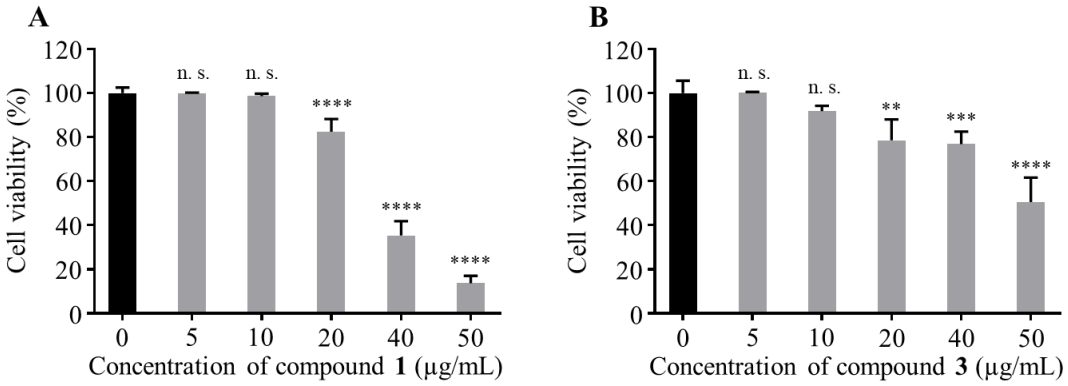

Figure 2.3 Effects of compounds **1** and **3** on cell viability of RAW 264.7 cells. RAW 264.7 macrophages were cultured with compounds 1 and 3 for 24 h, and then cell viability based on intracellular dehydrogenase was measured, as seen in (A) and (B), respectively. Values represent the mean ± SD (n = 4). Statistical significance was calculated by t-test and one-way ANOVA. ** p < 0.01; *** p < 0.001; ****, p < 0.0001 vs. cells treated with media only; n. s., not significant.

Therefore, the concentration at 5, 10 μg/mL of these compounds were investigated the anti-inflammatory effects through nitric oxide (NO) production. NO is known as a signal molecule, which plays an essential role in inflammation response [46]. As shown in

Figure 2.4, only compound 1 at 5 µg/mL significantly reduced the production of NO in comparison with LPS.

Taken together, a new 2′-*O*-methylnordivaricatic acid **3**, an isomer of **3a**, could be generated from the late-stage functionalization in the biosynthesis pathway of *Dirinaria* species. These findings might contribute to chemotaxonomy for determining *D. applanata* among a pool of lichen species.

In conclusion, from the extract of the lichen *Dirinaria applanata*, three compounds were isolated and fully characterized by both 1D and 2D-NMR. Notably, compound **1** was a new hopanoic acid while compound **3** was a new depside. Moreover, compound **2** was firstly isolated from *D. applanata*. Additionally, only compound **1** shows the anti-inflammatory potential through testing to reduce NO production in LPS-stimulated cells, while others do not show activity.

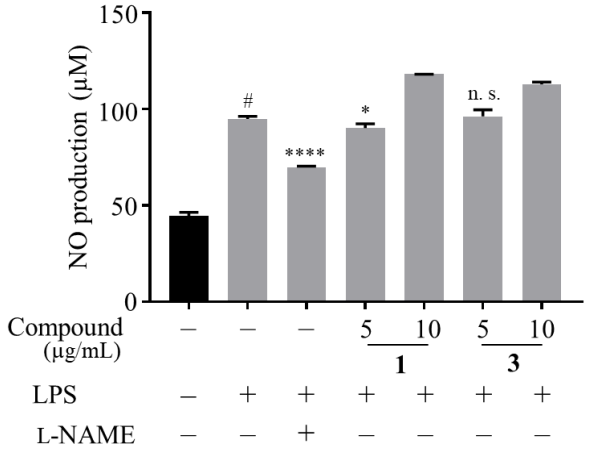

Figure 2.4 Effects of compound **1** and **3** on the production of NO in LPS-stimulated RAW 264.7 cells. Cells were pretreated with the concentration of compounds 1 and 3 for 24 h. After washing with phosphate-buffered saline (PBS), cells were stimulated with 1 µg/mL LPS for 18 h. The level of NO in the medium was quantified by Griess reagent was analyzed. *N*-Nitro-*L*-arginine methyl ester (L-NAME; 100 µM) was used as a control in the NO assay. Values represent the mean ± SD (n = 3). Statistical significance was calculated by *t*-test and one-way ANOVA. #, $p < 0.05$ vs. cells treated with media only; n. s., not significant; *, $p < 0.05$ and ****, $p < 0.0001$ vs. cells treated with LPS only.

Chapter 3

Anti-inflammatory effects of *Lasia spinosa* leaf extract in lipopolysaccharide-induce RAW 264.7 macrophages

3.1 Introduction

Inflammation is a mechanism used to defend against various infections and injuries; it is a well-appreciated aspect of complex biological responses that maintain homeostasis in the human body [47]. However, chronic inflammatory processes are implicated in the pathogenesis of common inflammation-associated diseases such as rheumatoid arthritis, chronic hepatitis, pulmonary fibrosis, and cancer [48]. Notably, innate immune cells (particularly macrophages) initiate an inflammatory response via the overwhelming production of pro-inflammatory mediators, such as nitric oxide (NO) and prostaglandin E_2 (PGE_2), and inflammatory cytokines such as tumor necrosis factor-α (TNF-α), interleukin-1β (IL-1β), and interleukin-6 (IL-6) [49]. As such, levels of pro-inflammatory mediators and cytokines are reflective of the degree of inflammation and are used to evaluate the effect of pharmacological agents on inflammatory processes. In particular, lipopolysaccharide (LPS), a bacterial endotoxin, can induce inflammation signaling pathways via Toll-like receptor 4 (TLR-4), which stimulates the recruitment of cytoplasmic MyD88 and Toll-like receptor-domain-containing adapter-inducing interferon-β (TRIF) adaptor proteins to increase the secretion of pro-inflammatory mediators and cytokines [50,51]. LPS initiates a signaling cascade and subsequent activation of the nuclear factor-kappa B (NF-κB) pathway, the mitogen-activated protein kinase (MAPKs: extracellular signal-regulated kinases 1/2 (ERK 1/2), c-Jun N-terminal kinase (JNK), and p38 MAPK) pathways, and the phosphatidylinositol (PI) 3-kinase (PI3K)/protein kinase B (Akt) signaling pathway [52]. Inflammation is related to oxidative stress, which elevates the levels of intracellular reactive oxygen species (ROS) and regulates the production of antioxidant enzymes [53]. The induction of phase II detoxifying enzymes, including heme oxygenase-1 (HO-1), is controlled by translocation of the nuclear factor-erythroid-2-related factor (Nrf2) in the Nrf2/HO-1 signaling pathway, which is a master cellular sensor that protects cells against inflammation and oxidative stress [54].

Nonsteroidal anti-inflammatory drugs (NSAIDs) are used to treat many inflammatory diseases. These drugs attack cyclooxygenase-2 (COX-2) and inhibit the synthesis of prostaglandins, thereby causing undesirable side effects such as toxicity and myocardial infarction [55]. These issues necessitate the development of novel agents to treat acute inflammation and chronic inflammatory diseases in a more effective and less toxic manner [56]. Because of the side effects associated with NSAIDs, natural compounds are used as dietary supplements and herbal treatments to reduce pain and inflammation. Many of these natural compounds and herbs inhibit inflammatory pathways to a similar degree as NSAIDs [57].

Lasia spinosa (L.) Thwaites (LS) is used in traditional Vietnamese medicine to alleviate the symptoms of many inflammatory diseases. Furthermore, the phytochemicals in LS include alkaloids, polyphenols, and flavonoids, which have antioxidant, anti-bacterial, anti-hyperglycemic, and anti-cancer properties [58–60]. A recent study showed that *L. spinosa* leaf extract possesses a considerable level of efficacy against Trichinella spiralis infections in mice [61]. In this study, we examined the anti-inflammatory properties of ethanol extracts from LS leaves in LPS-stimulated RAW 264.7 macrophages. We found that LS leaf ethanol extracts inhibited activation of the TLR-4 pathway and promoted the Nrf2/HO-1 pathway. Thus, we demonstrate that LS could be used as a potential anti-inflammatory agent.

3.2 Material and methods

3.2.1 Preparation of LS leaf ethanol extracts

LS leaves were collected in An Giang province, Vietnam (lat. 10°22’52’’ north latitude and 105°25’12’’ east longitude), dried naturally, and ground with a waring blender. 10 g of dried powder was extracted with 100 mL of ethanol (FUJIFILM-Wako, Tokyo, Japan) at 25 °C, then centrifuged to collect the supernatant, and was obtained 1.27 g extract. The residue was extracted three more times and supernatants were combined. The extract was concentrated under reduced pressure using a rotary evaporator (Rotavapor R-300, BUCHI, Switzerland), freeze-dried, and then stored at 4 °C until use. Voucher specimens of LS were deposited in the Laboratory of Plant Biology, Department of Biology, Can Tho University, Vietnam under code number (Ls01.2018-AG006).

3.2.2 Radical scavenging activity and total polyphenolic content

The radical scavenging effects of LS leaf extract on 2,2-diphenyl-1-picrylhydrazyl (DPPH; Sigma-Aldrich, MA, USA) and 2,2-azino-bis(3-ethylbenzothiazoline-6-sulfonic acid) diammonium salt (ABTS; Sigma-Aldrich) radicals were evaluated by previously described methods with slight modifications [62,63]. Briefly, various concentrations of LS leaf extracts (0, 4, 8, 12, 16, 20, 28 µg/mL) in 0.96 mL of methanol were mixed with 0.04 mL of DPPH in methanol (1 mg/mL). The mixtures were incubated in the dark at room temperature for 30 min. The absorbance was measured at 517 nm using a V-730 UV-Vis Spectrophotometer (Jasco, Tokyo, Japan). Vitamin C (FUJIFILM-Wako) was used as a positive control.

For the ABTS assay, the stock solution was prepared by mixing 0.2 mL of 7 mM ABTS solution with 0.2 mL of 2.4 mM potassium persulfate solution (pH 7.4) and allowed to generate ABTS radicals by incubation in the dark at room temperature for 14 h. The solution was then diluted with methanol to obtain an absorbance of 0.71 ± 0.01 at 734 nm. The scavenging activity was measured by mixing 1 mL of ABTS solution with 0.25 mL of various concentrations of LS sample, and the absorbance was measured at 734 nm after 6 min incubation. Trolox (6-hydroxy-2,5,7,8-tetramethyl chromane 2-carboxylic acid, FUJIFILM-Wako) was used as a positive control.

In both DPPH and ABTS assays, the scavenging activity was calculated with the following equation (1):

$$\textbf{Radical scavenging activity}\ (\%) = \frac{(\mathbf{A_{cs}} - \mathbf{A_{Blank\,1}}) - (\mathbf{A_s} - \mathbf{A_{Blank\,2}})}{\mathbf{A_{cs}} - \mathbf{A_{Blank\,1}}}$$

where A_{cs} is the absorbance of the control reaction (without test or standard sample), A_s is the absorbance in the presence of test or standard sample, $A_{Blank\ 1}$ is the absorbance of Blank 1 containing only methanol, and $A_{Blank\ 2}$ is the absorbance of Blank 2 containing test or standard sample in methanol.

The total polyphenolic content of LS leaf extract was determined using the Folin-Ciocalteu reagent with a slight modification [64]. A volume of 0.25 mL of plant extract in methanol (50 µg/mL) was mixed with 0.25 mL of the Folin-Ciocalteu reagent and neutralized with 0.25 mL of 10% sodium carbonate solution (w/v). The reaction mixture was incubated at 40 °C for 30 min with intermittent shaking for color development and then the absorbance at 765 nm was measured. Gallic acid (FUJIFILM-Wako), was used as a control for generating the calibration curve. The total polyphenolic content was expressed as mg/g gallic acid equivalent (GAE) of dried leaf.

3.2.3 Cell culture, cell viability, and LDH activity

RAW 264.7 murine leukemia macrophage cells (ATCC TIB-71^{TM}, USA) were maintained with Dulbecco's modified Eagle's medium (DMEM; FUJIFILM-Wako, Japan) containing 10% fetal bovine serum (FBS; GIBCO BRL, Grand Island, NY, USA) and 1% penicillin-streptomycin (PS; FUJIFILM-Wako, Japan) in a humidified incubator containing 5% CO_2 at 37 °C.

For cell experiments, LS leaf ethanol extract (1 g/mL) was dissolved in 5% (v/v) dimethyl sulfoxide (DMSO; FUJIFILM-Wako, Japan) as a stock. The stock solution was diluted to an appropriate sample concentration with DMEM and then added to the culture medium in 96-well plates that were incubated for 24 h. During treatment, the DMSO concentration was kept at 0.5% (v/v).

Cell viability was measured using the Cell Counting Kit-8 assay (CCK-8; Dojindo Molecular Technologies Inc., Rockville, USA), which is based on the measurement of intracellular dehydrogenase activity. Briefly, the cells were treated with serial concentrations of LS leaf extract (0, 50, 100, 200, 400, 800, and 1000 µg/mL) for 24 h in 96 well-plates at a density of 2 x 10^4 cells/well, followed by incubation with or without 1 µg/mL LPS (from *Escherichia coli*, Sigma-Aldrich, USA) for 18 h. Then, absorption at 450 nm was read using a SH-1200 microplate reader (CORONA electric, Ibaraki, Japan). To assess cell damage, LDH activity in the medium was measured using the Cytotoxicity LDH assay Kit-WST (Dojindo Molecular Technologies). Whole-cell extracts were prepared by cell lysis using 2% (v/v) Triton X-100.

3.2.4 NO production and ROS accumulation

RAW 264.7 cells were pretreated with the indicated concentration of LS extract dissolved in DMEM for 24 h, the medium was removed, and cells were washed with PBS. Then, cells were stimulated with 1 µg/mL LPS in DMEM for 18 h. To quantify NO, the conditioned medium (0.1 mL) was removed and mixed with an equal volume of Griess reagent (FUJIFILM-Wako) dissolved in water for 10 min at room temperature. The absorbance at 540 nm was measured with a SH-1200 microplate reader, and NO concentration was calculated based on a standard curve generated with sodium nitrite [65]. *N*-Nitro-*L*-arginine methyl ester (L-NAME; FUJIFILM-Wako) (100 µM) was used as a standard iNOS inhibitor (positive control).

ROS production was assayed using the Cellular ROS assay Kit (Abcam, Tokyo, Japan). After removing the media, the cells were stained with 10 µM *2',7'-dichlorodihydrofluorescein diacetate* ($DCFH_2$ –DA) at 37 °C for 45 min. The fluorescence, which corresponds to the intracellular ROS level, was measured using a

Wallac 1420 spectrofluorometer (Perkin-Elmer, Turku, Finland) at an excitation wavelength of 488 nm and an emission wavelength of 535 nm.

3.2.5 ELISA

The expression level of TNF-*α* protein in LPS-stimulated RAW 264.7 cells was analyzed by ELISA using the TNF-α ELISA Ready-SET-Go Kit (eBiosciences, California, USA). TNF-*α* concentration was calculated based on the standard curve made using the TNF-*α* mouse standard set in the kit. RAW 264.7 macrophages were incubated with 1 μg/mL LPS in the presence of various concentrations of LS extract for 24 h. The supernatants were collected and stored at -80 ℃ until analysis.

3.2.6 Quantitative RT-PCR (qRT-PCR)

RAW 264.7 cells were incubated for 24 h in 6-well plates with LS leaf extract, washed with PBS, and then stimulated with or without LPS 1 μg/mL for 18 h. Total RNA was extracted using Trizol reagent (Invitrogen; Carlsberg, CA, USA) followed by purification with the Qiagen RNeasy Kit (Qiagen; Hilden, Germany). cDNA was synthesized using Transcriptor Universal cDNA Master Mix (Roche, Mannheim, Germany) and s SimpliAmp™ Thermal Cycler (Life Technologies, Singapore) according to the manufacturer's instructions. Quantitative polymerase chain reaction (PCR) was performed using the FastStart Essential DNA Green Master Mix (Roche, Mannheim, Germany) and a Light-Cycler 96 (Roche). β-Actin was used as a normalization control. The primers used in this study are listed in Table 1.

Table 3.1 Primers used for qRT-PCR analysis

Gene[1]	**Primer sequence**	
	Forward Primer (5' – 3')	**Reverse Primer (5' – 3')**
iNOS (NOS2)	GGAGCCTTTAGACCTCAACAGA	AAGGTGAGCTGAACGAGGAG
IL-6	GCTACCAAACTGGATATAATCAGGA	CCAGGTAGCTATGGTACTCCAGAA
IL-1β	AGTTGACGGACCCCAAAAG	AGCTGGATGCTCTCATCAGG
TNF-α	CTGTAGCCCACGTCGTAGC	TTGAGATCCATGCCGTTG
IL-10	CGCTTGGAATCCCGAATTA	CTCAGGTTGGTCACAGTGAAAT
COX-2	GATGCTCTTCCGAGCTGTG	GGATTGGAACAGCAAGGATTT
HO-1	AGGGTCAGGTGTCCAGAGAA	CTTCCAGGGCCGTGTAGATA
Nrf2	CATGATGGACTTGGAGTTGC	CCTCCAAAGGATGTCAATCAA
β-Actin	GGAGGGGGTTGAGGTGTT	GTGTGCACTTTTATTGGTCTCAA

[1] Primer's name; nitric oxide synthase-2 (NOS2), interleukin-6 (IL-6), interleukin-1β (IL-1β), tumor necrosis factor-α (TNF-α), interleukin-10 (IL-10), cyclooxygenase-2 (COX-2), heme oxygenase-1 (HO-1), nuclear factor erythroid-2-related factor 2 (Nrf2), β-Actin.

3.2.7 Western Blotting

RAW 264.7 cells were seeded in 6-well plates and incubated with different concentrations of LS leaf extract for 24 h prior to stimulation with 1 µg/mL LPS for 18 h. Total protein was extracted from cells using RIPA lysis buffer (FUJIFILM-Wako) containing a cocktail of protease and phosphatase inhibitors. Cytoplasmic and nuclear proteins were separated using a Nuclear Extraction Kit (Abcam), and protein concentrations were analyzed using a Pierce ™ BCA protein assay kit (Thermo Fisher Scientific, Waltham, MA USA). The protein samples were separated by 10% SDS-PAGE and transferred onto polyvinylidene fluoride (PDVF) membranes. After blocking for 1 h with a solution containing 5% skim milk (FUJIFILM-Wako), the membrane was incubated with the primary antibodies overnight at 4℃. The primary antibodies and phospho-specific antibodies (IκB*α*, p-IκB*α*, p-NF-κB p65, p38, p-p38, ERK1/2, p-ERK1/2, JNK, Akt, p-Akt, β-actin [Cell Signaling Technology, Tokyo, Japan], p-JNK, NF-κB p65 [*Sigma-Aldrich*], Nrf2 [Proteintech, Japan], Lamin-B1, and GAPDH [Santa Cruz Biotechnology, Dallas, TX, USA]) were diluted according to the manufacturer's recommendation. After washing in Tris-buffered saline containing 0.5% Tween 20 (TBST), the membrane was incubated with horseradish-peroxidase-conjugated secondary antibody (*Sigma-Aldrich*) in TBST containing 5% skim milk or 3% bovine serum albumin (BSA fraction V; Roche, Mannheim, Germany) at room temperature for 1 h. Proteins were visualized using Pierce™ ECL Western Blotting Substrate (Thermo Fisher Scientific). Quantification of *band intensity* was *performed using Image J software* (NIH, USA) and normalized to *β*-Actin or GAPDH.

3.2.8 Immunofluorescent staining

Cells were seeded in 8-well chamber slides (Thermo Fisher Scientific, Nunc™ Lab-Tek® Chamber Slides, Waltham, MA USA). After treatment with LS leaf extract followed by LPS stimulation, the cells were fixed with 4% paraformaldehyde phosphate buffer solution (FUJIFILM-Wako) according to previously described methods [66]. Cells were incubated with rabbit anti-NF-κB p65 (1:500) followed by anti-rabbit IgG Alexa Fluor™ 488-conjugate (1:800; Molecular Probes, Invitrogen, Carlsbad, CA, USA), or rabbit anti-Nrf2 (1:500) followed by anti-rabbit IgG Alexa Fluor™ 594-conjugate (1:800; Molecular Probes). For staining of nuclei, 4′,6-diamidino-2-phenylindole (DAPI; Molecular Probes, Eugene, OR, USA) was used for 30 min. Samples were then mounted on a glass slide in Vectashield mounting medium (Vector Laboratories, Tokyo, Japan), and inspected

using a fluorescence FV10i microscope (Olympus, Tokyo, Japan). The fluorescent intensity was analyzed using MetaMorph software (version 7.7.7.0; Molecular Devices, Sunnyvale, CA, USA).

3.2.9 Statistical analysis

Experiments were repeated at least three times, and all data are expressed as means ± S.D. Statistical significance was evaluated using *t*-tests and one-way ANOVAs, where $p < 0.05$ was considered significant.

3.3 Results

3.3.1 Antioxidant activity of LS leaf ethanol extracts

To test the antioxidant activity of LS leaf ethanol extracts, radical scavenging ability was indirectly evaluated by DPPH (2,2-diphenyl-1-picrylhydrazyl) and ABTS (2,2-azino-bis (3-ethylbenzothiazoline-6-sulfonic acid) diammonium salt) assays. The free radical-scavenging activities increased linearly with increasing concentration of LS leaf extract in both assays (Figure 1). The concentrations of LS leaf extract required to scavenge 50% of the free radicals (SC_{50}) in the DPPH and ABTS assays were 17.25 μg/mL (equivalent to 5.38 μg/mL vitamin C) and 16.47 μg/mL (equivalent to 3.17 μg/mL Trolox), respectively (Figure 3.1).

Additionally, the total amount of polyphenols expressed as gallic acid equivalent (GAE) was 158 ± 0.56 mg GAE/g of extract (20.08 ± 0.07 mg GAE/g dried leaf). These results demonstrated that the LS leaf ethanol extract could effectively scavenge free radicals.

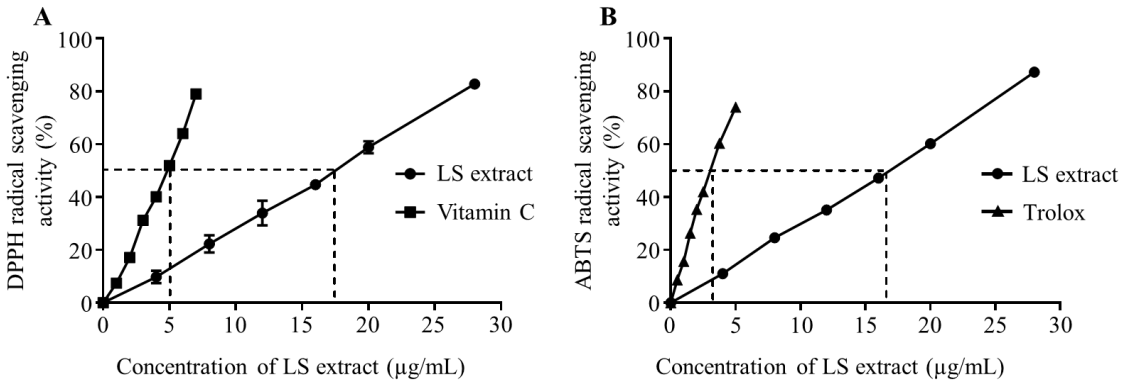

Figure 3.1 Radical scavenging activity of the LS leaf ethanol extract. Varying concentrations of LS leaf extract were mixed with DPPH (A) or ABTS (B). Vitamin C and Trolox were used as positive controls in (A) and (B), respectively. After incubation, the absorbance at 517 nm in the DPPH

assay or 734 nm in the ABTS assay was measured, and radical scavenging activity was calculated. The dotted line indicates the concentration of LS leaf extract or control substance which is required for 50% radical scavenging (SC_{50}). Data are expressed as means ± SD. Significant differences between the LS leaf extract and Vitamin C or Trolox controls (n = 3) were evaluated by t-test.

3.3.2 Effect of LS leaf extract on RAW 264.7 cells viability

The cytotoxicity of LS leaf extract was examined using RAW 264.7 cells in order to find the optimal concentration (effective in providing anti-inflammatory with minimum toxicity). At an LS leaf extract concentration of 800 µg/mL, cell survival was reduced by ~10% (Figure 3.2A) and lactate dehydrogenase (LDH) activity was increased (Figure 3.2B), suggesting cell toxicity. No cytotoxicity was observed with a concentration of LS leaf extract (<400 µg/mL).

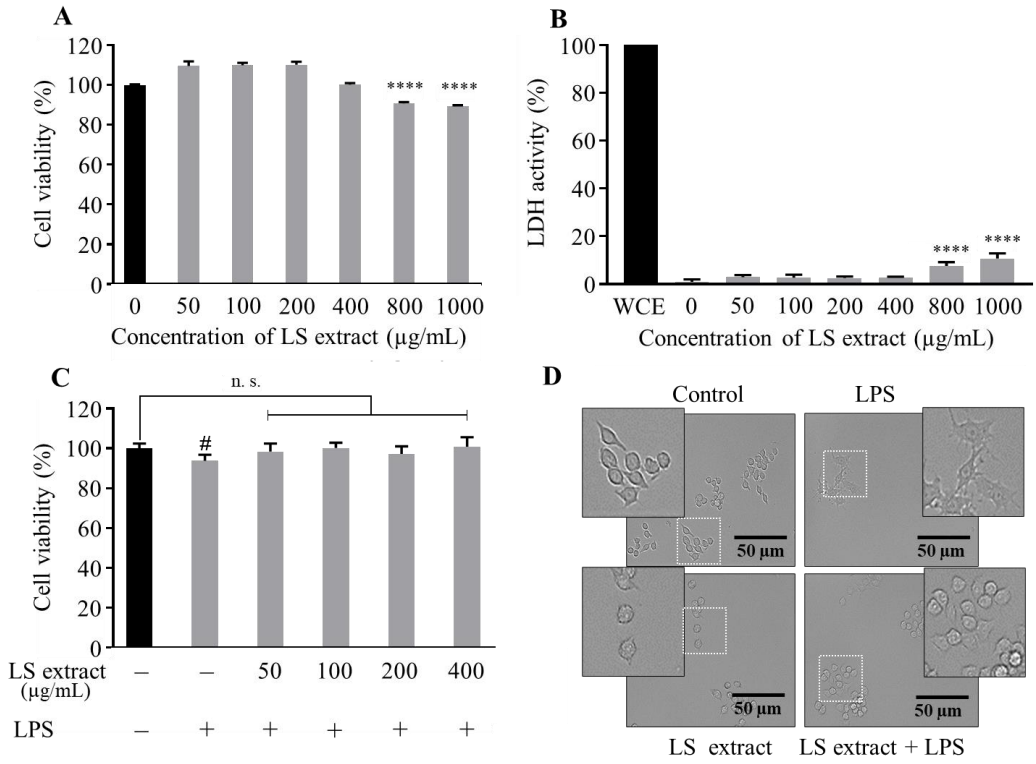

Figure 3.2 Effects of LS leaf extract on cell viability and morphology of RAW 264.7 cells. RAW 264.7 macrophages were cultured with LS leaf extract for 24 h, and then cell viability based on intracellular dehydrogenase activity (A) and cytotoxicity based on LDH activity released in culture medium (B) were measured. Whole-cell extract (WCE) was prepared as a positive control representing 100% activity in (B). After pretreatment with LS extract for 24 h, RAW 264.7 cells were stimulated by LPS (1 µg/mL) for 18 h, and then cell viability was measured (C). RAW 264.7 cells were treated with medium only (control), LPS, or LS extract (400 µg/mL) for 24 h. The LS

extract + LPS group was treated with LPS (1 μg/mL) for 18 h. Cell morphology was observed under a phase-contrast microscope (D). Magnification of the region framed with a dotted white line is shown in the frame with a black line. Values represent the mean ± S.D. (n = 6). Statistical significance was calculated by t-test- and one-way ANOVA. Scale bar in (D), 50 μm; #, $p < 0.05$; ****, $p < 0.0001$ vs. cells treated with media only; n. s., not significant.

Since LPS is known to reduce cell viability, the cytotoxicity of a mixture of LS leaf extract and LPS was also examined. As shown in Figure 3.2C, cell survival was significantly reduced by LPS but not by the mixture of LPS and LS leaf extract (<400 μg/mL). The LPS-stimulated cells had an abnormal shape (spindle-shaped pseudopodia and spreading) (Figure 3.2D). This phenomenon is one of the characteristics of LPS-activated RAW 264.7 macrophages [67]. Consistent with the above result, RAW 264.7 cells did not show the abnormal shape by treatment with a mixture of LPS and LS leaf extract at 400 μg/mL (Figure 3.2D). Taken together, these data indicate that the viability of RAW 264.7 cells is not affected by the LS leaf extract (<400 μg/mL), and the LS leaf extract protects the cell from LPS-induced toxicity.

3.3.3 LS leaf extract Inhibits the production of NO, ROS, and TNF-α in LPS-stimulated RAW 264.7 cells

NO, a signaling molecule produced by inducible nitric oxide synthase (iNOS), plays an essential role in the inflammatory response and is produced at higher concentrations in response to inflammation or injury [68,69]. To investigate the anti-inflammatory effect of LS leaf extract in LPS-stimulated RAW 264.7 cells, the amount of NO in culture medium was quantified. N-Nitro-L-arginine methyl ester (L-NAME) (100 μM) was used as a positive control. NO production was significantly increased by stimulation with LPS; however, pretreatment with LS leaf extract (50–400 μg/mL) significantly inhibited NO production in a dose-dependent manner (Figure 3.3A).

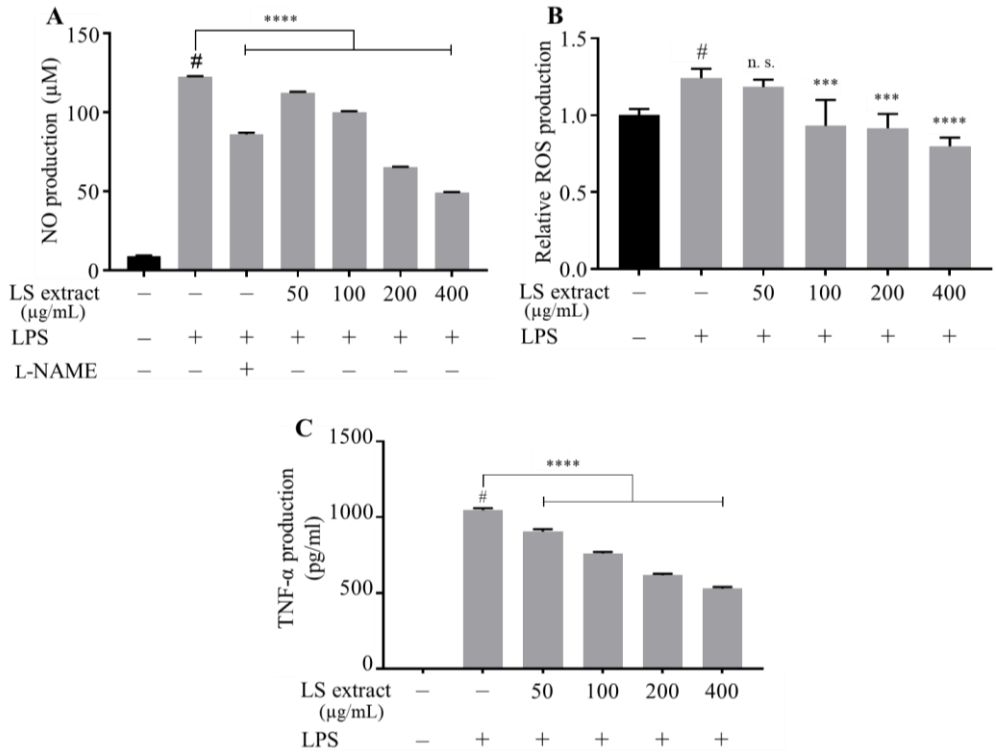

Figure 3.3 Effects of LS leaf extract on the production of NO, ROS, and TNF-α in LPS-stimulated RAW 264.7 cells. Cells were pretreated with LS leaf extract for 24 h. After washing with PBS, cells were stimulated with 1 μg/mL LPS for 18 h. The level of NO in the medium was quantified by Griess reagent (A), and cellular ROS concentration was analyzed (B). L-NAME (100 μM) was used as a control in the NO assay. The levels of TNF-α in RAW 264.7 cells were analyzed by an ELISA (C). Values represent the mean ± S.D. (n = 3). Statistical significance was calculated by t-test and one-way ANOVA. #, $p < 0.05$ vs. cells treated with media only; n. s., not significant, ***, $p < 0.001$ and ****$p < 0.0001$ vs. cells treated with LPS only.

ROS are signaling molecules that play an essential role in the progression of inflammatory disorders [70]. Thus, we evaluated the effect of pretreatment with LS leaf extract on intracellular ROS production in LPS-stimulated RAW 264.7 cells. Figure 3.3B demonstrates that ROS production was upregulated by LPS-stimulation and significantly reduced by pretreatment with LS leaf extract (except for the 50 μg/mL dose). These results indicate that LS leaf extract not only suppresses NO production but also inhibits intracellular ROS production in LPS-stimulated RAW 264.7 cells.

Since TNF-α is a strong pro-inflammatory cytokine that plays a crucial role in the immune system during inflammation [71], its expression in RAW 264.7 cells was analyzed using an enzyme-linked immunosorbent assay (ELISA). As illustrated in Figure 3.3C, LPS-stimulated RAW 264.7 cells increased TNF-α levels, while pretreatment with LS leaf

extract (50–400 μg/mL) significantly suppressed TNF-α expression. Taken together, these data suggest that the LS leaf extract suppresses the production of inflammatory mediators in LPS-stimulated RAW 264.7 cells.

3.3.4 LS leaf extract Inhibits the expression of inflammatory genes in LPS-stimulated RAW 264.7 cells

We tested whether LS leaf extract suppressed the transcription of inflammatory mediators using qRT-PCR. We analyzed three concentrations, 100, 200, and 400 μg/mL, of LS extract that are non-toxic and showed clear suppressive effects on the production of inflammatory mediators as shown in Figure 3.3. As expected, LS leaf extract strongly suppressed the up-regulation of *iNOS (NOS2)*, *COX-2*, and cytokine (*TNF-α*, *IL-1β*, *IL-6*) messenger RNA (mRNA) levels (Figure 3.4A–C,E,F). In contrast, LS leaf extract (>200 μg/mL) significantly induced the expression of *IL-10*, an anti-inflammatory cytokine that limits the host immune response (Figure 3.4D). These results indicate that LS leaf extract inhibits the expression of inflammatory mediators at the transcriptional level.

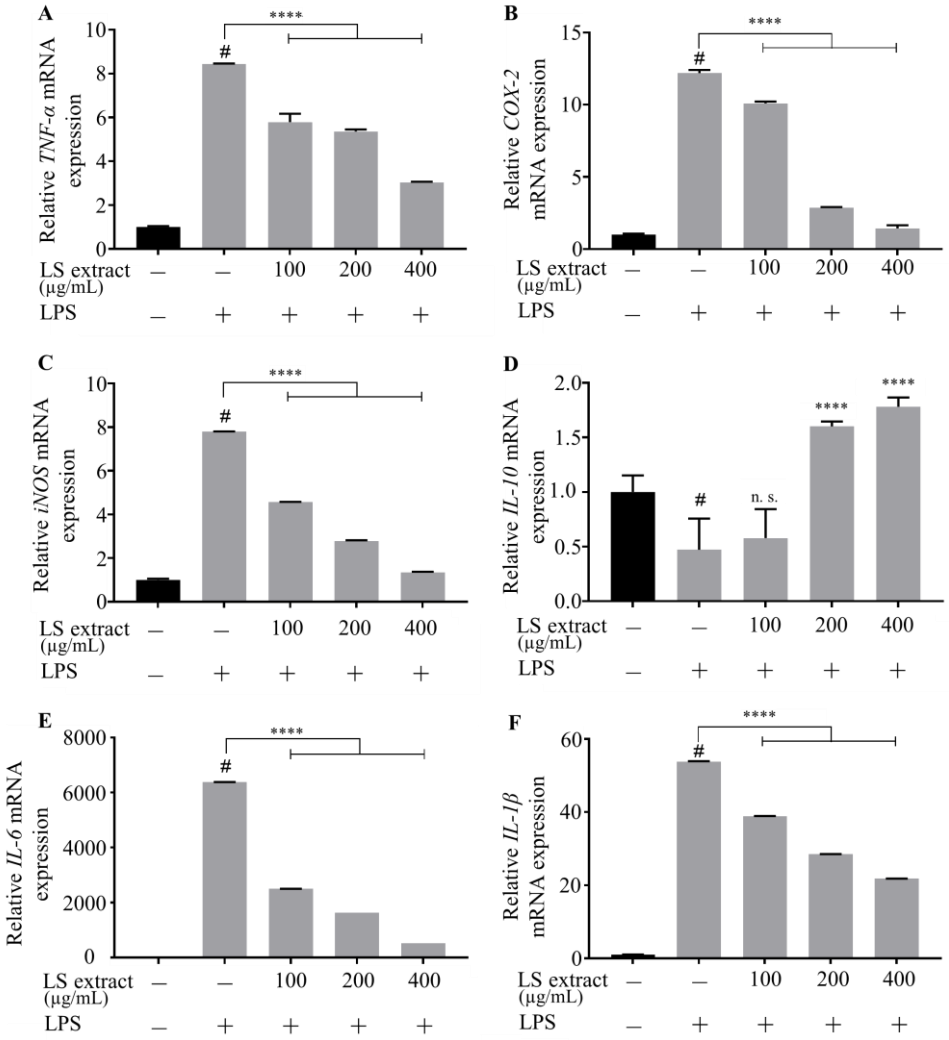

Figure 3.4 Effects of LS leaf extract on the expression of pro-inflammatory cytokines in LPS-stimulated RAW264.7 macrophages. RAW264.7 cells were pretreated with LS leaf extract for 24 h, followed by LPS (1 μg/mL) stimulation for 18 h. The expression of *TNF-α* (A), *cyclooxygenase-2* (*COX-2*) (B), inducible nitric oxide synthase (*iNOS*) (*NOS2*) (C), *interleukin-10* (*IL-10*) (D), *IL-6* (E), and *IL-1β* (F) was analyzed by qRT-PCR (n = 3). Values represent the mean ± SD. Statistical significance was calculated by t-test and one-way ANOVA. # $p < 0.05$ vs. cells treated with media only; n. s., not significant; **** $p < 0.0001$ vs. cells treated with LPS only.

3.3.5 LS leaf extract inhibits phosphorylation and translocation of NF-κB in LPS-stimulated RAW 264.7 cells

NF-κB proteins are heterodimers consisting of two p50 and p65 monomers that are regulated by the degradation of nuclear factor of kappa light polypeptide gene enhancer in B-cells inhibitor, alpha (IκBα). IκBα phosphorylation induces the translocation of phosphorylated-NF-κB (p-NF-κB) from the cytoplasm to the nucleus, in order for it to transcriptionally regulate genes associated with the inflammatory processes. To investigate

the effect of LS leaf extract on the regulation of the NF-κB pathway, the levels of phosphorylated p65 (p-p65) and phosphorylated-IκBα (p-IκBα) in whole-cell extracts were examined by Western blot. As shown in Figure 3.5, p-p65 and p-IκBα were significantly reduced by treatment with the LS leaf extract (100 – 400 μg/mL).

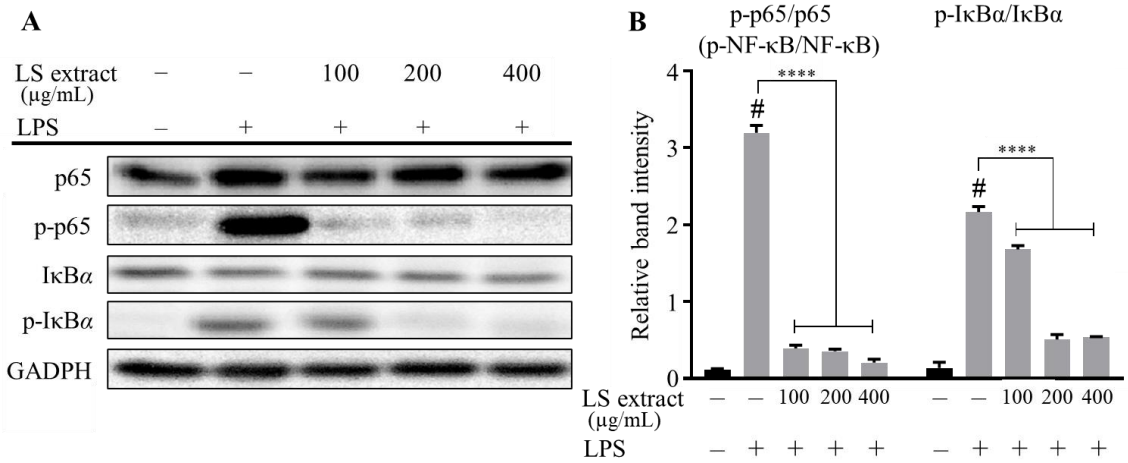

Figure 3.5 Effects of LS leaf extract on LPS-induced activation of the nuclear factor kappa B (NF-κB) pathway in RAW 264.7 cells. Cells were pretreated with LS extract for 24 h, followed by LPS (1 μg/mL) stimulation for 18 h. Whole-cell lysates were subjected to Western blotting (A). Glyceraldehyde 3-phosphate dehydrogenase (GAPDH) was used as a control. The relative band intensity of phosphorylated target protein to total target protein was analyzed using Image J (B) (n = 3). Values represent the mean ± SD. Statistical significance was calculated by t-test and one-way ANOVA. # $p < 0.05$ vs. cells treated with media only; n. s., not significant; **** $p < 0.0001$ vs. cells treated with LPS only.

Moreover, levels of the p65 NF-κB subunit in the nucleus also significantly decreased in response to LS leaf extract treatment (100–400 μg/mL) (Figure 3.6A,B). The p65 NF-κB subunit was visualized using a fluorescence-labeled antibody to confirm the effect of LS leaf extract on its translocation. Consistent with the Western blot results, LS leaf extract inhibited the translocation of p65 from the cytoplasm to the nucleus (Figure 3.6C,D). These data indicate that the LS leaf extract controls the inflammatory response of RAW 264.7 cells by inhibiting the activation of NF-κB.

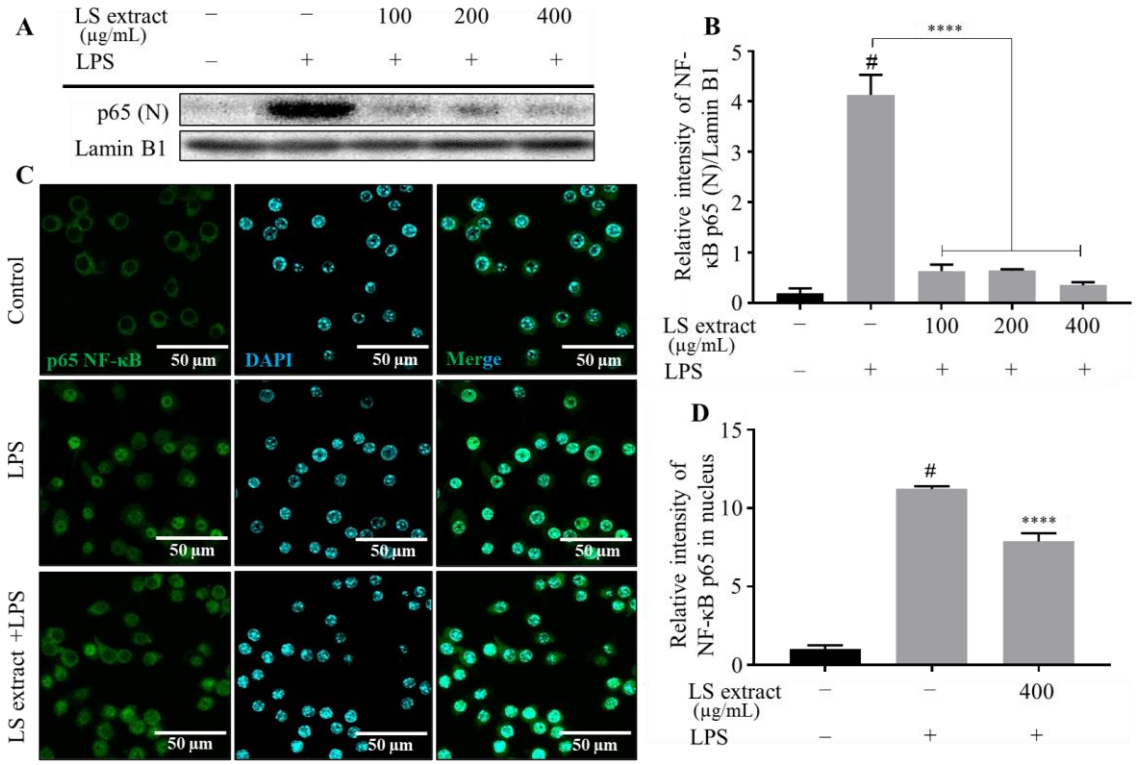

Figure 3.6 The inhibitory effects of LS leaf extract on translocation of the p65 NF-κB subunit in LPS-stimulated RAW 264.7 cells. Cells were pretreated with LS leaf extract for 24 h, followed by LPS (1 μg/mL) stimulation for 18 h. The nuclear (N) p65 NF-κB subunit was detected by Western blotting (n = 3) (A). The relative band intensity of p65 (N) to lamin B1 (nuclear loading control) was quantified using Image J (B). Cells were pretreated without or with 400 μg/mL of LS leaf extract followed by LPS stimulation and then labeled with an anti-NF-κB p65 antibody tagged with Alex Fluor 488 (Green) and nuclear-counterstaining 40,6-diamidino-2-phenylindole (DAPI; blue) (C). The fluorescent intensity of nuclei was analyzed using MetaMorph software (n = 30) (D). Control, cells treated with only culture medium; LPS, cells treated with LPS only (1 μg/mL); LS extract + LPS, cells treated LS leaf extract (400 μg/mL) followed by LPS (1 μg/mL). Values represent the mean ± SD; scale bar, 50 μm. Statistical significance was calculated by t-test and one-way ANOVA. # $p < 0.05$ vs. cells treated with media only; n. s., not significant; **** $p < 0.0001$ vs. cells treated with LPS only.

3.3.6. LS leaf extract Inhibits the phosphorylation of MAPKs and Akt in LPS-stimulated RAW 264.7 cells

The MAPKs and PI3K/Akt signaling pathways are upstream of NF-κB signaling pathways, and play a critical role in LPS-induced inflammatory responses in RAW 264.7 cells [53,72]. Our Western blot results showed that LS leaf extract effectively reduced the

phosphorylation of MAPKs (p38, ERK, JNK) and Akt (Figure 3.7A,B). Thus, LS leaf extract suppresses the inflammatory responses by deactivating the MAPKs and PI3K/Akt signaling pathways in LPS-stimulated RAW 264.7 cells.

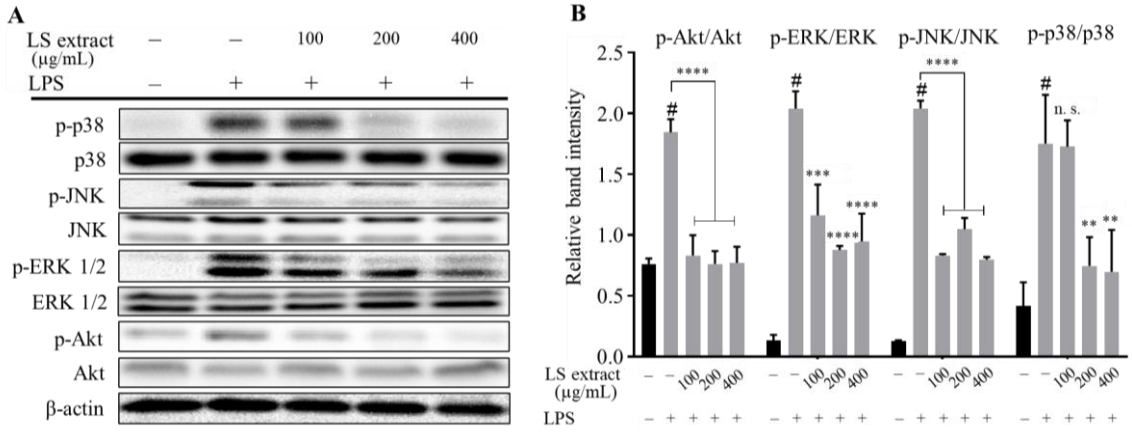

Figure 3.7 Effects of LS leaf extract on LPS-induced of mitogen-activated protein kinases (MAPKs) and phosphoinositide-3-kinase/protein kinase B (PI3K/Akt) pathways in RAW 264.7 cells. Cells were pretreated with LS leaf extract for 24 h, followed by LPS (1 μg/mL) stimulation for 18 h. The expression of p-p38, p38, p-c-Jun N-terminal kinase (JNK), JNK, p-extracellular signal-regulated kinases 1/2 (ERK 1/2), ERK1/2, p-Akt, and Akt was analyzed by Western blot (A). β-actin was used as a loading control. The relative band intensity of phosphorylated (p-) target protein compared to total target protein was quantified using Image J (B) (n = 3). Values represent the mean ± SD. Statistical significance was calculated by t-test and one-way ANOVA. # $p < 0.05$ vs. cells treated with media only; n. s., not significant; ** $p < 0.01$, *** $p < 0.001$, and **** $p < 0.0001$ vs. cells treated with LPS only.

3.3.7 LS leaf extract promotes the activation of Nrf2/HO-1 pathway in LPS-stimulated RAW 264.7 cells

The Nrf2/HO-1 signaling pathway plays an essential role in intracellular antioxidant systems [73]. To analyze the effect of LS leaf extract on the Nrf2/OH-1 pathway, we firstly measured the mRNA levels of transcription factor Nrf2 and HO-1 by qRT-PCR. Nrf2 and HO-1 mRNA levels were significantly upregulated by pretreatment of LPS-stimulated RAW cells with LS leaf extract (100–400 μg/mL) (Figure 3.8A,B). Although pretreatment with 400 μg/mL of LS extract showed the highest effect, the upregulation of Nrf2 and HO-1 seems not to be dose-dependent with respect to LS extract. Further study is needed to clarify this reason.

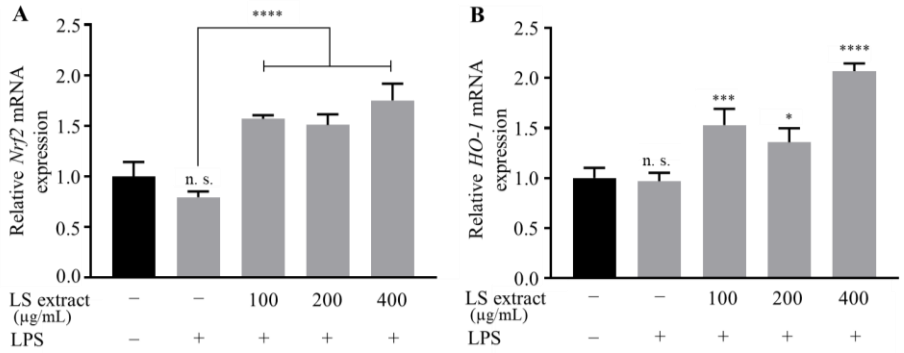

Figure 3.8 Effects of LS leaf extract on the expression of transcription factor *nuclear factor-erythroid-2- related factor* (*Nrf2*) (A) and phase II enzyme *heme oxygenase-1* (*HO-1*) (B) in LPS-stimulated RAW 264.7 cells. Cells were pretreated with LS leaf extract for 24 h, followed by LPS (1 μg/mL) stimulation for 18 h. The expression of *Nrf2* and *HO-1* genes was analyzed by qRT-PCR (n = 3). Values represent the mean ± SD. Statistical significance was calculated by *t*-test and one-way ANOVA. n. s., not significant; * $p < 0.05$, *** $p < 0.001$, and **** $p < 0.0001$ vs. cells treated with LPS only.

Next, Western blotting of nuclear proteins demonstrated that LS leaf extract promoted Nrf2 nuclear translocation in RAW264.7 cells (Figure 3.9A,B). Furthermore, the location of Nrf2 in the nucleus was confirmed by immunostaining (Figure 3.9C,D). These results imply that the anti-inflammatory properties of LS leaf extract relate to induction of the Nrf2/HO-1 signaling pathway.

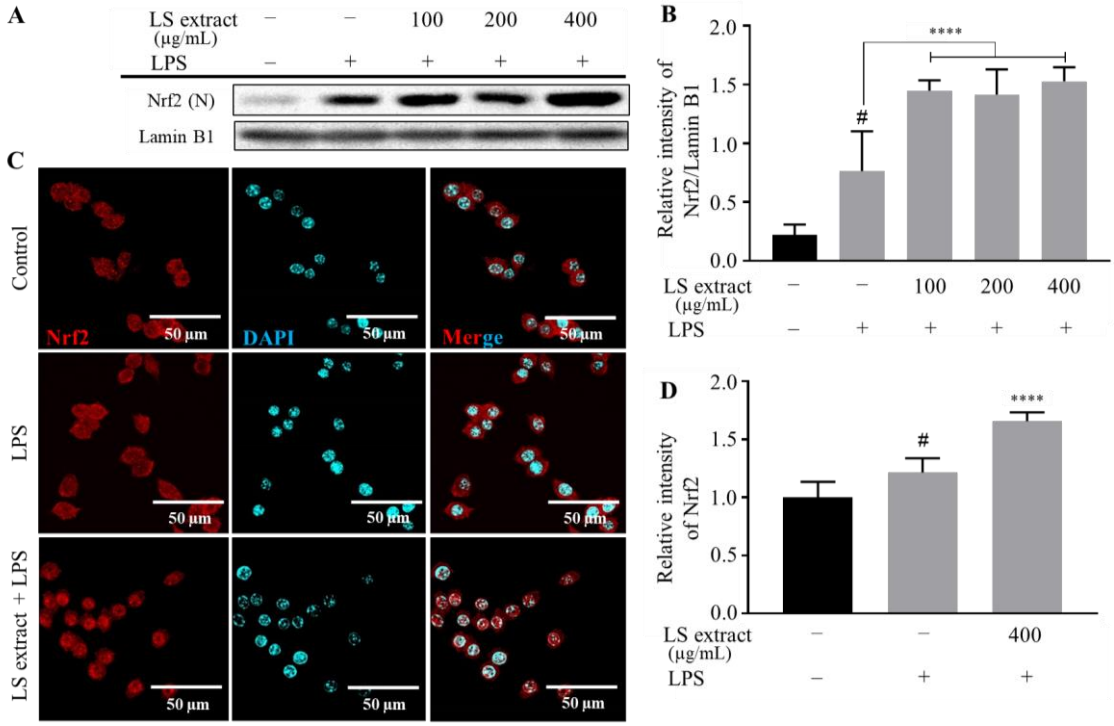

Figure 3.9 Effects of LS leaf extract on Nrf2 translocation in LPS-stimulated RAW 264.7 cells. Cells were pretreated with LS leaf extract for 24 h, followed by LPS (1 μg/mL) stimulation or 18

h. Nuclear (N) Nrf2 was analyzed by Western blot (n = 3) (A). Lamin B1 was used as a nuclear loading control. The relative band intensity of Nrf2 (N) compared to lamin B1 was quantified using Image J (B). The cells were treated with culture medium only (control), LPS only (1 μg/mL), or LS leaf extract (400 μg/mL) and LPS (1 μg/mL), and stained with an Nrf2 antibody labeled with Alex Fluor 594 (red) and DAPI (blue). Representative images acquired by confocal fluorescence microscopy are shown in (C). Fluorescent intensity was analyzed using MetaMorph software (D) (n = 30). Values represent the mean ±SD; scale bar, 50 μm. Statistical significance was calculated by t-test and one-way ANOVA. # $p < 0.05$ vs. cells treated with media only; n. s., not significant; **** $p < 0.0001$ vs. cells treated with LPS only.

3.4 Discussion

Inflammation is described as an immune response that defends against infection or injury. When our body fails to respond to inflammation, tissues are destroyed and lose their function, a phenomenon which is characteristic of many serious diseases such as diabetes, cardiovascular disorders, Alzheimer's disease, autoimmune and pulmonary disease, and cancer. Currently, epidemiological evidence suggests that plants have various bioactivities that are associated with anti-inflammatory effects. Therefore, traditional medicines or natural products are potential sources of novel anti-inflammatory active compounds that could lead to the innovative therapeutics with fewer toxic side effects [74,75]. LS was previously reported to have many pharmacological effects that are used in traditional Vietnamese medicine to treat inflammatory diseases [58,59,76]. However, the mechanisms behind its pharmacological properties and its chemical constituents are not yet elucidated. We found that, consistent with previous studies, LS leaf extract had high DPPH and ABTS scavenging activity [59,77]. Antioxidants act as oxygen scavengers capable of catalyzing the oxidative process [78]. Lin et al. (2016) showed that polyphenolic is the major donor in the anti-oxidative process [79]. LS leaf extract possessed anti-oxidative ability, likely due to its high polyphenolic content (158 ± 0.56 mg GAE/g of dried extract, 20.08 mg ±0.07 mg GAE/g dried leaf) compared to other plant extracts. For example, ethanol extract of the *Aniseia martinicense* leaf contains phenolics, 10.61 ± 3.12 mg GAE/g of dried leaf, which is much lower than that of the LS leaf extract [80]. Additionally, both ginger and turmeric are herbs that possess powerful antioxidant and anti-inflammatory properties, which could help decrease pain and protect against disease [81]. In this study, polyphenolic compounds were

found to be good scavengers of free radicals to a much higher than previously reported on these herbs [82,83]. This suggests that the *L. spinosa* leaf should not only be further evaluated at a scientific level but also as an adjunct herb that may potentially have wide applications.

Antioxidants have important roles in redox mechanisms by protecting the cell against inflammation and apoptosis [79]. Oxidative stress caused by LPS or other stimuli may trigger the activation of macrophages, thereby leading to an excessive inflammatory response [84]. As illustrated in Figure 3.2A and 3.2B, the high concentration of LS leaf extract (>400 µg/mL) reduced cell viability, suggesting that an overdose of LS leaf extract or its active components may be toxic, giving rise to cell damage. In contrast, cell viability and morphology analyses revealed that LS leaf extract (50–400 µg/mL) protects RAW 264.7 cells from LPS-induced damage (Figure 3.2C,D).This effect may relate to the anti-oxidative and anti-inflammatory effects of the extract. Here, we clearly showed that LS leaf extract suppressed LPS-induced production of the important inflammatory mediator TNF-α, intracellular ROS, and NO in RAW 264.7 macrophages (Figure 3.3). This suggests that LS leaf extract can alleviate several inflammatory symptoms as a result of its anti-inflammatory properties.

Pro-inflammation cytokines (TNF-α, IL-6, IL-1β) and enzymes (iNOS, COX-2) are induced by the immune system during inflammation. Interestingly, our extract inhibited the expression of these cytokines and enzymes (Figure 3.4). Noticeably, IL-6 and TNF-α are the primary mediators of local inflammation and sepsis [85]. Elevated expression of IL-1β was observed in various human cancers, such as melanoma, colon, breast, and lung cancers [86]. On the other hand, IL-10 is a potent anti-inflammatory cytokine that controls the inflammatory processes by inhibiting various pro-inflammatory cytokines [87,88]. Here, we found that the LS leaf extract enhances IL-10 expression in LPS-stimulated macrophages (Figure 4D). Previous studies suggested that IL-10 induction may exert beneficial effects in reducing the chronic inflammatory response [89]. This suggests that the LS leaf extract not only inhibits the inflammatory response but also promotes anti-inflammatory factors. Thus, further research should aim to uncover the exact mechanism(s) behind the anti-inflammatory effects of LS leaves in order to develop drugs for inflammatory diseases.

The activation of innate immunity by LPS starts with its binding to TLR-4, a receptor for pathogen-derived molecules such as LPS and lipoteichoic acid [90]. TLR-4 activation

leads to activation of the canonical NF-κB signaling pathway. At basal conditions, the NF-κB p50/p65 heterodimers are sequestered in the cytoplasm through the formation of a complex with inhibitory IκB [91]. When macrophages are stimulated by LPS, IκB is rapidly phosphorylated, leading to its degradation by the ubiquitination-mediated 26S proteasome. NF-κB dimers are subsequently liberated and translocated to the nucleus to promote the expression of pro-inflammatory cytokines [92,93]. Our study showed that LS leaf extract strongly inhibits the phosphorylation of IκBα and the NF-κB p65 subunit (Figure 3.5) and the nuclear translocation of NF-κB p65 in LPS-stimulated RAW264.7 cells (Figure 3.6), suggesting that the activation of TLR-4 pathway is suppressed. Apart from functioning as modulators of the inflammatory response, pro-inflammatory cytokines also facilitate the induction of free radicals such as NO and ROS. In addition, the excessive appearance of free radicals (ROS and NO) leads to a state of oxidative stress; thus, free radicals can both activate and repress NF-κB signaling [94,95]. The reduction of intracellular ROS by LS leaf extract may, therefore, affect the activation of NF-κB signaling. In TLR-4-stimulated cells, MyD88 and TRIF are recruited to phosphorylate interleukin-1 (IL-1)-receptor-associated kinase (IRAK) and its downstream targets to activate NF-κB signaling, which is necessary to initiate the expression of pro-inflammatory cytokines [96]. Thus, we cannot exclude the possibility that LS leaf extract inhibits these molecules, thereby affecting activation of the TLR-4 pathway. In addition, we found that LS leaf extract strongly reduced pro-inflammatory factors (Figure 3.4), suggesting that activation of the TLR-4 signaling pathway is inhibited by LS leaf extract in the initial steps of inflammation. NF-κB activation is related to several signaling pathways, including MAPKs and PI3K/Akt pathways that are crucial for regulating inflammation and producing inflammatory factors [97,98]. Previous studies showed that LPS stimulation increases the phosphorylation of MAPKs (JNK, p38, MAPK, ERK) in macrophages [99]. PI3K/Akt signal transduction involves the activation of the TLR-4 pathway by LPS [43]. Li et al. reported that Akt (downstream of the NF-κB, MAPKs, and interferon regulatory factor-3 (IRF-3) pathways) is indirectly involved in the activation of macrophages by Astragalus polysaccharide [100]. Saponaro et al. reported that LPS-induced p-Akt activation occurs upstream of NF-κB activation in microglia [101]. Despite the discrepancy in the position of TLR-4 in the pathway, these reports suggest the involvement of PI3K/Akt in the activation of NF-κB-dependent inflammatory responses. Our data (Figure 3.7) indicated that LS leaf

extract inhibits the phosphorylation of MAPKs (p38, ERK, JNK) and Akt in response to LPS stimulation. These results demonstrate that LS leaf extract may suppress the inflammatory response by inhibiting the activation of MAPKs and PI3K/Akt. Previous reports described that the suppression of NF-κB and MAPK pathway activation leads to the inhibition of NO, PGE_2, iNOS, COX-2, TNF-α, and IL-6 production in LPS-stimulated RAW 264.7 cells [98]. Taken together, our evidence reinforces the hypothesis that the anti-inflammatory capacity of LS leaf extract relates to the regulation of the TLR-4 pathway in LPS-stimulated RAW 264.7 cells.

In this study, we demonstrated that LS leaf extract has strong antioxidant effects (Figure 3.1), possibly due to its high levels of polyphenolic compounds. A previous study showed that LPS causes oxidative stress that may trigger the activation of macrophages, leading to an excessive inflammatory response [102]. Therefore, we further analyzed the antioxidant effects underlying the inhibition of LPS-stimulated macrophage activation. LPS stimulation rapidly increases the ROS level in macrophages. This response not only causes DNA damage but also leads to the overproduction of inflammatory cytokines and enzymes [103]. Nrf2 is an upstream mediator of the antioxidant response element. Under normal conditions, Nrf2 is anchored in its inactive form in the cytoplasm through its interaction with Kelch-like encoded in human (ECH)-associated protein (Keap1), a sensor of oxidative signals and electrophilic reactions. In response to oxidative stress, Nrf2 dissociates from Keap1, translocates to the nucleus, and induces the expression of phase II anti-oxidative enzymes such as HO-1, glutathione synthesis enzyme, and drug transporters. We found that pretreatment with LS leaf extract increased the expression of *Nrf2* and *HO-1* (Figure 3.8), repressed the expression of *iNOS* and *COX-2* (a PGE2-producing enzyme) (Figure 4), and suppressed the production of ROS and NO (Figure 3.3) in LPS-stimulated RAW 264.7 cells. Moreover, nuclear translocation of Nrf2 was enhanced by pretreatment with LS leaf extract (Figure 3.9). These findings illustrate that LS leaf extract is able to activate the Nrf2/HO-1 pathway to promote the downstream expression of HO-1, in order to reduce ROS production. These findings coincide with the findings from Yao et al. (2019) that nardochinoid B isolated from *Nardostachys chinensis* inhibits the activation of RAW 264.7 cells stimulated by LPS through activation of the Nrf2/HO-1 pathway [104]. However, nardochinoid B did not inhibit the activation of the NF-κB and MAPK pathways. Polyphenols are considered anti-oxidative and anti-inflammatory agents due to their effects

on radical scavenging, inhibition of certain enzymes involved in ROS production, and upregulation of endogenous antioxidant enzymes [105]. Therefore, activation of the Nrf2/HO-1 pathway in LPS-stimulated macrophages may be promoted by the polyphenols in LS leaf extract.

Previous studies mentioned that TLR-4 plays a crucial role in various diseases, especially cancer [106,107]. In the present study, we demonstrated that LS leaf extract inhibits the inflammatory response in LPS-stimulated macrophages by not only inhibiting TLR-4 activation but also promoting the Nrf2/HO-1 pathway. Interestingly, under the investigated conditions, pretreatment of LS leaf extract induced cell death at a high concentration. However, at a low concentration, it protected cells from the cytotoxicity effect of LPS-induced inflammation. Furthermore, our data suggest that the effect of LS leaf extract, in a concentration-dependent manner, might suppress inflammation by LPS-induced RAW 264.7 cells. Thus, *L. spinosa* leaf extract may contain components that are either beneficial or harmful to cells. To address this hypothesis, further studies are needed to identify potentially active compounds and to assess the effects of anti-inflammatory agents. In conclusion, this study provides the first evidence that LS leaf extract suppresses the inflammatory response. Therefore, LS may be a promising alternative anti-inflammatory agent.

Chapter 4. Conclusions

Traditional herbal medicines still play an important role in future drug development based on their variety and specific medicinal properties in various diseases. In dissertation, the composition of compounds from two potential herbs as well as their anti-inflammatory ability have been evaluated and explained clearly. Notably, three new compounds from lichen *Dirinaria applanata* were isolated and fully characterized based on both 1D and 2D-NMR. Additionally, *1β-Acetoxy-3β-hydroxy-21α-hopane-29-oic acid* shows its anti-inflammatory properties by inhibiting NO production in LPS-induced RAW 264.7 macrophages. Besides, these results also provide crucial information that *Lasia spinosa* leaf extract, with the enrichment of polyphenol components, possesses an activity to inhibit the LPS-induced inflammatory response though the blocking of PI3K/Akt, MAPK, NF-κB and activating Nrf2/HO-1 signaling pathways. Thereby, the potential unique anti-inflammatory mechanism of *L. spinosa* leaf provides a new therapeutic solution for oxidative damage and inflammation-related diseases. These findings lead to further research on the main active components of lichen *D. applanata*, *L. spinosa* as a basis for extending evidence to develop and apply natural compounds in the treatment of excessive inflammation and oxidative stress.

References

1. Yuan, H.; Ma, Q.; Ye, L.; Piao, G. The traditional medicine and modern medicine from natural products. *Molecules* **2016**, *21*.

2. Zhu, F.; Ma, X.H.; Qin, C.; Tao, L.; Liu, X.; Shi, Z.; Zhang, C.L.; Tan, C.Y.; Chen, Y.Z.; Jiang, Y.Y. Drug discovery prospect from untapped species: Indications from approved natural product drugs. *PLoS One* **2012**, *7*, 1–9.

3. Ngo, L.T.; Okogun, J.I.; Folk, W.R. 21st Century natural product research and drug development and traditional medicines. *Nat. Prod. Rep.* **2013**, *30*, 584–592.

4. Galm, U.; Shen, B. Natural Product Drug Discovery: The Times Have Never Been Better. *Chem. Biol.* **2007**, *14*, 1098–1104.

5. Parasuraman, S.; Thing, G.S.; Dhanaraj, S.A. Polyherbal formulation: Concept of ayurveda. *Pharmacogn. Rev.* **2014**, *8*, 73–80.

6. Li, Y. Qinghaosu (artemisinin): Chemistry and pharmacology. *Acta Pharmacol. Sin.* **2012**, *33*, 1141–1146.

7. Mansukh C. Wani and Susan Band Horwitz Nature as a Remarkable Chemist: A Personal Story of the Discovery and Development of Taxo. *Anticancer Drugs.* **2014**, *25*, 482–487.

8. Ashraf, K.; Sultan, S. A comprehensive review on Curcuma longa Linn.: Phytochemical, pharmacological, and molecular study. *Int. J. Green Pharm.* **2017**, *11*, S671–S685.

9. T.R, P.K.; Ramesh, Dhanya, Dhatri Ramesh, Sunita C. Mesta Sunita C. Mesta, O.; R, O.; K.S, and V. Radical Scavenging, Antimicrobial and Insecticidal Efficacy of Parmotrema cristiferum and Dirinaria applanata. *Sci. Technol. Arts Res. J.* **2015**, *4*, 95–102.

10. Ahmed, E.F.; Elkhateeb, W.A.; Taie, H.A.A.; Rateb, M.E.; Fayad, W. Biological capacity and chemical composition of secondary metabolites from representatives Japanese lichens. *J. Appl. Pharm. Sci.* **2017**, *7*, 98–103.

11. Lin, W.; Karin, M. A cytokine-mediated link between innate immunity , inflammation , and cancer Find the latest version : Review series A cytokine-mediated link between innate immunity, inflammation , and cancer. *J. Clin. Invest.* **2007**, *117*, 1175–1183.

12. Multhoff, G.; Molls, M.; Radons, J. Chronic inflammation in cancer development. *Front. Immunol.* **2012**, *2*, 1–17.

13. Geng, J.G. Directional migration of leukocytes: Their pathological roles in inflammation and strategies for development of anti-inflammatory therapies. *Cell Res.* **2001**, *11*, 85–88.

14. Guzik, T.J.; Korbut, R.; Adamek-Guzik, T. Nitric oxide and superoxide in inflammation and immune regulation. *J. Physiol. Pharmacol.* **2003**, *54*, 469–487.

15. Maeda, H.; Akaike, T. *Infection, Inflammation, and Cancer Mediated by Oxygen Radicals and Nitric Oxide*; 1998;

16. Morgan, M.J.; Liu, Z.G. Crosstalk of reactive oxygen species and NF-κB signaling. *Cell Res.* **2011**, *21*, 103–115.

17. Grisham, M.B.; Jourd'heuil, D.; Wink, D.A. I. Physiological chemistry of nitric oxide and its metabolites: Implications in inflammation. *Am. J. Physiol. - Gastrointest. Liver Physiol.* **1999**, *276*, 315–321.

18. MacMicking, J.; Xie, Q.; Nathan, C. Nitric Oxide and Macrophage Function. *Annu. Rev. Immunol.* **1997**, *15*, 323–350.

19. Vallabhapurapu, S.; Karin, M. Regulation and Function of NF-κB Transcription Factors in the Immune System. *Annu. Rev. Immunol.* **2009**, *27*, 693–733.

20. Bonizzi, G.; Karin, M. The two NF-κB activation pathways and their role in innate and adaptive immunity. *Trends Immunol.* **2004**, *25*, 280–288.

21. Xiao, G.; Fong, A.; Sun, S.C. Induction of p100 processing by NF-κB-inducing kinase involves docking IκB kinase α (IKKα) to p100 and IKKα-mediated phosphorylation. *J. Biol. Chem.* **2004**, *279*, 30099–30105.

22. Pearson, G.; Robinson, F.; Gibson, T.B.; Xu, B.E.; Karandikar, M.; Berman, K.; Cobb, M.H. Mitogen-activated protein (MAP) kinase pathways: Regulation and physiological functions. *Endocr. Rev.* **2001**, *22*, 153–183.

23. Read, M.A.; Whitley, M.Z.; Gupta, S.; Pierce, J.W.; Best, J.; Davis, R.J.; Collins, T. Tumor necrosis factor α-induced E-selectin expression is activated by the nuclear factor-κB and c-JUN N-terminal kinase/p38 mitogen-activated protein kinase pathways. *J. Biol. Chem.* **1997**, *272*, 2753–2761.

24. Qiang Ma Role of Nrf2 in Oxidative Stress and Toxicity. *Annu. Rev. Pharmacol. Toxicol.* **2015**, 401–426.

25. Ying Huang, Wenji Li, Z.S. and A.-N.T.K. The complexity of the Nrf2 pathway: Beyond the antioxidant response. *J Nutr Biochem.* **2015**, *26*, 1401–1403.

26. I. I. I. Nash and H. Thomas. Lichen Biology, Cambridge University Press, Cambridge **2015**.

27. M. J. Calcott, D. F. Ackerley, A. Knight, R. A. Keyzers and J. G. Owen. Secondary metabolism in the lichen symbiosis, *Chem. Soc. Rev.* 2018, **47**, 1730-1760.

28. G. Shrestha and L. L. S. Clair. Lichens: a promising source of antibiotic and anticancer drugs, *Phytochem. Rev.* 2013, **12**, 229-244.

29. V. P. Zambare and L. P. Christopher. Biopharmaceutical potential of lichens, *J. Pharm. Biol.* 2012, **50**,778-798.

30. Y. Yamamoto, K. Hara, H. Kawakami and M. Komine, Lichen substances and their biological activities, In: Recent Advances in Lichenology. Springer, 2015, 181-199.

31. U. Jayalal, S. S. Oh, S. Joshi, S. O. Oh and J. S. Hur . The lichen *Dirinaria picta* new to South Korea, *Mycobiology* 2013, **41**, 155-158.

32. E. Ahmed, W. Elkhateeb, H. Taie, M. Rateb and W. Fayad. Biological capacity and chemical composition of secondary metabolites from representatives Japanese lichens, *J. Appl. Pharm. Sci.* 2017, **7**, 98-103.

33. T. T. Nguyen, Q. C. T. Nguyen, V. H. Mai, Q. T. Phan, P. Q. Do, T. D. Nguyen, P. D. Nguyen, T. T. T. Nguyen, T. D. Le, T. X. T. Dai, K. Kamei and K. Kanaori. A new hopane derivative from the lichen *Dirinaria applanata*, *Nat. Prod. Res.* 2019, 1-5 (in press).

34. J. A. Elix (2009). Dirinaria, *Fl. Australia.* **57**, 509–517.

35. S. Huneck and I. Yoshimura. Identification of lichen substances, Springer 1996

36. D. Joulain and R. Tabacchi. Lichen extracts as raw materials in perfumery. Part 1: oakmoss, *Flavour Frag. J.*, 2009, **24**, 49-61.

37. L. F. G. Brandão, G. B. Alcantara, M. F. C. Matos, D. Bogo, D. Dos Santos Freitas, N. M. Oyama and N. K. Honda. Cytotoxic evaluation of phenolic compounds from lichens against melanoma cells, *Chem. Pharm. Bull.* 2013, **61**, 176-183.

38. P. Kumboonma, T. Senawong, S. Saenglee, C. Yenjai and C. Phaosiri. New histone deacetylase inhibitors from the twigs of *Melanorrhoea usitata*, *Med. Chem. Res.* 2018, **27**, 2004-2015.

39. C. Seo, J. HanYim, H. Kum Lee and H. Oh. PTP1B inhibitory secondary metabolites from the Antarctic lichen *Lecidella carpathica*, *Mycology* 2011, **2**, 18-23.

40. G. M. König and A. D. Wright. ^{1}H and ^{13}C-NMR and biological activity investigations of four lichen-derived compounds, *Phytochem. Anal.*1999, **10**, 279-284.

41. M. Cuellar, W. Quilhot, C. Rubio, C. Soto, L. Espinoza and H. Carrasco. Phenolics, depsides and triterpenes from the chilean lichen *Pseudocyphellaria nudata* (Zahlbr.) DJ Galloway, *J. Chil. Chem. Soc.*, 2008, **53**, 1624-1625.

42. D. T. M. Nguyen, L. T. M. Do, H. T. N. Tuyet, M. K. Q. Ho, H. T. Nguyen, J. Mortier and P. K. P. Nguyen. Chemical constituents of the lichen *Dendriscosticta platyphylloides*, Lobariaceae, *Sci. Technol. Dep. J.*, 2019, **22**, 165-172.

43. J. Sichaem, H. H. Nguyen and T. H. Duong. Hopane-6*α*, 16*α*, 22-triol: A new hopane triterpenoid from the lichen *Parmotrema sancti-angelii*, *Nat. Prod. Commun.* 2019, **14**.

44. R. Corbett and A. Wilkins. Lichens and fungi. XV. Revised structures for hopane triterpenoids isolated from the lichen *Pseudocyphellaria mougeotiana*, *Aust. J. Chem.* 1977, **30**, 2329-2332.

45. M. C. Fritis, C. R. Lagos, N. Q. Sobarzo, I. M. Venegas, C. S. Sánchez, H. C. Altamirano, L. E. Catalán and W. Q. Palma. Depsides and triterpenes in *Pseudocyphellaria coriifolia* (lichens) and biological activity against *Trypanosoma cruzi*, *Nat. Prod. Res.*2013, **27**, 1607-1610.

46. Krishna Chaithanya K, Gopalakrishnan V.K, Zenebe Hagos, K.K. and G.R.D. Anti-inflammatory activity of bioactive flavonoid mesuaferrin-A from Mesua ferrea L. on Lipopolysaccharide-induced pro-inflammatory cytokines in raw 264.7 cells. *J. Pharm. Res.* **2018**, *12*, 593–598.

47. Fürst, R.; Zündorf, I. Plant-derived anti-inflammatory compounds: Hopes and disappointments regarding the translation of preclinical knowledge into clinical progress. *Mediat. Inflamm*. **2014**, 9, 1–9.

48. Scrivo, R.; Vasile, M.; Bartosiewicz, I.; Valesini, G. Inflammation as “common soil” of the multifactorial diseases. *Autoimmun. Rev.* **2011**, 10, 369–374.

49. Ji, K.Y.; Kim, K.M.; Kim, Y.H.; Im, A.R.; Lee, J.Y.; Park, B.; Na, M.K.; Chae, S. The enhancing immune response and anti-inflammatory effects of *Anemarrhena asphodeloid*es extract in RAW 264.7 cells. Phytomedicine, **2019**, 59, 1–9.

50. Modlin, H.D.B.; Modlin, R.L. Toll-like receptors: Molecular mechanisms of the mammalian immune response. *Immunology*, **2000**, 101, 1–10.

51. Savva, A.; Roger, T. Targeting Toll-like receptors: Promising therapeutic strategies for the management of sepsis-associated pathology and infectious diseases. *Front. Immunol.* **2013**, 4, 1–16.

52. Choi, Y.H.; Kim, G.Y.; Lee, H.H. Anti-inflammatory effects of cordycepin in lipopolysaccharide-stimulated RAW 264.7 macrophages through Toll-like receptor 4-mediated suppression of mitogen-activated protein kinases and NF-κB signaling pathways. *Drug Des. Dev. Ther.* **2014**, 8, 1941–1953.

53. Kwon, D.H.; Cha, H.J.; Choi, E.O.; Leem, S.H.; Kim, G.Y.; Moon, S.K.; Chang, Y.C.; Yun, S.J.; Hwang, H.J.; Kim, B.W.; et al. Schisandrin A suppresses lipopolysaccharide-induced

inflammation and oxidative stress in RAW 264.7 macrophages by suppressing the NF-κB, MAPKs and PI3K/Akt pathways and activating Nrf2/HO-1 signaling. *Int. J. Mol. Medicine,* **2018**, 41, 264–274.

54. Leung, W.S.; Yang, M.L.; Lee, S.S.; Kuo, C.W.; Ho, Y.C.; Huang-Liu, R.; Lin, H.W.; Kuan, Y.H. Protective effect of zerumbone reduces lipopolysaccharide-induced acute lung injury via antioxidative enzymes and Nrf2/HO-1 pathway. *Int. Immunopharmacol.* **2017**, 46, 194–200.

55. Ren, J.; Li, L.; Wang, Y.; Zhai, J.; Chen, G.; Hu, K. Gambogic acid induces heme oxygenase-1 through Nrf2 signaling pathway and inhibits NF-κB and MAPK activation to reduce inflammation in LPS-activated RAW264.7 cells. *Biomed. Pharmacother.* **2019**, 109, 555–562.

56. Dinarello, C.A. Anti-inflammatory agents: Present and future. *Cell,* **2010**, 140, 935–950.

57. Bost, J.; Maroon, A.; Maroon, J. Natural anti-inflammatory agents for pain relief. *Surg. Neurol. Int.* **2010**, 1, 1–2.

58. Hasan, M.N.; Munshi, M.; Rahman, M.H.; Alam, S.N.; Hirashima, A. Evaluation of antihyperglycemic activity of Lasia spinosa leaf extracts in Swiss albino mice. *World J. Pharm. Pharm. Sci.* **2014**, 3, 118–124.

59. Rahman, A.; Siddiqui, S.A.; Oke-Altuntas, F.; Okay, S.; Gül, F.; Demirtas, I. Phenolic profile, essential oil composition and bioactivity of *Lasia spinosa* (L.) thwaites. *Braz. Arch. Biol. Technol.* **2019**, 62, 1–14.

60. Muthukrishnan, S.; Sivakkumar, T. Physicochemical evaluation, preliminary phytochemical investigation, fluorescence and TLC analysis of leaves of *Lasia spinosa* (Lour.) thwaites. I*nt. J. Pharm. Pharm. Sci.* **2013**, 5, 306–310.

61. Yadav, A.K. Temjenmongla. Efficacy of *Lasia spinosa* leaf extract in treating mice infected with Trichinella spiralis. *Parasitol. Res.* **2012**, 110, 493–498.

62. Tailor Chandra Shekhar, G.A. Antioxidant Activity by DPPH Radical Scavenging Method of *Ageratum conyzoides*. *Orient,* **2014**, 1, 244–249.

63. Roberta, R.; Nicoletta, P.; Anna, P.; Ananth, P.; Min, Y. Catherine Rice-Evans Antioxidant activity applying an improved ABTS radical cation decolorization assay. *Free Radic. Biol. Med.* **1999**, 26, 1231–1237.

64. Singleton, V.L.; Rudof, O.; Rosa, M.L.R. Analysis of total phenols and other oxidation substrates and antioxidants by means of Folin-Ciocalteu reagent. *METHODS Enzymol.* **1999**, 299, 152–178.

65Schmölz, L.; Wallert, M.; Lorkowski, S. Optimized incubation regime for nitric oxide measurements in murine macrophages using the Griess assay. *J. Immunol. Methods*, **2017**, 449, 68–70.

66. Chen, R. Immunofluorescence (Indirect Staining) Protocol for Adherent Cells. *Bio-Protoc.* **2012**, 2, 3–5.

67. Dai, B.; Wei, D.; Zheng, N.N.; Chi, Z.H.; Xin, N.; Ma, T.X.; Zheng, L.Y.; Sumi, R.; Sun, L. Coccomyxa gloeobotrydiformis polysaccharide inhibits lipopolysaccharide-induced inflammation in RAW 264.7 macrophages. *Cell. Physiol. Biochem.* **2019**, 51, 2523–2535.

68. Sharma, J.N.; Al-Omran, A.; Parvathy, S.S. Role of nitric oxide in inflammatory diseases. *Inflammopharmacology* **2007**, 15, 252–259.

69. Ruhee, R.T.; Ma, S.; Suzuki, K. Sulforaphane protects cells against lipopolysaccharide-stimulated inflammation in murine macrophages. *Antioxidants*, **2019**, 8, 577.

70. Forrester, S.J.; Kikuchi, D.S.; Hernandes, M.S.; Xu, Q.; Griendling, K.K. Reactive oxygen species in metabolic and inflammatory signaling. *Circ. Res.* **2018**, 122, 877–902.

71. Rogler, G.; Andus, T. Cytokines in inflammatory bowel disease. *World J. Surgery*, **1998**, 22, 382–389.

72. Zong, Y.; Sun, L.; Liu, B.; Deng, Y.S.; Zhan, D.; Chen, Y.L.; He, Y.; Liu, J.; Zhang, Z.J.; Sun, J.; et al. Resveratrol inhibits LPS-induced MAPKs activation via activation of the phosphatidylinositol 3-kinase pathway in murine RAW264.7 macrophage cells. *PLoS ONE* **2012**, 7, 1–13.

73. Loboda, A.; Damulewicz, M.; Pyza, E.; Jozkowicz, A.; Dulak, J. Role of Nrf2/HO-1 system in development, oxidative stress response and diseases: An evolutionarily conserved mechanism. *Cell. Mol. Life Sci.* **2016**, 73, 3221–3247.

74. Yuan, H.; Ma, Q.; Ye, L.; Piao, G. The traditional medicine and modern medicine from natural products. *Molecules* **2016**, 21, 559.

75. Beg, S.; Swain, S.; Hasan, H.; Barkat, M.A.; Hussain, M.S. Systematic review of herbals as potential anti-inflammatory agents: Recent advances, current clinical status and future perspectives. *Pharmacogn. Rev.*, **2011**, 5, 120–137.

76. Kankanamge, S.U.; Amarathunga, A.A.M.D.D.N. Phytochemical and ethnopharmacological properties of Lasia spinosa (Kohila): A review. *World J. Pharm. Res.* **2017**, 6, 1–9.

77. Shafie, N.H.; Idris, S.L.; Hamdan, N.N.; Bakar, S.A.; Ishak, A.H.; Nai'mah, H.B.; Kadir, K.K.A. Nutritional composition, antioxidative and inhibitory effects against pancreatic lipase, α-amylase and α-glucosidase of *Lasia spinosa*. *J. Eng. Appl. Sci.* **2018**, 13, 8898–8905.

78. Dzoyem, J.P.; Eloff, J.N. Anti-inflammatory, anticholinesterase and antioxidant activity of leaf extracts of twelve plants used traditionally to alleviate pain and inflammation in South Africa. *J. Ethnopharmacol.* **2015**, 160, 194–201.

79. Lin, D.; Xiao, M.; Zhao, J.; Li, Z.; Xing, B.; Li, X.; Kong, M.; Li, L.; Zhang, Q.; Liu, Y.; et al. An overview of plant phenolic compounds and their importance in human nutrition and management of type 2 diabetes. *Molecules* **2016**, 21, 1374.

80. Wong, J.Y.; Matanjun, P.; Ooi, Y.B.H.; Chia, K.F. Evaluation of antioxidant activities in relation to total phenolics and flavonoids content of selected Malaysian wild edible plants by multivariate analysis. *Int. J. Food Prop.* **2014**, 17, 1763–1778.

81. Ghasemian, M.; Owlia, S.; Owlia, M.B. Review of Anti-Inflammatory Herbal Medicines. *Adv. Pharmacol. Sci.* **2016**, 1–11.

82. Tohma, H.; Gülçin, ˙I.; Bursal, E.; Gören, A.C.; Alwasel, S.H.; Köksal, E. Antioxidant activity and phenolic compounds of ginger (Zingiber offcinale Rosc.) determined by HPLC-MS/MS. *J. Food Meas. Charact.* **2017**, 11, 556–566.

83. Akter, J.; Hossain, M.A.; Takara, K.; Islam, M.Z.; Hou, D.X. Antioxidant activity of different species and varieties of turmeric (*Curcuma spp*): Isolation of active compounds. Comp. Biochem. Physiol. Part C *Toxicol. Pharmacol.* **2019**, 215, 9–17.

84. Xu, X.; Li, H.; Hou, X.; Li, D.; He, S.;Wan, C.; Yin, P.; Liu, M.; Liu, F.; Xu, J. Punicalagin induces Nrf2/HO-1 expression via upregulation of PI3K/AKT pathway and inhibits LPS-induced oxidative stress in RAW 264.7 macrophages. *Mediat. Inflamm.* **2015**, 11, 1–11.

85. Leon, L.R.; White, A.A.; Kluger, M.J. Role of IL-6 and TNF in thermoregulation and survival during sepsis in mice. *Am. J. Physiol.-Regul. Integrative Comp. Physiol.* **1998**, 275, 269–277.

86. Baker, K.J.; Houston, A.; Brint, E. IL-1 family members in cancer; two sides to every story. *Front. Immunol.* **2019**, 1, 1–16.

87. Hovsepian, E.; Penas, F.; Siffo, S.; Mirkin, G.A.; Goren, N.B. IL-10 inhibits the NF-κB and ERK/MAPK-mediated production of pro-inflammatory mediators by up-regulation of SOCS-3 in Trypanosoma cruzi-infected cardiomyocytes. *PLoS ONE* **2013**, 8, 1–12.

88. Asadullah, K.; Sterry, W.; Volk, H.D. Interleukin-10 therapy—Review of a new approach. *Pharmacol. Rev.*, **2003**, 55, 241–269.

89. Tsai, T.T.; Chuang, Y.J.; Lin, Y.S.; Wan, S.W.; Chen, C.L.; Lin, C.F. An emerging role for the anti-inflammatory cytokine interleukin-10 in dengue virus infection. *J. Biomed. Sci.* **2013**, 20, 1–9.

90. Anwar, M.A.; Basith, S.; Choi, S. Negative regulatory approaches to the attenuation of Toll-like receptor signaling. *Exp. Mol. Med.* **2013**, 45, 1–14.

91. Liang, Y.; Zhou, Y.; Shen, P. NF-κB and its regulation on the immune system. *Cell. Mol. Immunol.* **2004**, 1, 343–350.

92. Tak, P.P.; Firestein, G.S. NF-κB: A key role in inflammatory diseases. *J. Clin. Invest.* **2001**, 107, 7–11.

93. Liu, T.; Zhang, L.; Joo, D.; Sun, S.C. NF-κB signaling in inflammation. *Sign. Transduct. Target. Ther.* **2017**, 2, 1–9.

94. Lingappan, K. NF-_B in Oxidative Stress. C*urr. Opin. Toxicol.* **2018**, 7, 8139–8186.

95. Akanda, M.R.; Kim, I.S.; Ahn, D.; Tae, H.J.; Nam, H.H.; Choo, B.K.; Kim, K.; Park, B.Y. Anti-inflammatory and gastroprotective roles of rabdosia inflexa through downregulation of pro-inflammatory cytokines and MAPK/NF-κB signaling pathways. *Int. J. Mol. Sci.* **2018**, 19, 584.

96. Brubaker, S.W.; Bonham, K.S.; Zanoni, I.; Kagan, J.C. Innate Immune Pattern Recognition: A Cell Biological Perspective. *Rev. Adv.* **2015**, 33, 257–290.

97. Jung, J.S.; Choi, M.J.; Lee, Y.Y.; Moon, B.I.; Park, J.S.; Kim, H.S. Suppression of lipopolysaccharide-induced neuroinflammation by morin via MAPK, PI3K/Akt, and PKA/HO-1 signaling pathway modulation. *J. Agric. Food Chem.* **2017**, 65, 373–382.

98. Huang, B.P.; Lin, C.H.; Chen, H.M.; Lin, J.T.; Cheng, Y.F.; Kao, S.H. AMPK activation inhibits expression of proinflammatory mediators through downregulation of PI3K/p38 MAPK and NF-κB signaling in murine macrophages. *DNA Cell Biol.* **2015**, 34, 133–141.

99. Han, J.M.; Lee, E.K.; Gong, S.Y.; Sohng, J.K.; Kang, Y.J.; Jung, H.J. Sparassis crispa exerts anti-inflammatory activity via suppression of TLR-mediated NF-κB and MAPK signaling pathways in LPS-induced RAW 264.7 macrophage cells. *J. Ethnopharmacol.* **2019**, 231, 10–18.

100. Zheng, Y.; Ren, W.; Zhang, L.; Zhang, Y.; Liu, D.; Liu, Y. A Review of the Pharmacological Action of Astragalus Polysaccharide. *Front. Pharmacol.* **2020**, 11, 1–15.

101. Saponaro, C.; Cianciulli, A.; Calvello, R.; Dragone, T.; Iacobazzi, F.; Panaro, M.A. The PI3K/Akt pathway is required for LPS activation of microglial cells. *Immunopharmacol. Immunotoxicol.* **2012**, 34, 858–865.

102. Zuo, L.; Prather, E.R.; Stetskiv, M.; Garrison, D.E.; Meade, J.R.; Peace, T.I.; Zhou, T. Inflammaging and oxidative stress in human diseases: From molecular mechanisms to novel treatments. *Int. J. Mol. Sci.* **2019**, 20, 4472.

103. Zhang, B.; Hirahashi, J.; Cullere, X.; Mayadas, T.N. Elucidation of molecular events leading to neutrophil apoptosis following phagocytosis. Cross-talk between caspase 8, reactive oxygen species, and MAPK/ERK activation. *J. Biol. Chem.* **2003**, 278, 28443–28454.

104. Yao, Y.D.; Shen, X.Y.; Machado, J.; Luo, J.F.; Dai, Y.; Lio, C.K.; Yu, Y.; Xie, Y.; Luo, P.; Liu, J.X.; et al. Nardochinoid B inhibited the activation of RAW264.7 macrophages stimulated by lipopolysaccharide through activating the Nrf2/HO-1 pathway. *Molecules* **2019**, 24, 2482.

105. Yahfoufi, N.; Alsadi, N.; Jambi, M.; Matar, C. The immunomodulatory and anti-inflammatory role of polyphenols. *Nutrients* **2018**, 10, 1618.

106. Oblak, A.; Jerala, R. Toll-like receptor 4 activation in cancer progression and therapy. *Clin. Dev. Immunol.* **2011**, 12, 1–12.

107. Awasthi, S. Toll-like receptor-4 modulation for cancer immunotherapy. *Front. Immunol.* **2014**, 5, 1–5.

Appendix A. Supporting information of chapter 2

1. Supplemental data for structure elucidation of compound 1

Table A1. The comparison of NMR data of compound **1** with similar compound **1a**

Position	Compound 1		1β-Acetoxy-21α-hopane-3β,22-diol (1a) [1]	
	^{13}C-NMR (150 MHz)	^{1}H-NMR (600 MHz)	^{13}C-NMR (125 MHz)	^{1}H-NMR (500 MHz)
1	80.9	4.59 (1H, *dd*, 11.34 & 4.62 Hz)	80.9	4.59 (1H, *dd*, J = 11.5 & 5.0 Hz)
2	33.4	1.91 (1H, *m*, H$_\alpha$)	33.4	1.62 (1H, *m*, H$_a$)
		1.62 (1H, *m*, H$_\beta$)		1.91 (1H, *m*, H$_b$)
3	75.2	3.31 (1H, *dd*, 12.24 & 4.26 Hz)	75.2	3.30 (1H, *dd*, J = 12.5 & 4.5 Hz)
4	38.8	-	38.8	-
5	53.0	0.65 (1H, *dd*, 11.58 & 2.04 Hz)	53.0	0.65 (1H, *dd*, J = 11.0 & 2.0 Hz)
6	17.9	1.57 (1H, *m*, H$_\alpha$)	17.8	1.58 (*m*, H$_a$)
		1.49 (1H, *m*, H$_\beta$)		1.50 (*m*, H$_b$)
7	33.1	1.40 (1H, *m*, H$_\alpha$)	33.0	1.42 (*m*, H$_a$)
		1.21 (1H, *m*, H$_\beta$)		1.22 (*m*, H$_b$)
8	42.2	-	42.2	-
9	50.7	1.45 (1H, *m*)	50.7	1.45 (*m*)
10	42.2	-	42.2	-
11	23.0	1.46 (2H, *m*)	23.0	1.46
12	23.8	1.46 (1H, *m*)	24.0	1.47 (*m*, H$_a$)
		1.32 (1H, *m*)		1.34 (*m*, H$_b$)
13	48.6	1.32 (1H, *m*)	49.3	1.34 (*m*)
14	41.9	-	41.9	-
15	33.5	1.16 (1H, *m*, H$_\alpha$)	34.5	1.36 (*m*, H$_a$)
		1.32 (1H, *m*, H$_\beta$)		1.23 (*m*, H$_b$)
16	19.8	1.28 (1H, *m*, H$_\alpha$)	21.9	1.93 (*m*, H$_a$)
		1.48 (1H, *m*, H$_\beta$)		1.57 (*m*, H$_b$)
17	53.6	1.25 (1H, *m*)	53.9	1.44 (*m*)
18	44.3		43.9	-
19	40.9	1.51 (1H, *m*, H$_\alpha$)	41.2	1.50 (*m*, H$_a$)
		0.90 (1H, *m*, H$_\beta$)		0.91 (*m*, H$_b$)
20	26.6	1.43 (1H, *m*, H$_\alpha$)	26.6	1.75 (*m*, H$_a$)
		1.87 (1H, *m*, H$_\beta$)		1.48 (*m*, H$_b$)
21	42.0	2.34 (1H, *m*)	51.1	2.20 (1H, *dt*, J = 11.0 & 8.5 Hz)
22	42.8	2.36 (1H, *m*)	73.9	-
23	27.9	0.97 (3H, *s*)	27.9	0.96 (3H, *s*)
24	15.0	0.77 (3H, *s*)	14.9	0.78 (3H, *s*)
25	12.8	0.98 (3H, *s*)	12.7	0.99 (3H, *s*)
26	16.9	0.94 (3H, *s*)	16.9	0.97 (3H, *s*)
27	16.6	0.91 (3H, *s*)	17.0	0.93 (3H, *s*)
28	15.7	0.70 (3H, *s*)	16.0	0.74 (3H, *s*)
29	183.6	-	28.7	1.17 (3H, *s*)
30	17.6	1.13 (3H, *d*, 6.48 Hz)	30.9	1.20 (3H, *s*)
1′	170.5	-	170.5	-
2′	21.9	1.99 (3H, *s*)	21.8	1.99 (3H, *s*)

**The highlighted rows showed the main differences between two compounds.*

2. Supplemental data for structure elucidation of compound 2

Compound **2** appeared as a white solid. The negative HR-ESI-MS gave a peak at 459.3840 $[M–H]^-$ (calcd. For $C_{30}H_{51}O_3^-$, 459.3843) which corresponded to chemical formula $C_{30}H_{52}O_3$. The FT-IR showed a hydroxy band at 3414 cm^{-1}. The ^{1}H-NMR indicated 8 singlet signals of methyl groups at δ_H 1.06 (3H, *s*, H-23), 1.16 (3H, *s*, H-24), 1.19 (3H, *s*, H-25), 1.30 (3H, *s*, H-26), 0.91 (3H, *s*, H-27), 0.77 (3H, *s*, H-28), 1.18 (3H, *s*, H-29), 1.21 (3H, *s*, H-30). Two peaks at δ_H 3.14 (1H, *m*, H-3), 4.55 (1H, *m*, H-6) belong to two oxygen-bearing carbons which were also confirmed by the presence of two signals these at δ_C 79.1 (C-3) and 69.0 (C-6) in ^{13}C-NMR and DEPT. Further analyzing carbon spectra proved that there was an oxygenated quaternary carbon at δ_C 73.9 (C-22) characterized for a 2-hydroxy-2-propylfragment. Based on these 1D-NMR characteristics, compound **2** can be reasonably inferred as a regioisomer of a hopanetriol [2].

To reveal the position of three hydroxy groups, HMBC analysis was recorded. The resulted spectra displayed that carbon at δ_C 79.1 was C-3 due to the correlation with neighboured protons, namely H-1, 2, 5, 23, 24. Additionally, the cross-peaks between carbon at δ_C 69.0 and H-5, 7, 23 proved that this oxygenated carbon was C-6. Finally, the obtained data also supported the presence of 2-hydroxy-2-propyl moiety at C-21 as indicated by the inter-correlations of H-17, 21, 29, 30 to hydroxyl carbon at δ_C 73.9 (C-22) [**Figure A1a**].

More specifically, the relative position of C-1, C-3 and C-21 were readily interpreted by analyzing NOESY spectrum. As shown in [**Figure A1b**], proton H-3 displayed a nuclear overhauled effect with H-1*α*, 2*α*, 5*α*, 23 evidenced that the hydroxy group of C-3 must be *beta*- configuration. By using the same approach, carbon C-6 was similarly assigned for *beta*- configuration due to two important cross-signals from H-6 to H-5, 23. Carbon C-21 was clearly proved to be *alpha*- configuration because of the H-21/H-17 correlated signal. Based on the above evidence, compound **2** was solidly elucidated as 21*α*-hopane-3*β*,6*β*,22-triol.

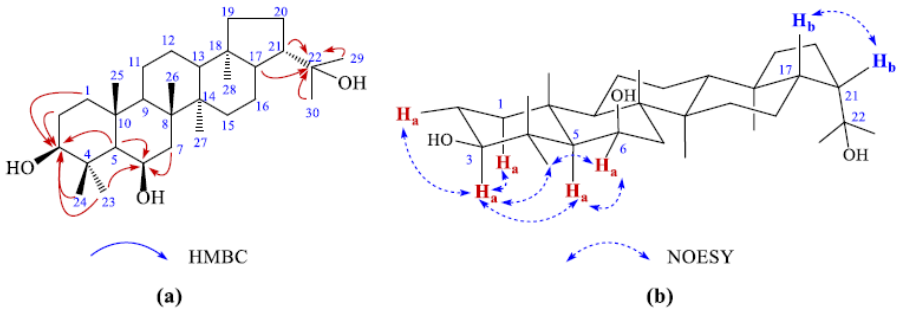

Figure A1. Some selected key HMBC (*a*) and NOESY (*b*) correlations of compound **2**

Table A2. The spectroscopic data of compound 2 ($CDCl_3$, δ in ppm, *J* in Hz)

No.	^{13}C-NMR (150 MHz)	^{1}H-NMR (600 MHz)	HMBC (^{1}H → ^{13}C)	NOESY (^{1}H → ^{1}H)
1	40.8	1.67 (1H, *m*, H_β)	C-2, 3, 5, 10, 25	H-1α, 25
		0.93 (1H, *m*, H_α)	C-5	H-1β, 2β, 3, 5, 9
2	27.6	1.64 (1H, *m*, H_β)	C-1, 3, 4, 10	H-1α, 3, 24, 25
		1.57 (1H, *m*, H_α)		H-3
3	79.1	3.14 (1H, *m*)	C-23	H-1α, 2β, 2α, 5, 23
4	39.6	-		
5	55.6	0.69 (1H, *m*)	C-3, 4, 6, 9, 10, 23, 24, 25	H-1α, 3, 6, 7α, 9, 23, 27
6	69.0	4.55 (1H, *s*)		H-5, 7α, 7β, 23, 24
7	41.0	1.72 (1H, *m*, H_α)	C-5, 6, 8, 14, 26	H-5, 6, 7β, 27
		1.47 (1H, *m*, H_β)	C-5, 6, 9	H-6, 7α
8	42.0	-		
9	50.9	1.26 (1H, *m*)	C-12	H-1β, 5, 23
10	36.7	-		
11	24.2	1.45 (2H, *m*)	C-9, 13	
12	21.1	1.57 (1H, *m*, H_β)	C-13	
		1.46 (1H, *m*, H_α)	C-9, 11, 13	H-27
13	48.8	1.47 (1H, *m*)	C-11, 12, 14	H-26
14	40.7	-		
15	34.5	1.44 (1H, *m*, H_β)	C-8	H-15α, 16β
		1.24 (1H, *m*, H_α)	C-8, 12, 13, 17, 27	H-7β, 15β, 16β, 27
16	21.9	1.94 (1H, *m*, H_β)	C-8, 15, 17, 18	H-15β, 15α, 16α, 17, 30
		1.58 (1H, *m*, H_α)		H-16β, 27
17	54.0	1.46 (1H, *m*)	C-16, 18, 22, 28	H-16β, 19β, 21
18	44.0	-		
19	41.3	1.55 (1H, *m*, H_α)	C-17, 18, 20, 21, 28	H-19β, 28
		0.97 (1H, *m*, H_β)	C-13, 18, 20, 28	H-17, 19α, 20β
20	26.6	1.76 (1H, *m*, H_β)	C-17, 18, 19, 21	H-19β, 20α, 21
		1.50 (1H, *m*, H_α)		H-20β, 28
21	51.1	2.23 (1H, *dt*, 10.8 & 9.0 Hz)	C-18, 22	H-17, 20β, 29, 30
22	73.9	-		
23	27.6	1.06 (3H, *s*)	C-3, 4,5, 6	H-3, 5, 6, 9, 24
24	16.9	1.16 (3H, *s*)	C-3, 4, 5, 23	H-2β, 6, 23, 25
25	17.6	1.19 (3H, *s*)	C-1, 5, 9, 10, 26	H-1β, 2β, 24, 26
26	17.3	1.30 (3H, *s*)	C-7,8, 9, 14, 25	H-6, 13, 25
27	17.0	0.91 (3H, *s*)	C-8, 13, 14, 15, 28	H-5, 7α, 12α, 15α, 16α, 28
28	16.3	0.77 (3H, *s*)	C-13, 17, 18, 19, 27	H'-19α, 20α, 27, 29, 30
29	28.8	1.18 (3H, *s*)	C-21, 22	H-21, 28
30	30.9	1.21 (3H, *s*)	C-21, 22	H-16β, 21, 28

3. Supplemental data for structure elucidation of compound 3

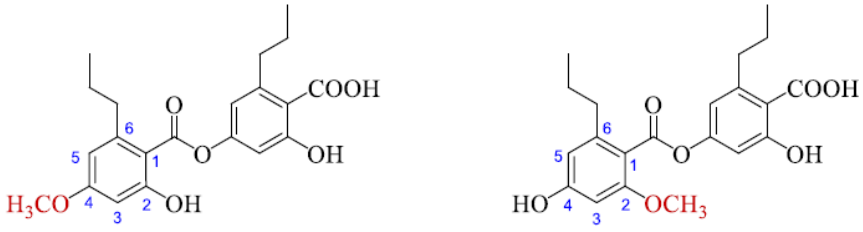

3a Divaricatic acid

3b 2-*O*-Methylnordivaricatic acid

Figure A2. The two possible structures of compound **3**

Appendix A - References

Table A3. ^{1}H and ^{13}C-NMR of compound **3** and divaricatic acid **3a** in acetone-*d6* and MeOD-*d4*

Position	Acetone-*d6*				MeOD-*d4*			
	Compound **3**		Divaricatic acid **3a** [3]		Compound **3**		Divaricatic acid **3a** [4]	
	^{13}C-NMR (125 MHz)	^{1}H-NMR (500 MHz)	^{13}C-NMR (150 MHz)	^{1}H-NMR (600 MHz)	^{13}C-NMR (125 MHz)	^{1}H-NMR (500 MHz)	^{13}C-NMR (100 MHz)	^{1}H-NMR (400 MHz)
1	105.7		105.4		107.3		105.5	
2	166.1		166.4		165.6		163.9	
3	99.8	6.39 (1H, *d*, 2.5 Hz)	99.9	6.41 (1H, *d*, 2.5 Hz)	100.1	6.40 (1H, *d*, 2.5 Hz)	98.54	6.30 (1H, *s*)
4	165.3		165.6		165.4		163.7	
5	111.3	6.45 (1H, *d*, 2.5 Hz)	111.6	6.46 (1H, *d*, 2.5 Hz)	111.2	6.42 (1H, *d*, 2.5 Hz)	109.4	6.08 (1H, *s*)
6	148.4		148.6*		148.4		146.8	
7	170.2		169.2		170.5		171.5	
8	39.3	2.95 (2H, overlap)	39.3*	2.93-3.00 (2H, *m*)	39.5	2.93 (2H, *t*, 7.5 Hz)	38.0	2.79 (2H, *t*, 7.6 Hz)
9	25.9	1.70 (2H, *m*)	25.7*	1.61-1.77 (2H, *m*)	26.4	1.65-1.73 (2H, *m*)	24.7	1.57 (2H, *m*)
10	14.4	0.95 (3H, *t*, 7.0Hz)	14.4*	0.93-1.00 (3H, *m*)	14.5	0.99 (3H, *t*, 7.5 Hz)	13.3	0.94 (3H, *t*, 7.2 Hz)
1′	116.2		112.2		116.9		110.1	
2′	165.3		165.2		164.5		157.9	
3′	114.5	6.57 (1H, *d*, 2.5Hz)	109.3	6.79 (1H, *d*, 2.3 Hz)	115.2	6.54 (1H, *d*, 2.0 Hz)	99.8	6.08 (1H, *d*, 2,4 Hz)
4′	152.8		155.0		153.4		159.3	
5′	108.2	6.50 (1H, *d*, 2.5Hz)	116.6	6.77 (1H, *d*, 2.3 Hz)	108.3	6.49 (1H, *d*, 2.5 Hz)	108.8	6.08 (1H, *d*, 2,4 Hz)
6′	149.3		149.1*		149.5		148.0	
7′	176.7		173.3		#		175.12	
8′	38.0	3.12 (2H, *t*, 7.5 Hz)	38.7*	2.93-3.00 (2H, *m*)	38.4	3.14 (2H, *t*, 7.5 Hz)	37.31	3.00 (2H, *t*, 7.6 Hz)
9′	25.5	1.63 (2H, *sextet*, 7.5 Hz)	25.9*	1.61-1.77 (2H, *m*)	26.1	1.65-1.73 (2H, *m*)	24.7	1.57 (2H, *m*)
10′	14.4	0.90 (3H, *t*, 7.0Hz)	14.5*	0.93-1.00 (3H, *m*)	14.6	0.98 (3H, *t*, 6.5 Hz)	13.1	0.93 (3H, *t*, 7.2 Hz)
2–OH	-	11.17 (1H, *s*)	-					
2′–OCH_3	55.9	3.86 (3H, *s*)	-	-	55.9	3.84 (3H, *s*)	-	-
4–OCH_3	-	-	55.9	3.86 (3H, *s*)			54.4	3.78 (3H, *s*)
–COOH		14.22 (1H, *brs*)						

[1] T. T. Nguyen, Q. C. T. Nguyen, V. H. Mai, Q. T. Phan, P. Q. Do, T. D. Nguyen, P. D. Nguyen, T. T. T.Nguyen, T. D. Le, T. X. T. Dai, K. Kamei and K. Kanaori. A new hopane derivative from the lichen *Dirinaria applanata*, *Nat. Prod. Res.*, 2019, 1-5.

[2] J. Sichaem, H. H. Nguyen and T. H. Duong. Hopane-6*α*,16*α*,22-triol: A New Hopane Triterpenoid from the Lichen *Parmotrema sancti-angelii*, *Nat. Prod. Commun.* 2019, 14

[3] L. F. G. Brandão, G. B. Alcantara, M. F. C. Matos, D. Bogo, D. Dos Santos Freitas, N. M. Oyama and N. K. Honda. Cytotoxic evaluation of phenolic compounds from lichens against melanoma cells, *Chem. Pharm. Bull.* 2013, **61**, 176-183.

[4] P. Kumboonma, T. Senawong, S. Saenglee, C. Yenjai and C. Phaosiri (2018). New histone deacetylase inhibitors from the twigs of *Melanorrhoea usitata, Med. Chem. Res.* 2018, **27**, 2004-2015.

4. Scanned spectra of all compounds

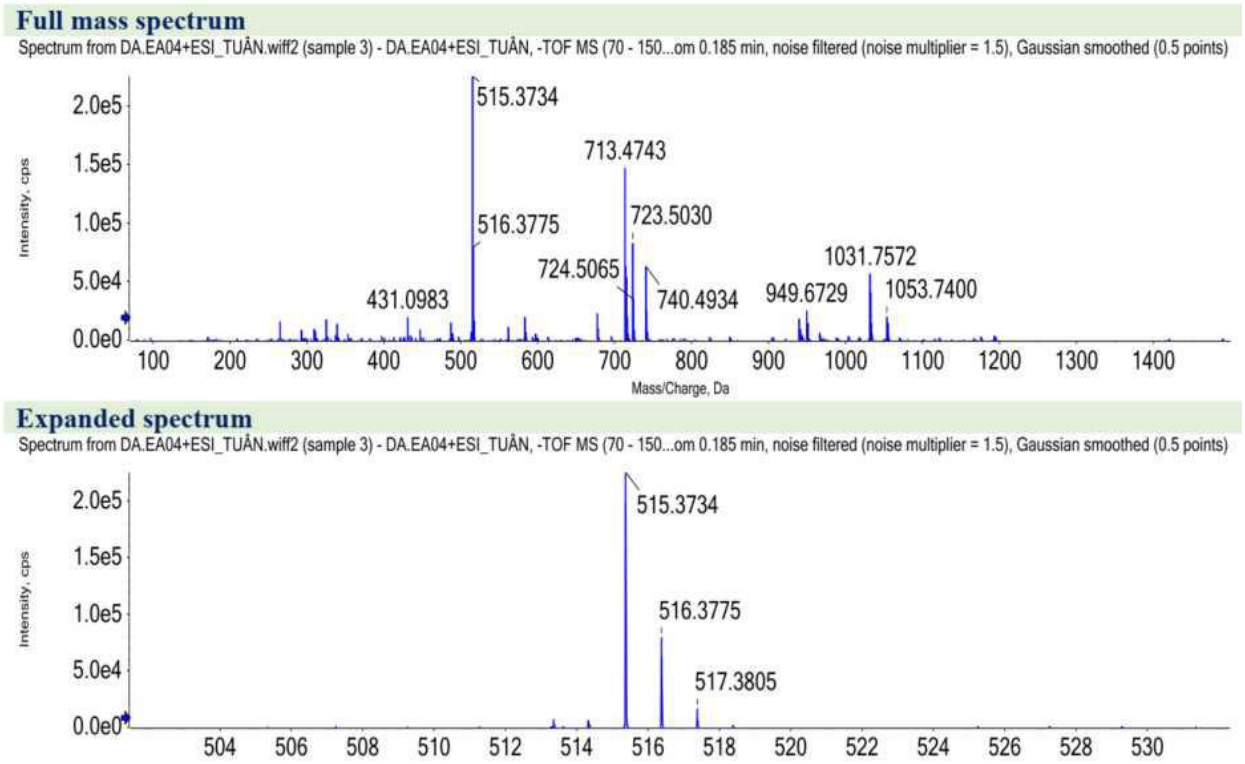

Formular (M)	Ion formula	m/z	Calcd m/z	Diff (ppm)
$C_{32}H_{52}O_5$	$C_{32}H_{51}O_5$	515.3734	515.3736	0.39 ppm

Figure A3: (–)HR-ESI-MS of compound **1**

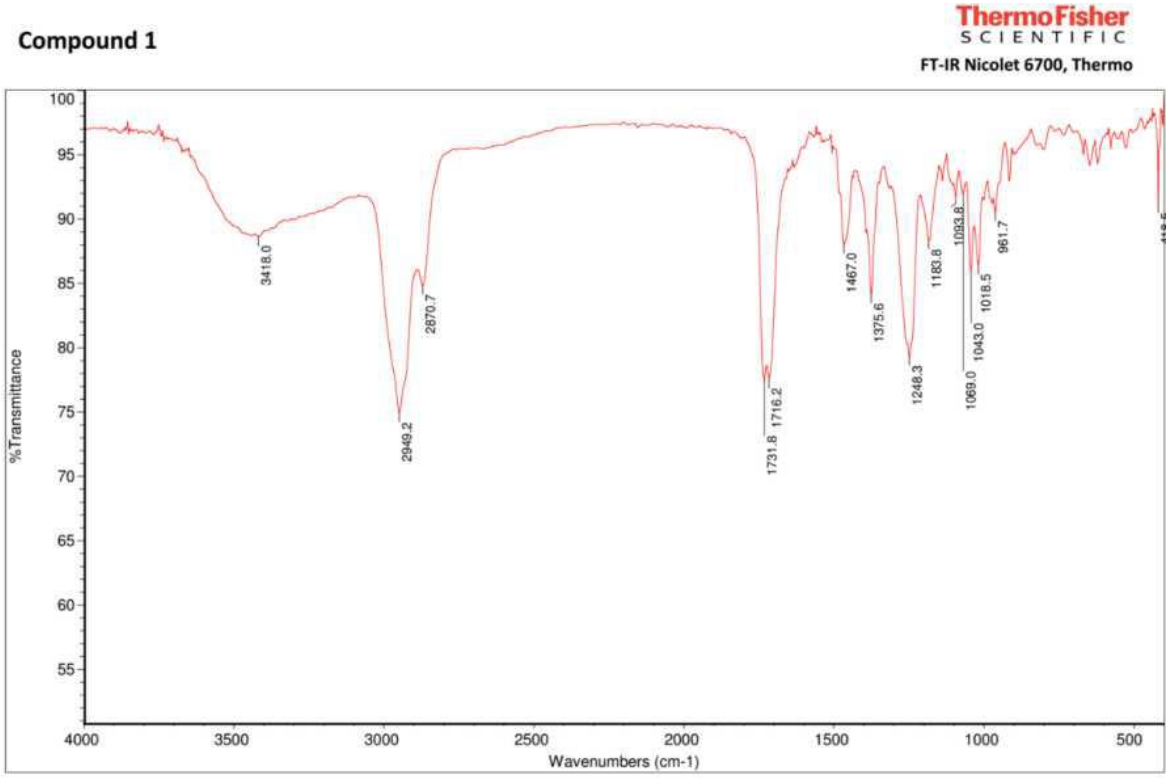

Figure A4: FT-IR of compound **1**

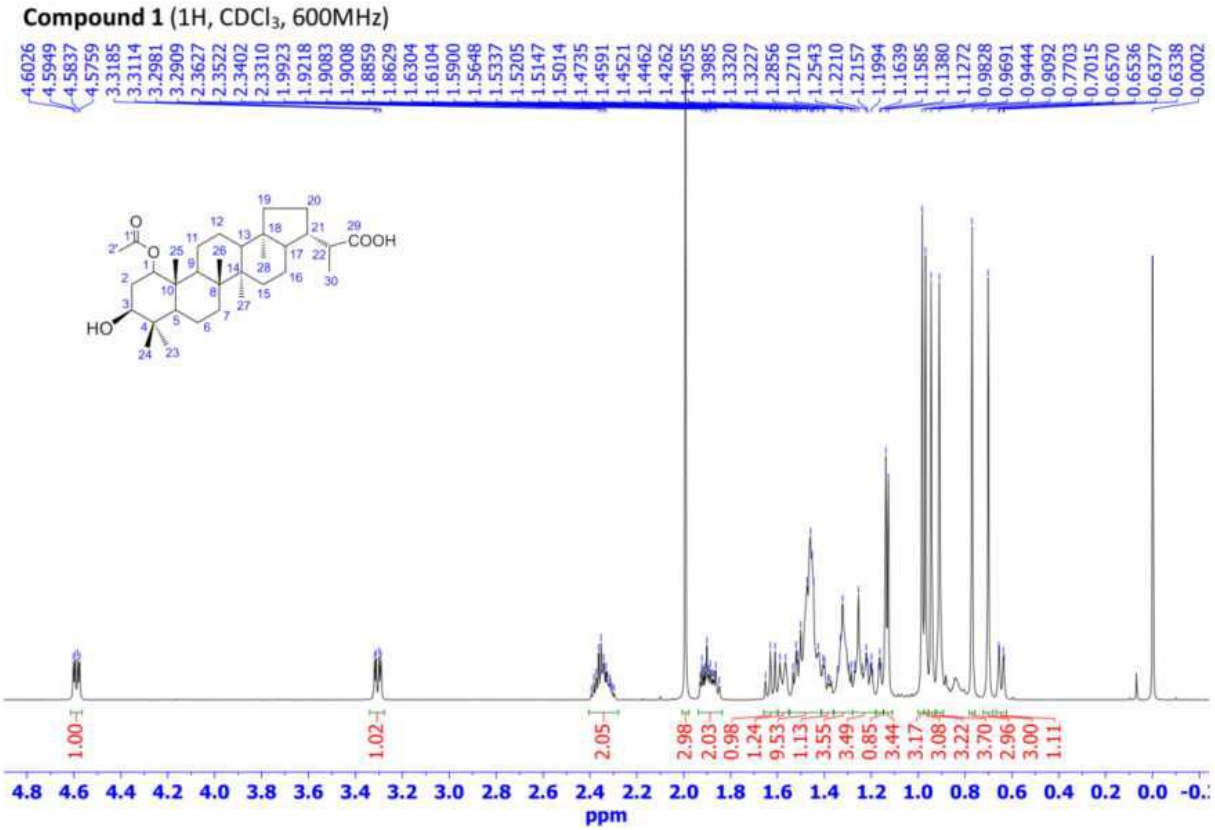

Figure A5: Full ^{1}H-NMR of compound **1**

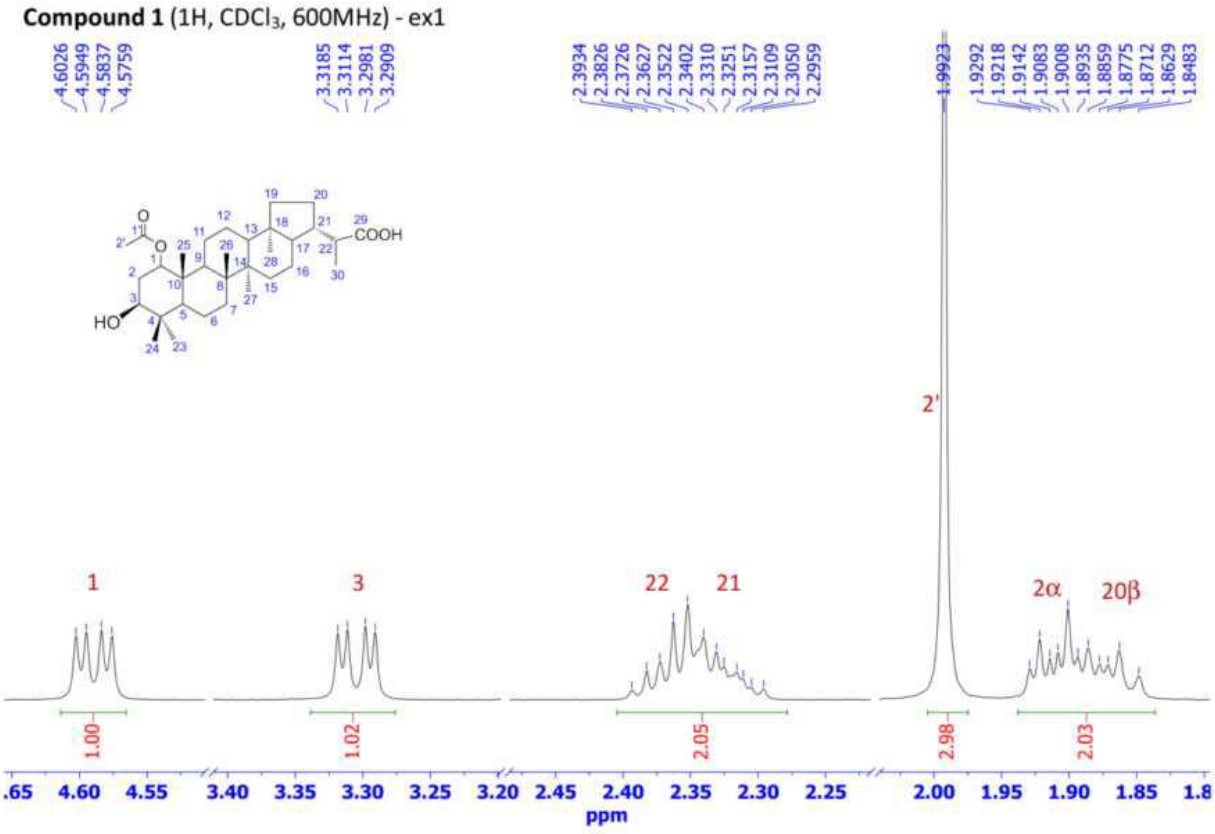

Figure A6: Extended ^{1}H-NMR of compound **1**

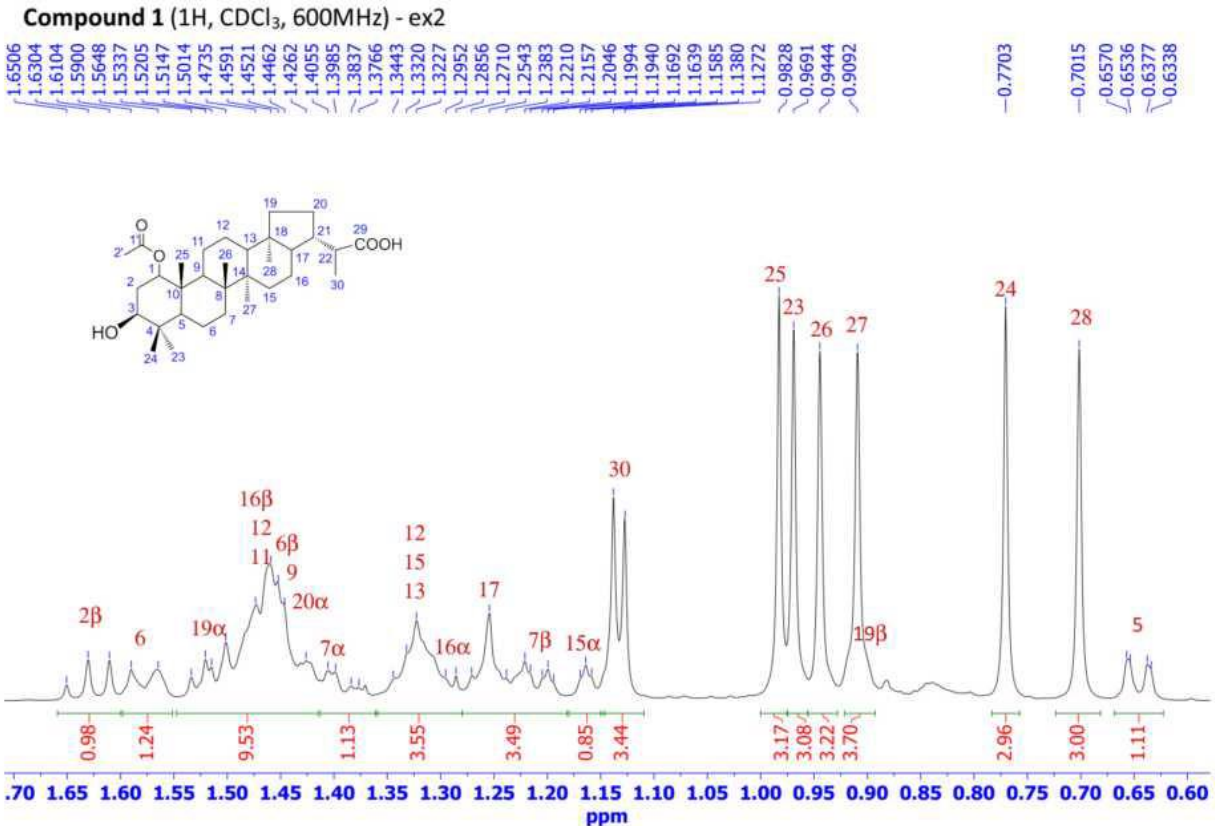

Figure A7: Extended ^{1}H-NMR of compound **1**

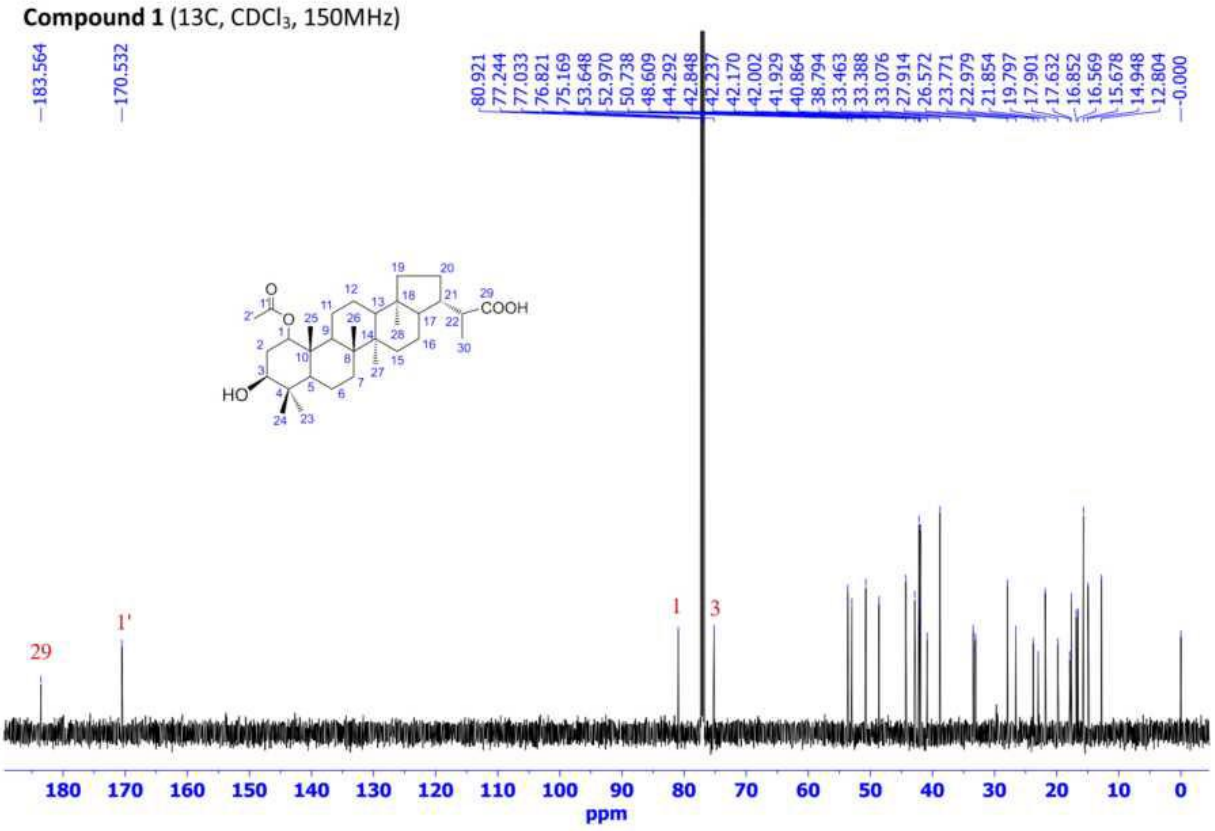

Figure A8: Full ^{13}C-NMR of compound **1**

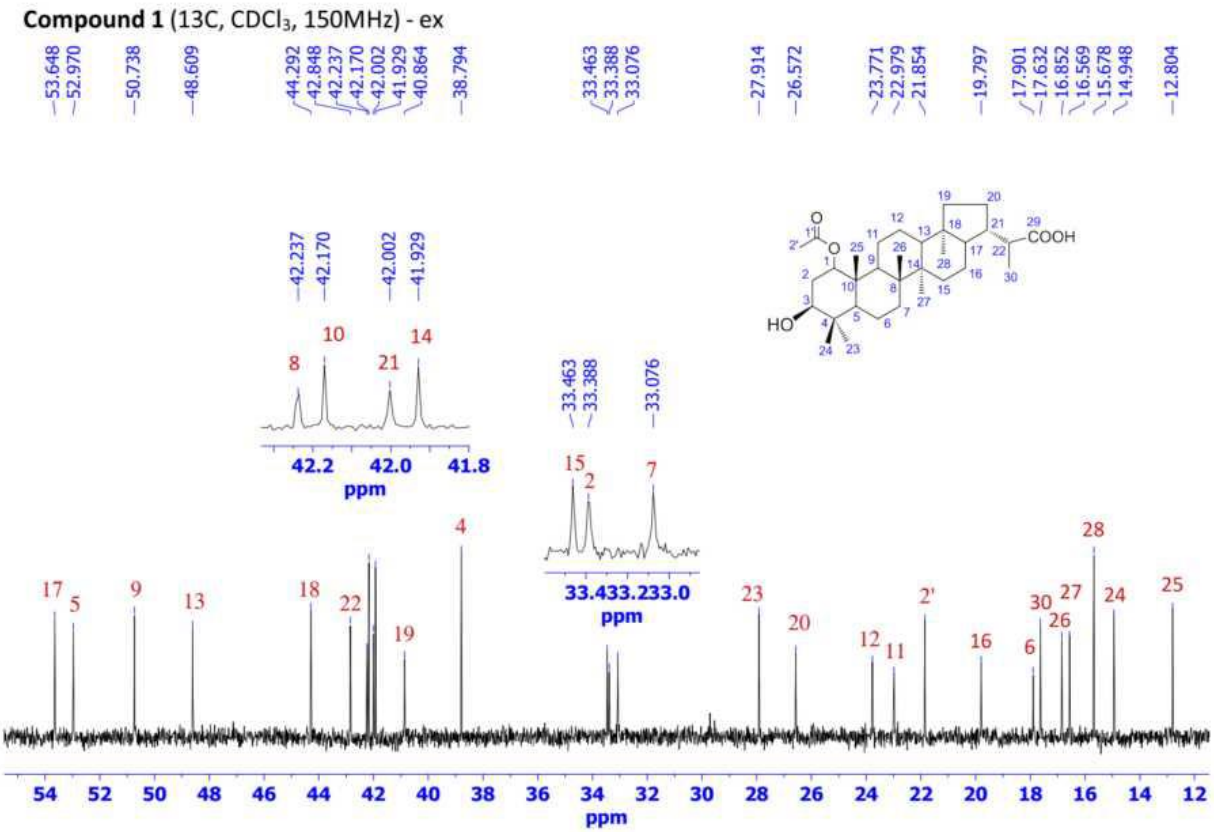

Figure A9: Extended ^{13}C-NMR of compound **1**

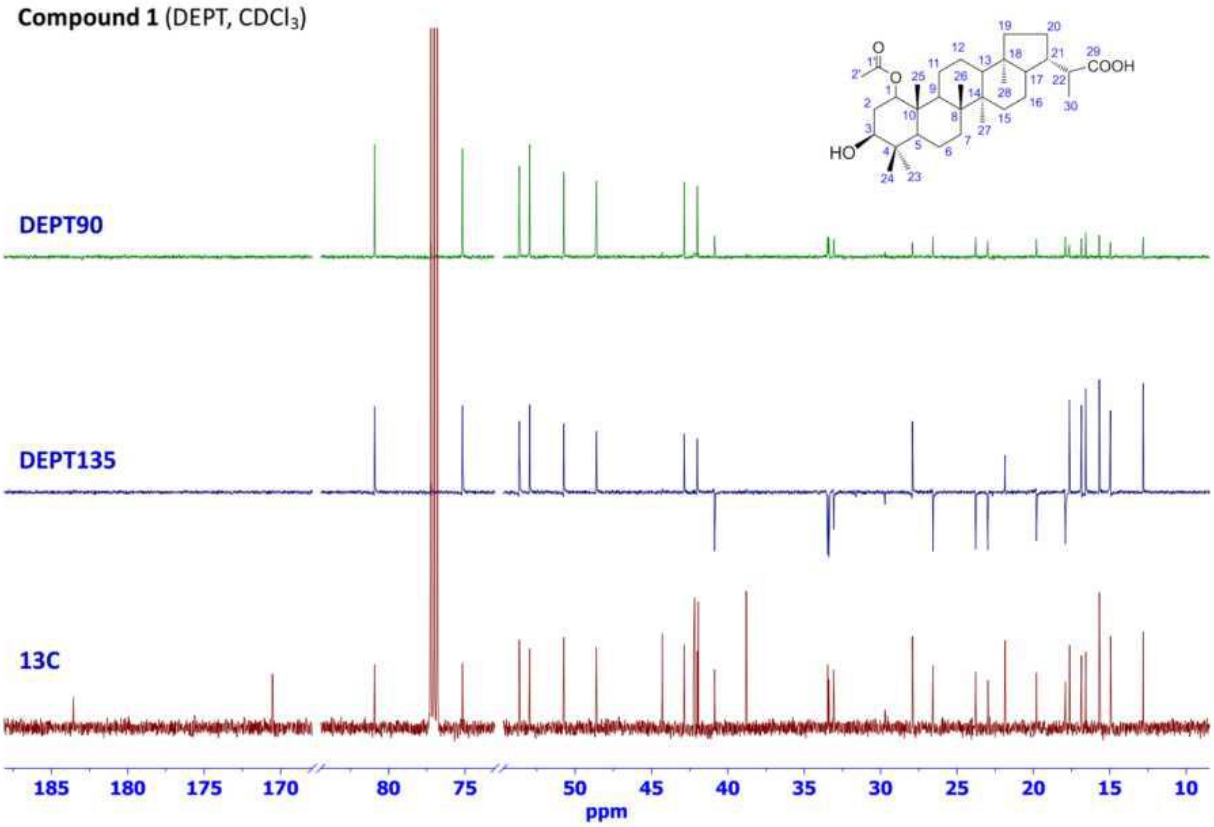

Figure A10: Full DEPT of compound **1**

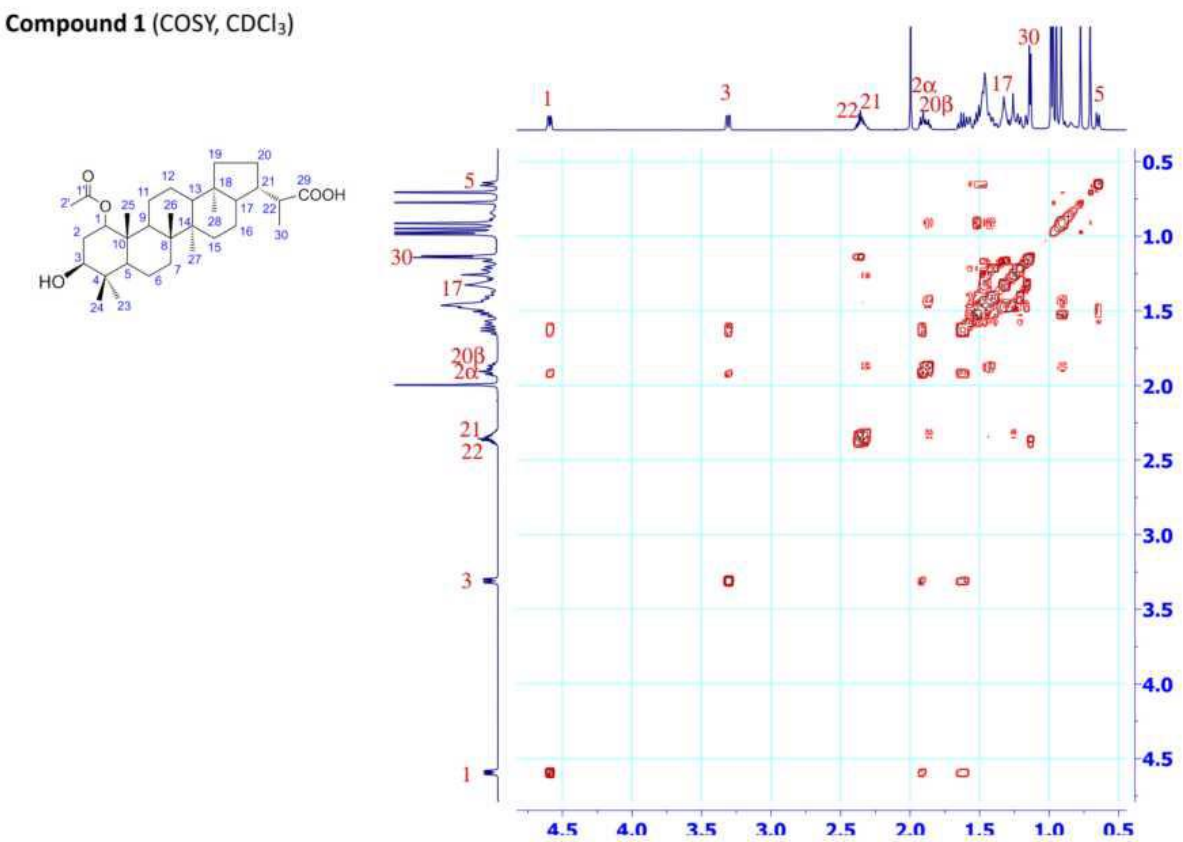

Figure A11: Full COSY of compound **1**

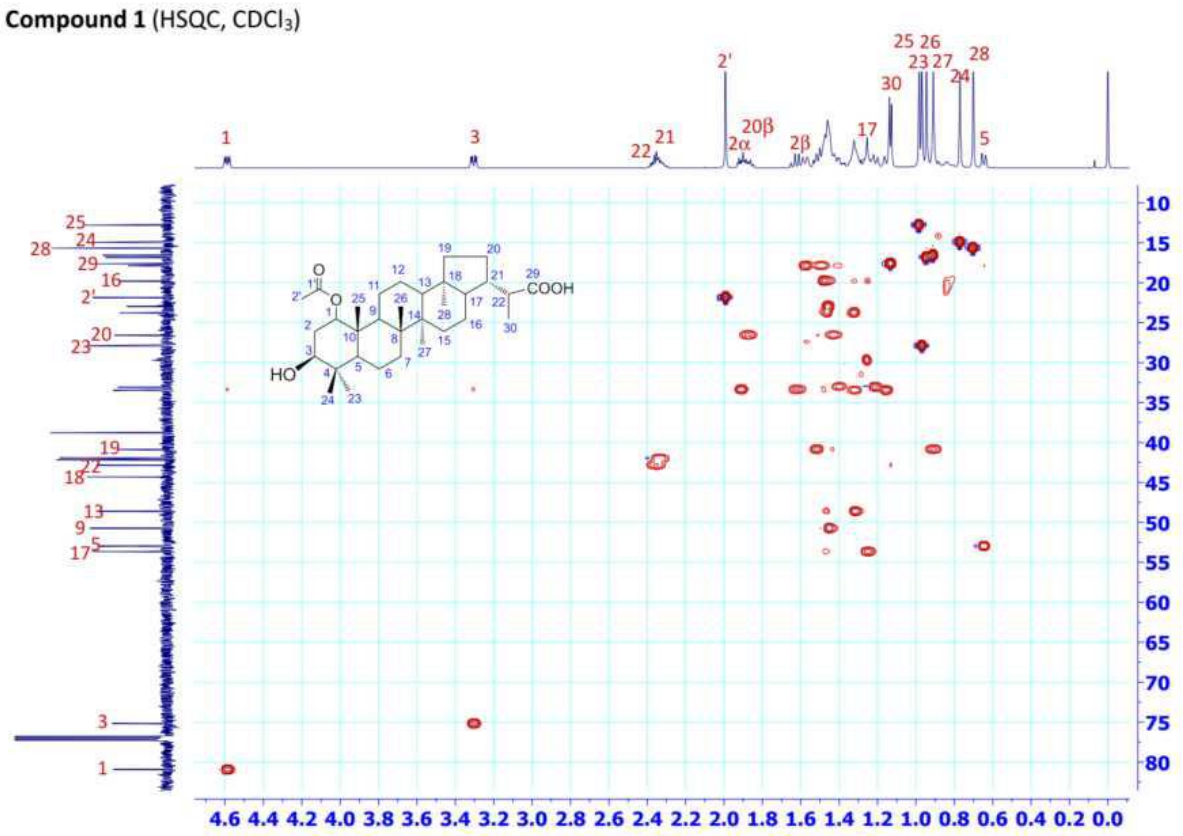

Figure A12: Full HSQC of compound **1**

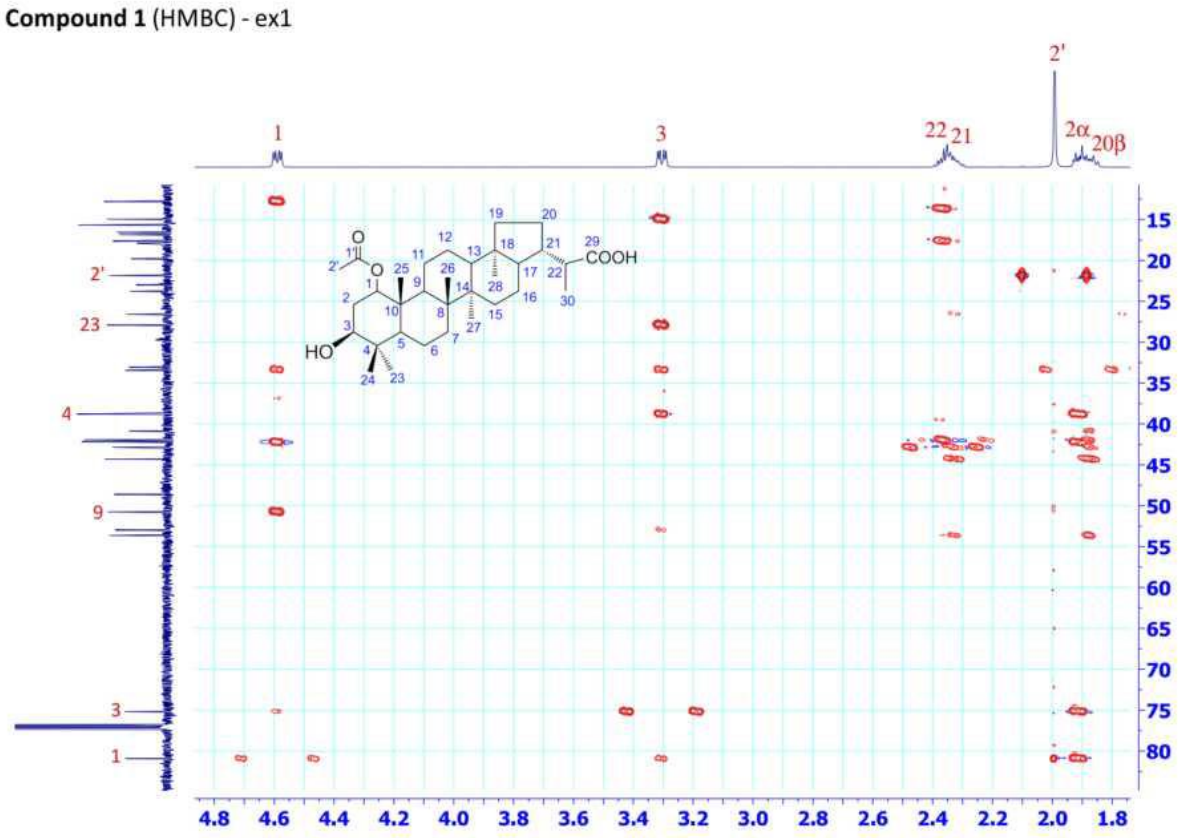

Figure A13: Extended HMBC of compound **1**

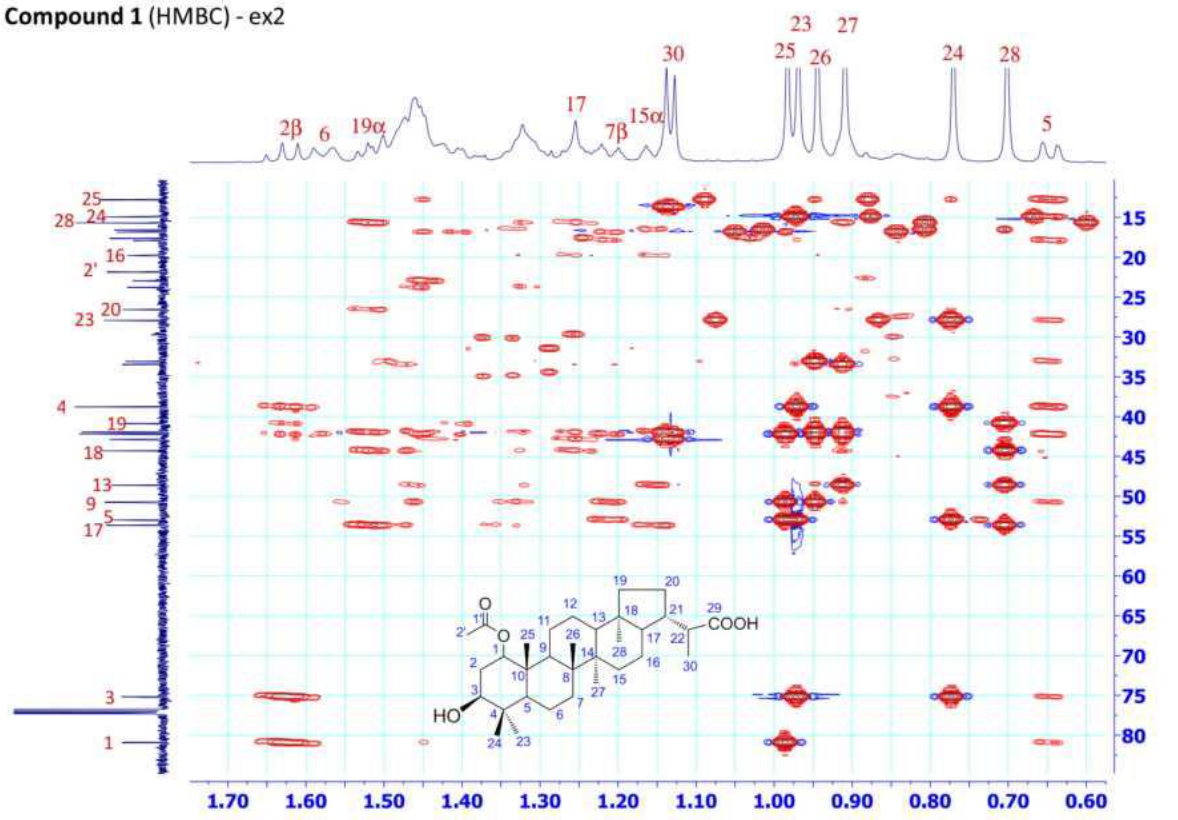

Figure A14: Extended HMBC of compound **1**

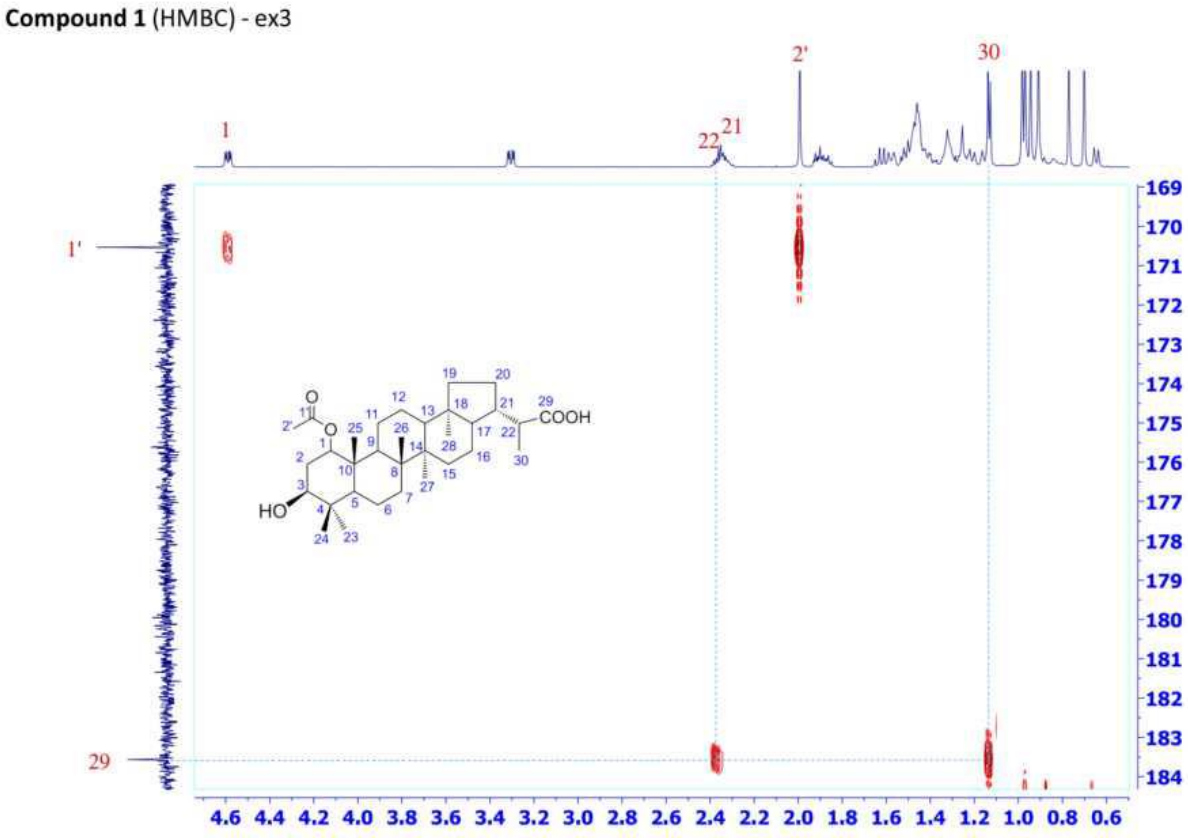

Figure A15: Extended HMBC of compound **1**

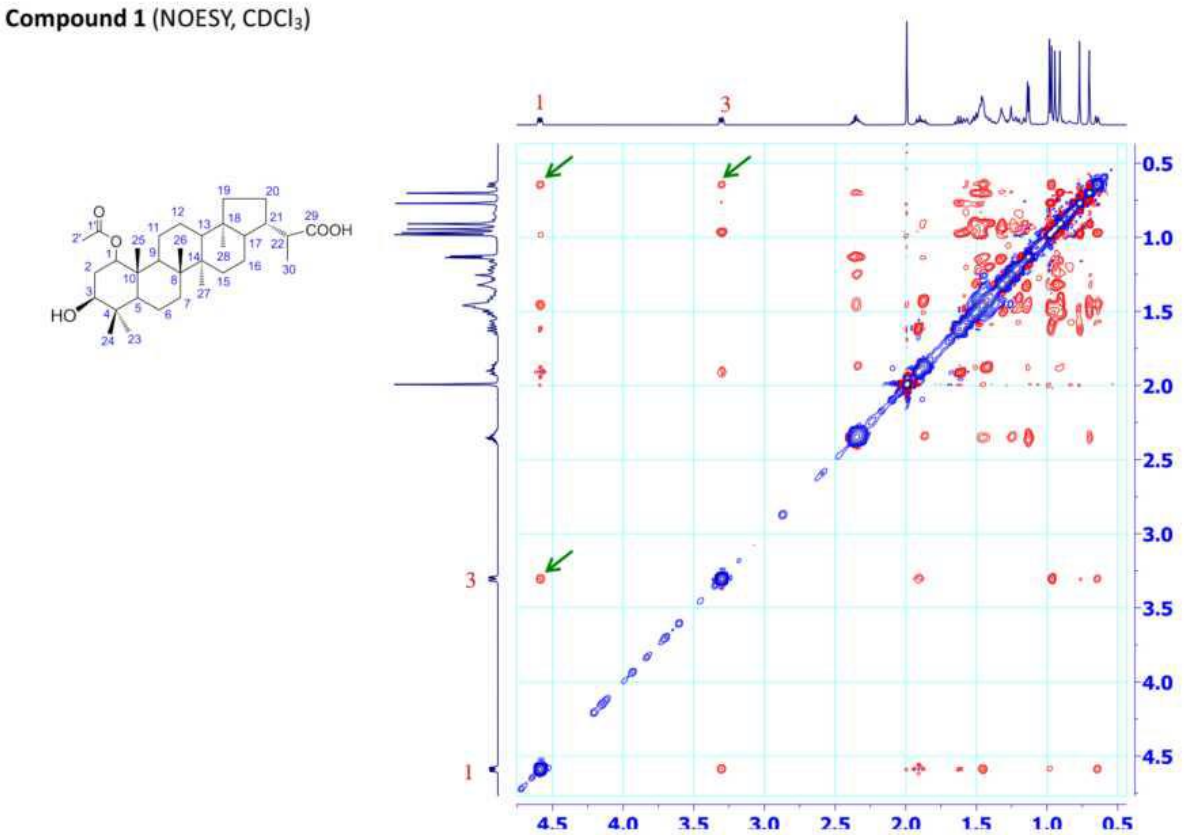

Figure A16: Full NOESY of compound **1**

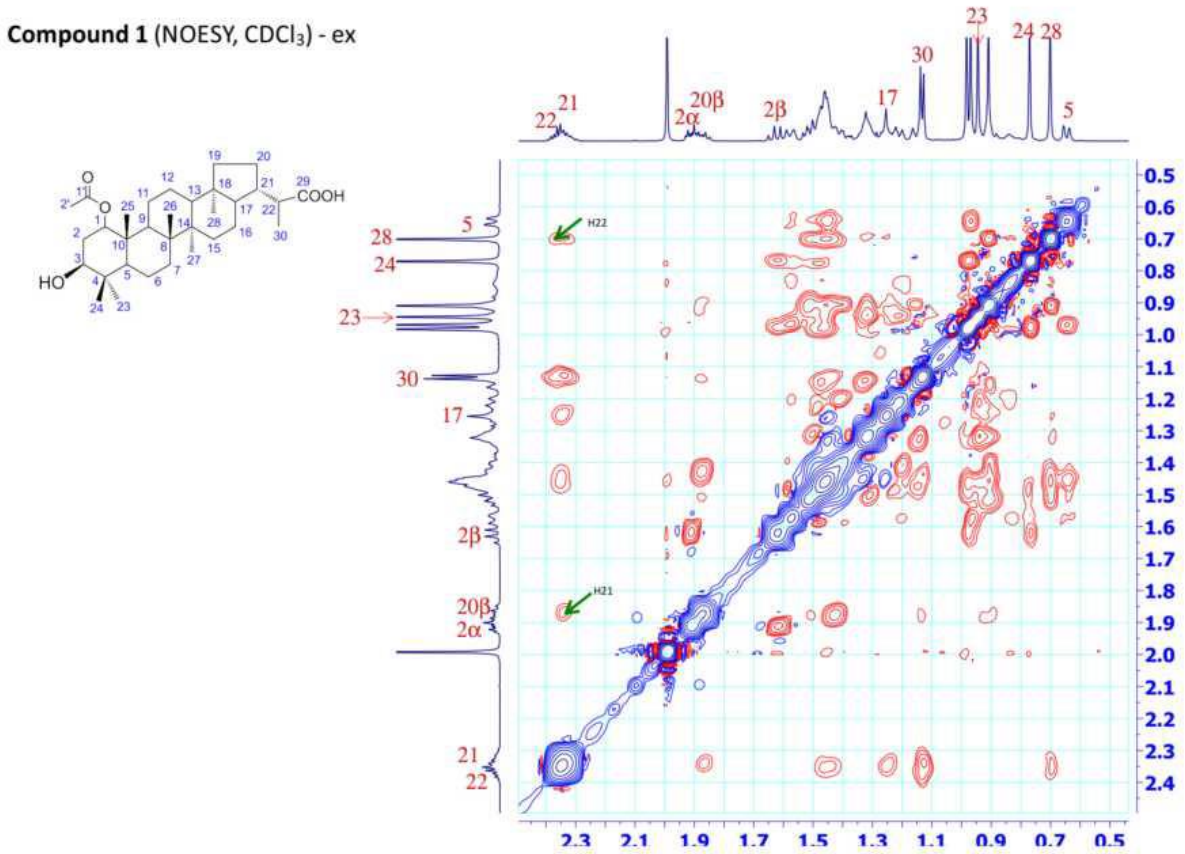

Figure A17: Extended NOESY of compound **1**

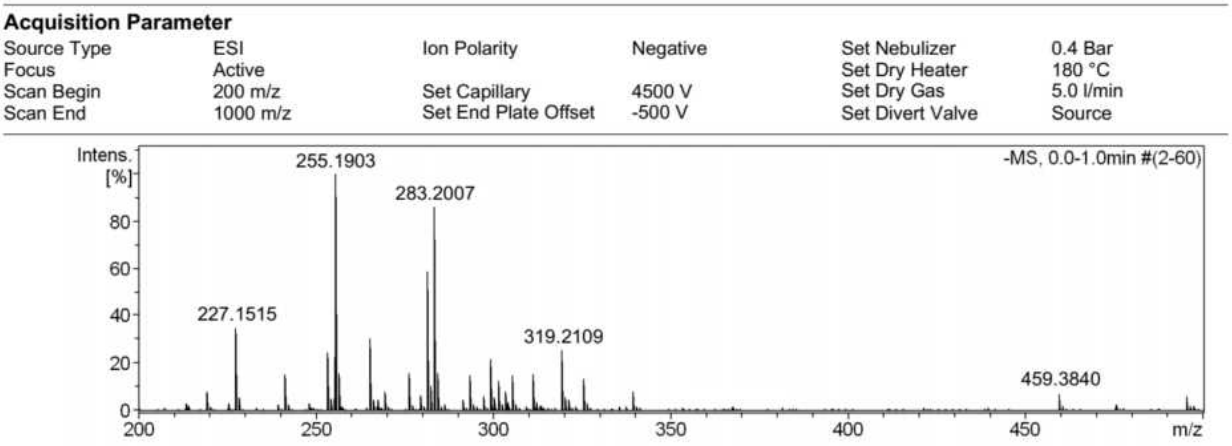

Formular (M)	Ion formula	m/z	Calcd m/z	Diff (ppm)
$C_{30}H_{52}O_3$	$C_{30}H_{51}O_3$	459.3840	459.3843	0.65

Figure A8. (–)HR-ESI-MS of compound **2**

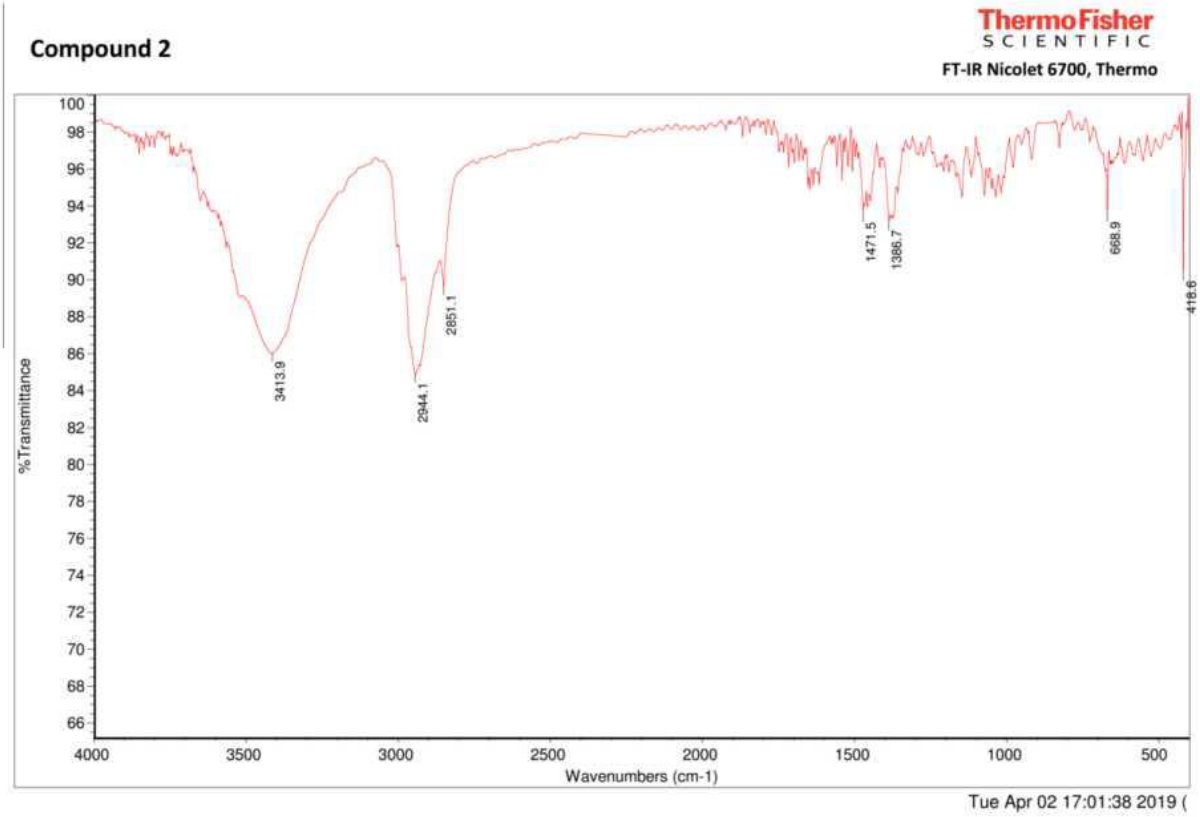

Figure A19: FT-IR of compound **2**

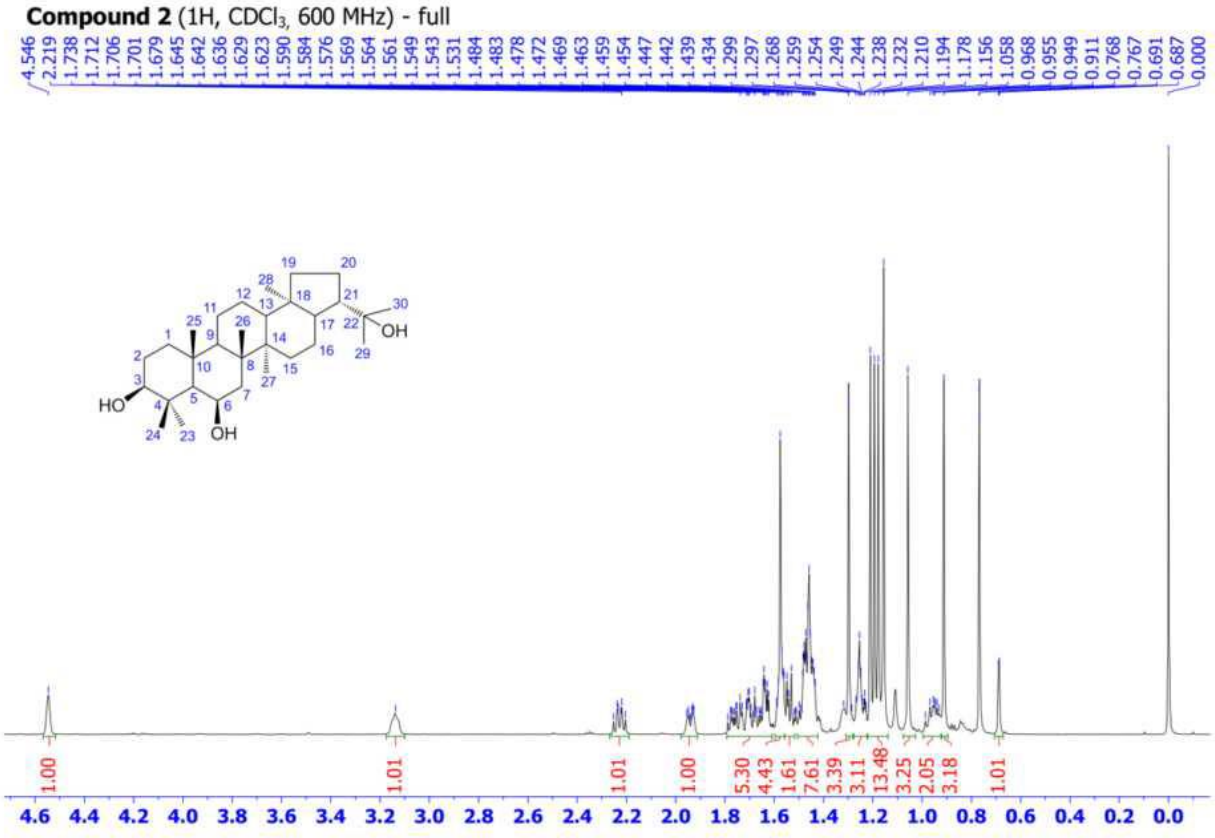

Figure S20: Full ^{1}H-NMR of compound **2**

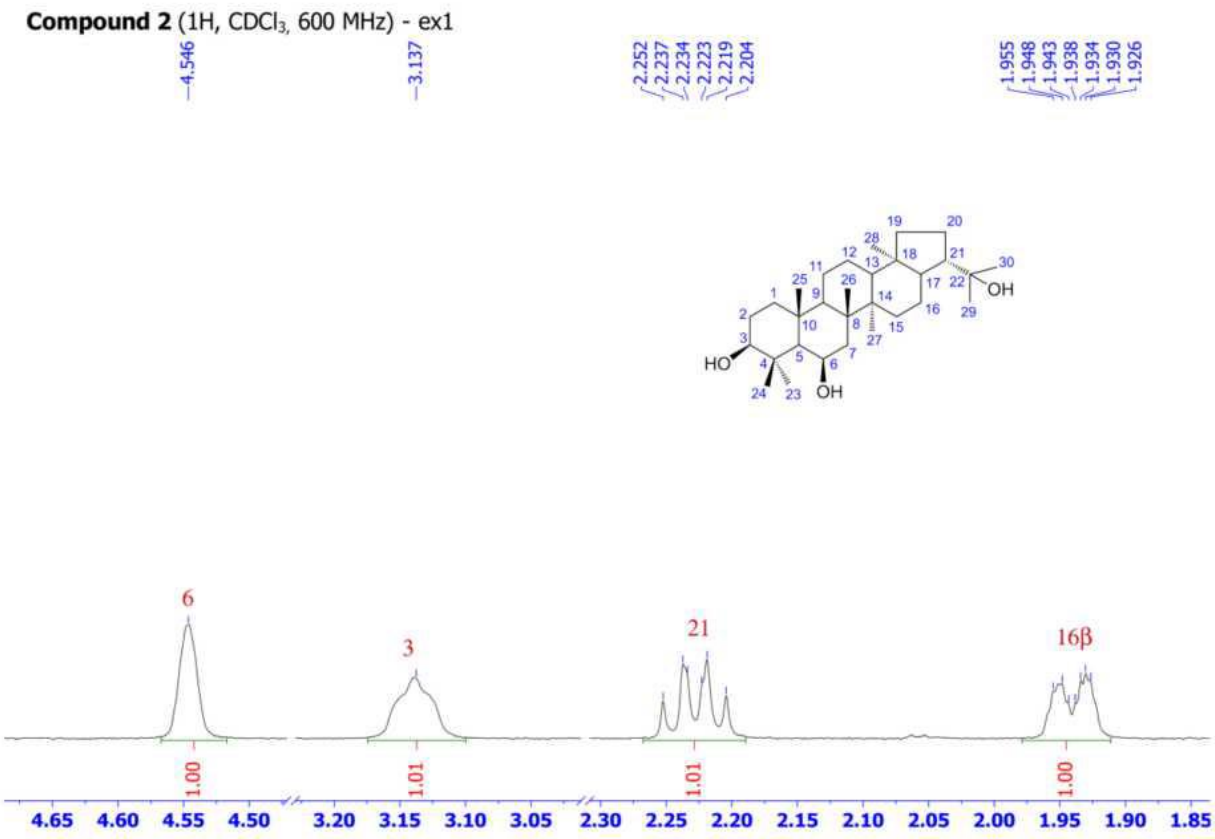

Figure A21: Extended [1]H-NMR of compound **2**

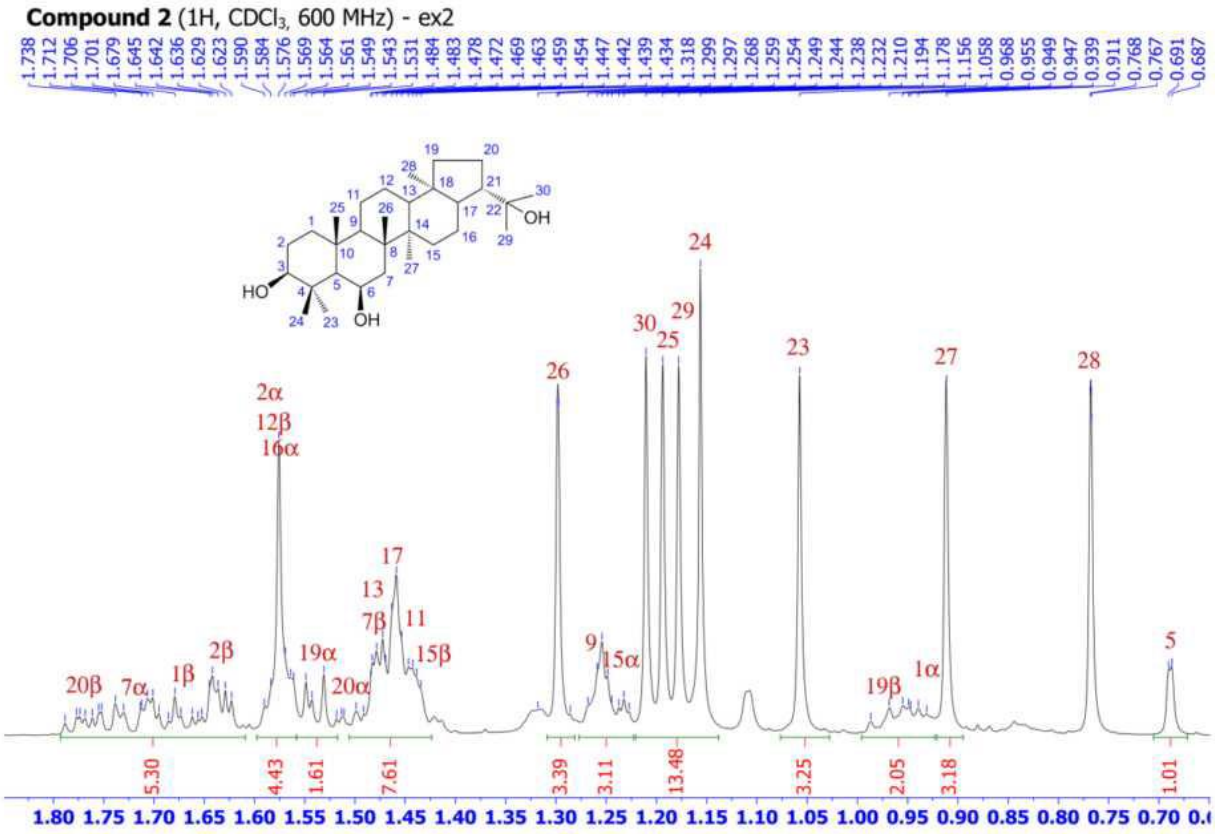

Figure A22: Extended [1]H-NMR of compound **2**

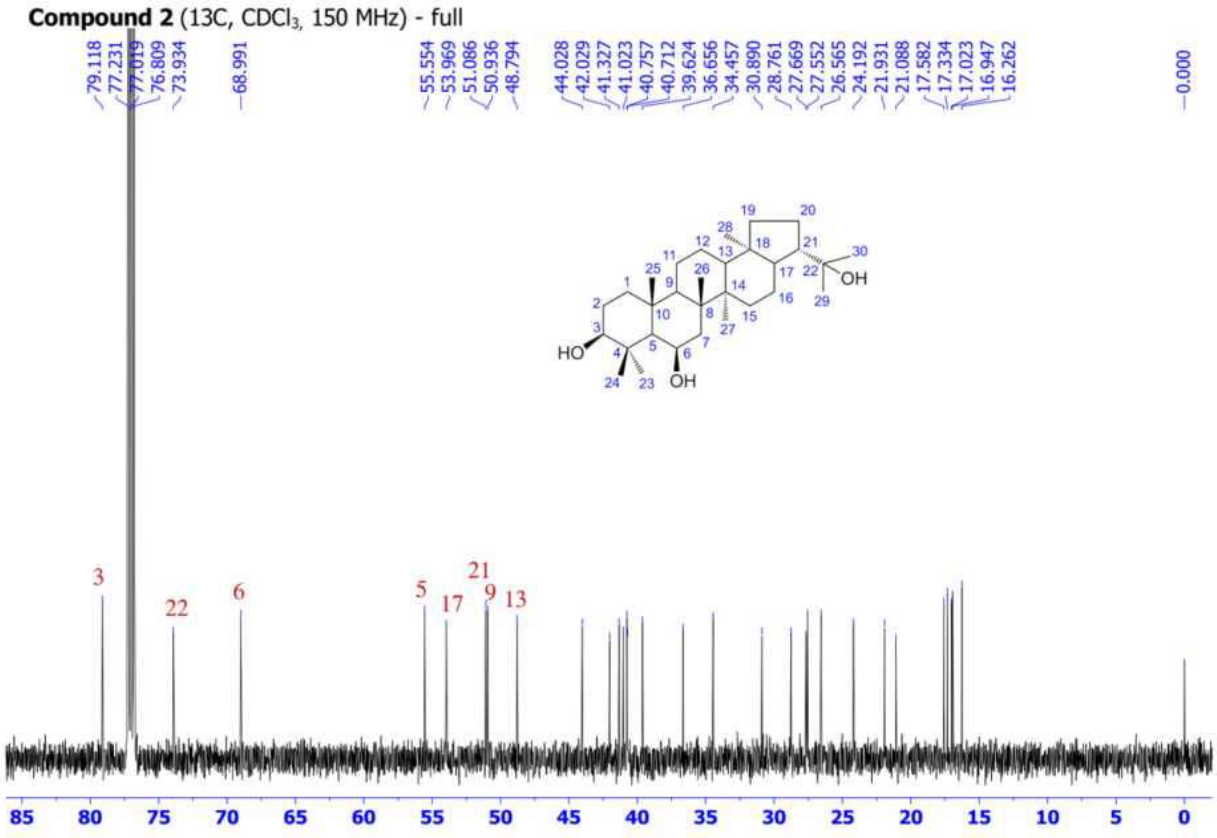

Figure A23: Full ^{13}C-NMR of compound **2**

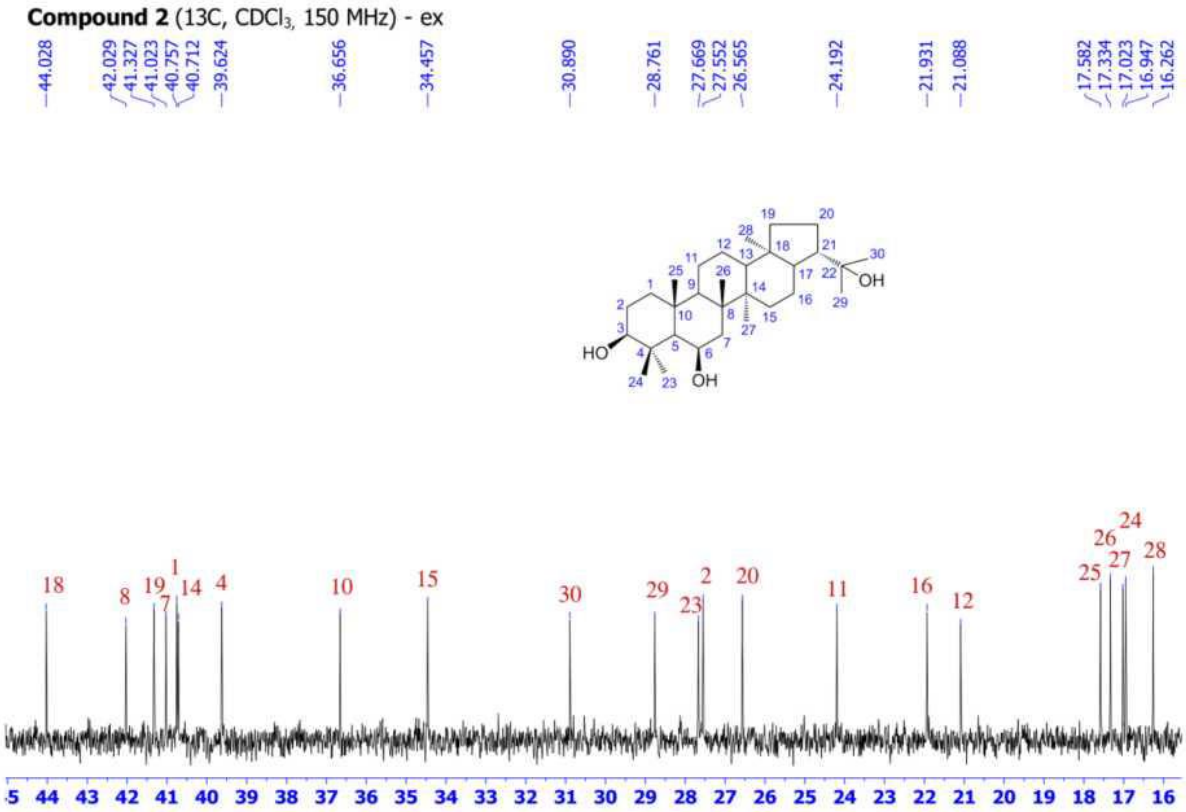

Figure A24: Extended ^{13}C-NMR of compound **2**

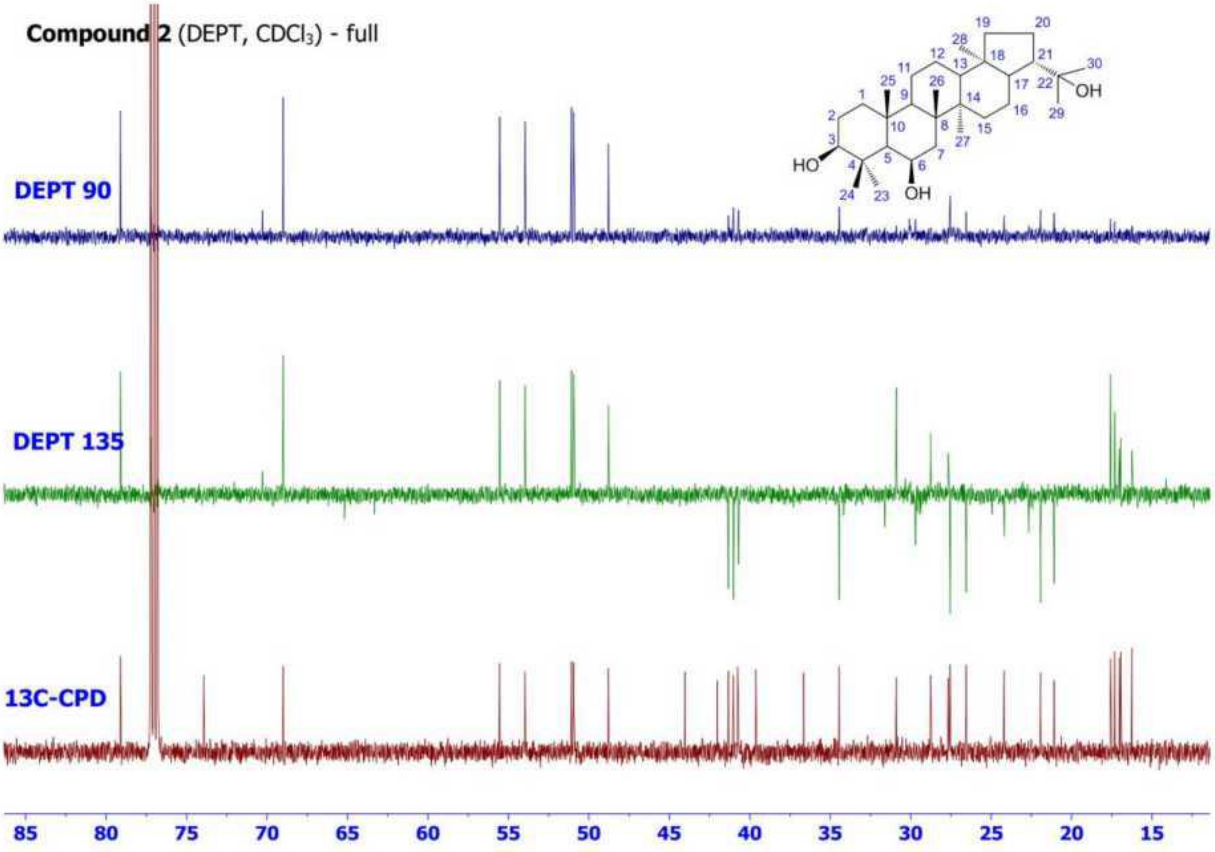

Figure A25: Full DEPT of compound **2**

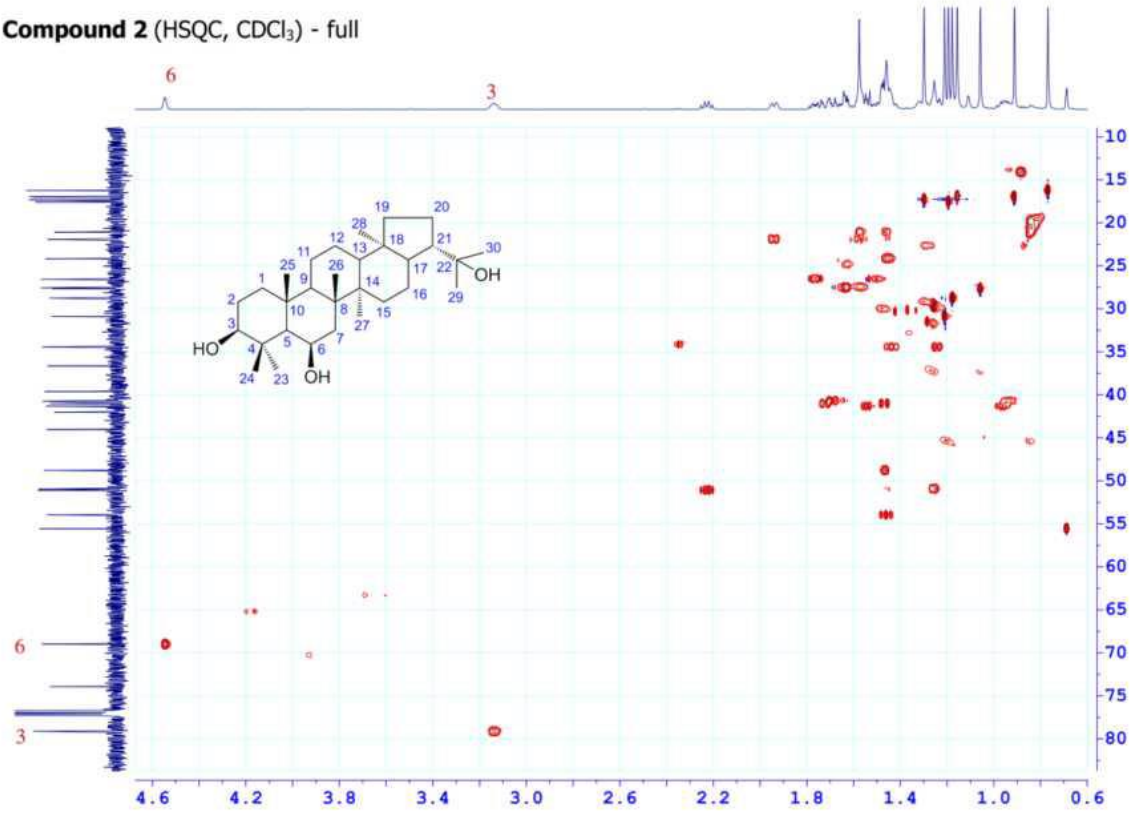

Figure A26: Full HSQC of compound **2**

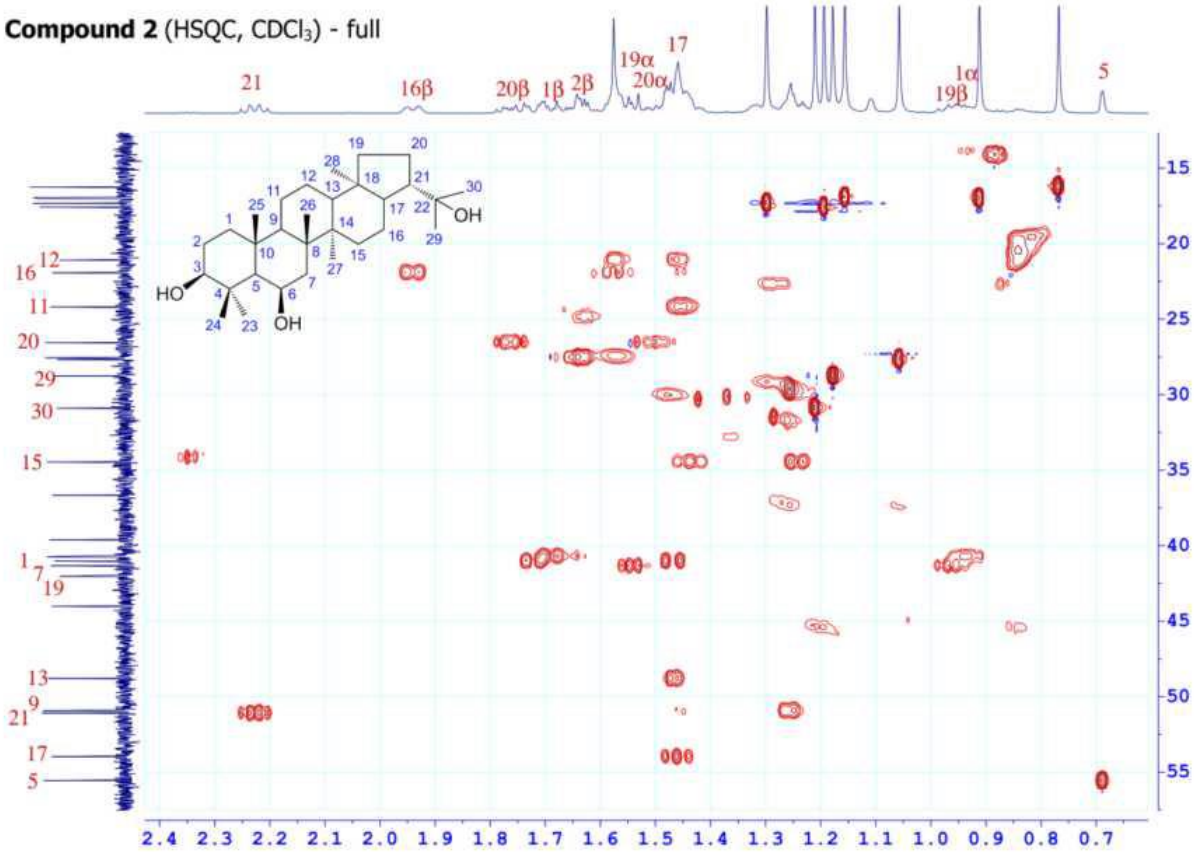

Figure A27: Extended HSQC of compound **2**

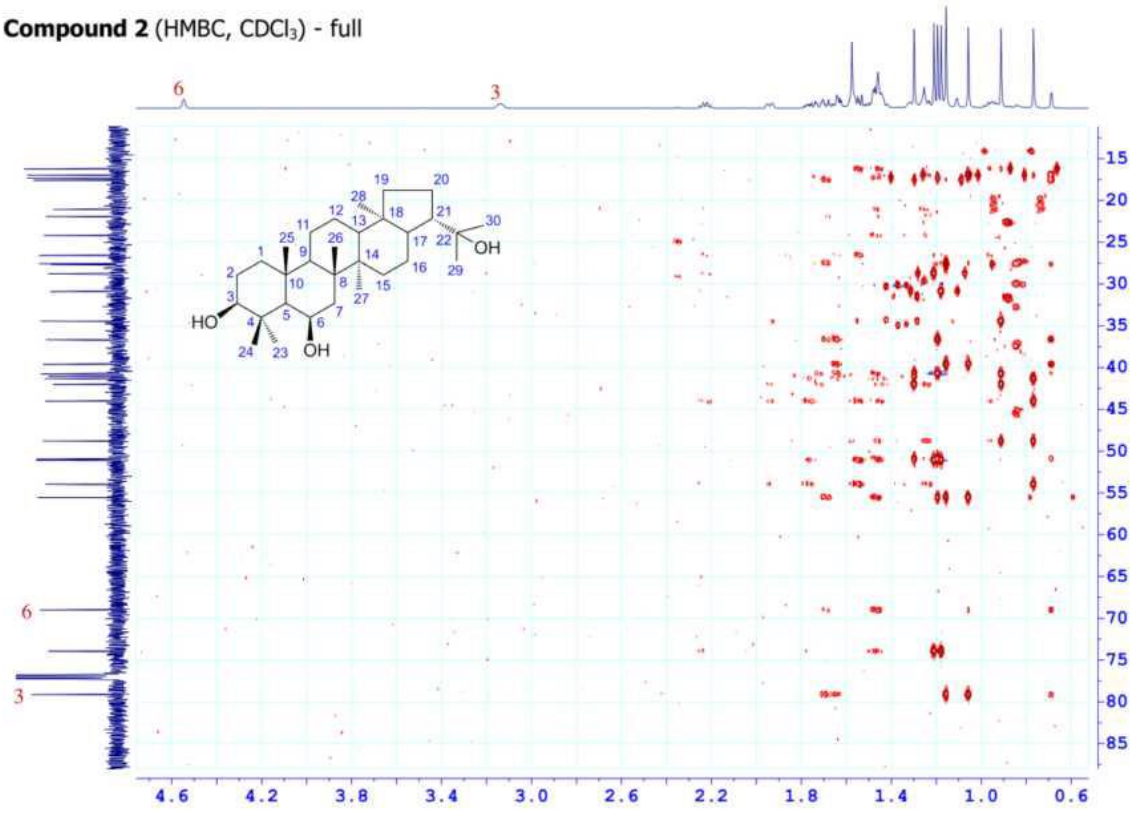

Figure A28: Full HMBC of compound **2**

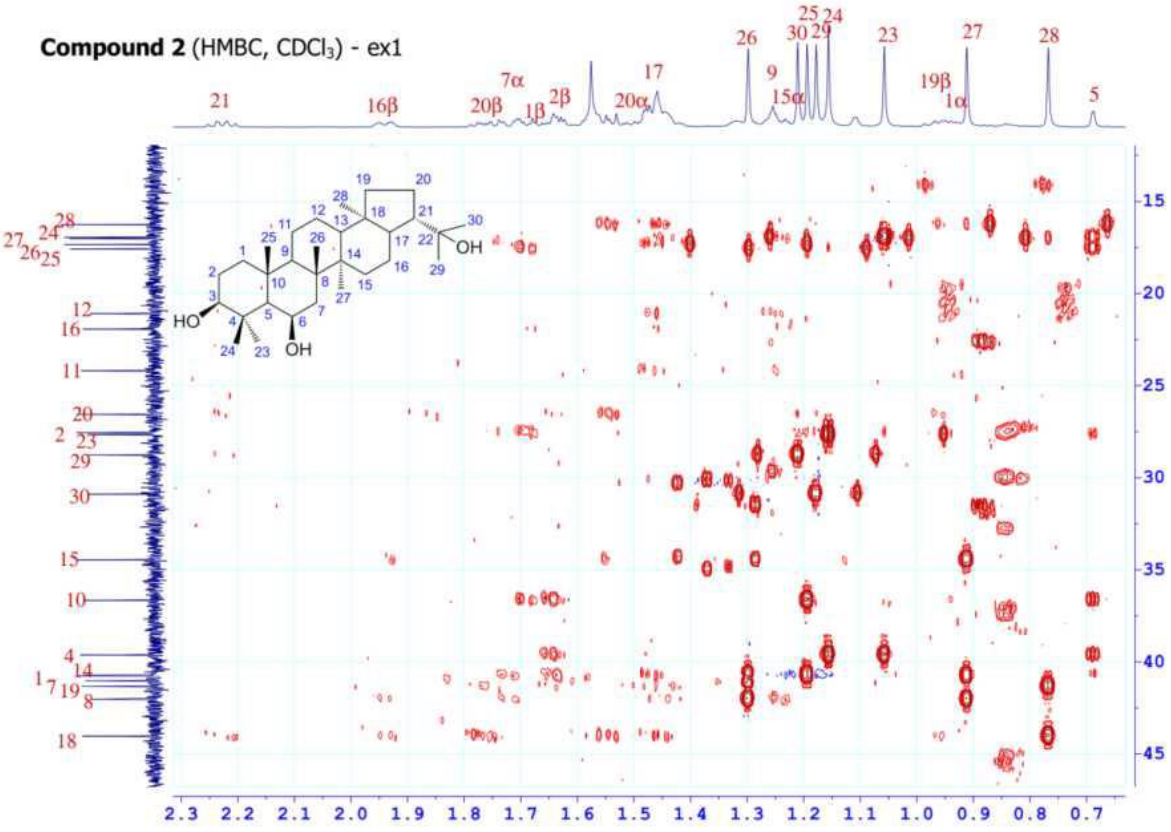

Figure A29: Extended HMBC of compound **2**

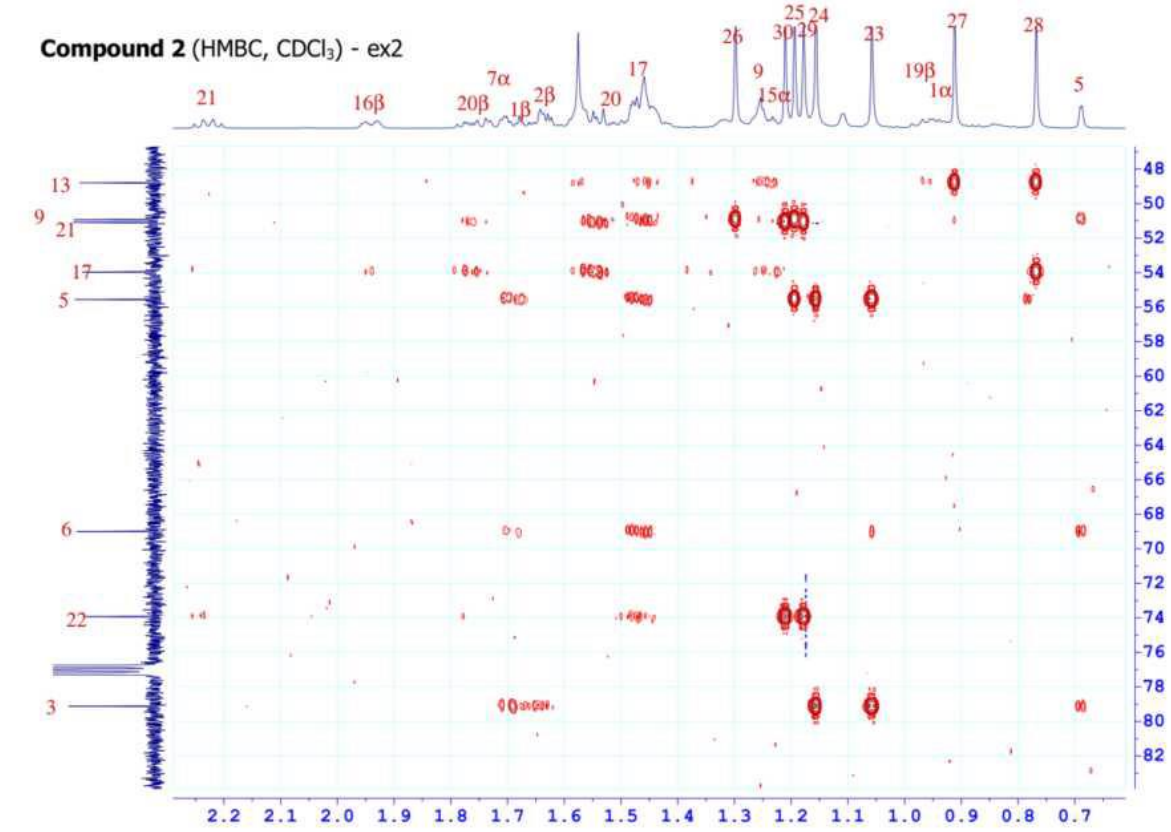

Figure A30: Extended HMBC of compound **2**

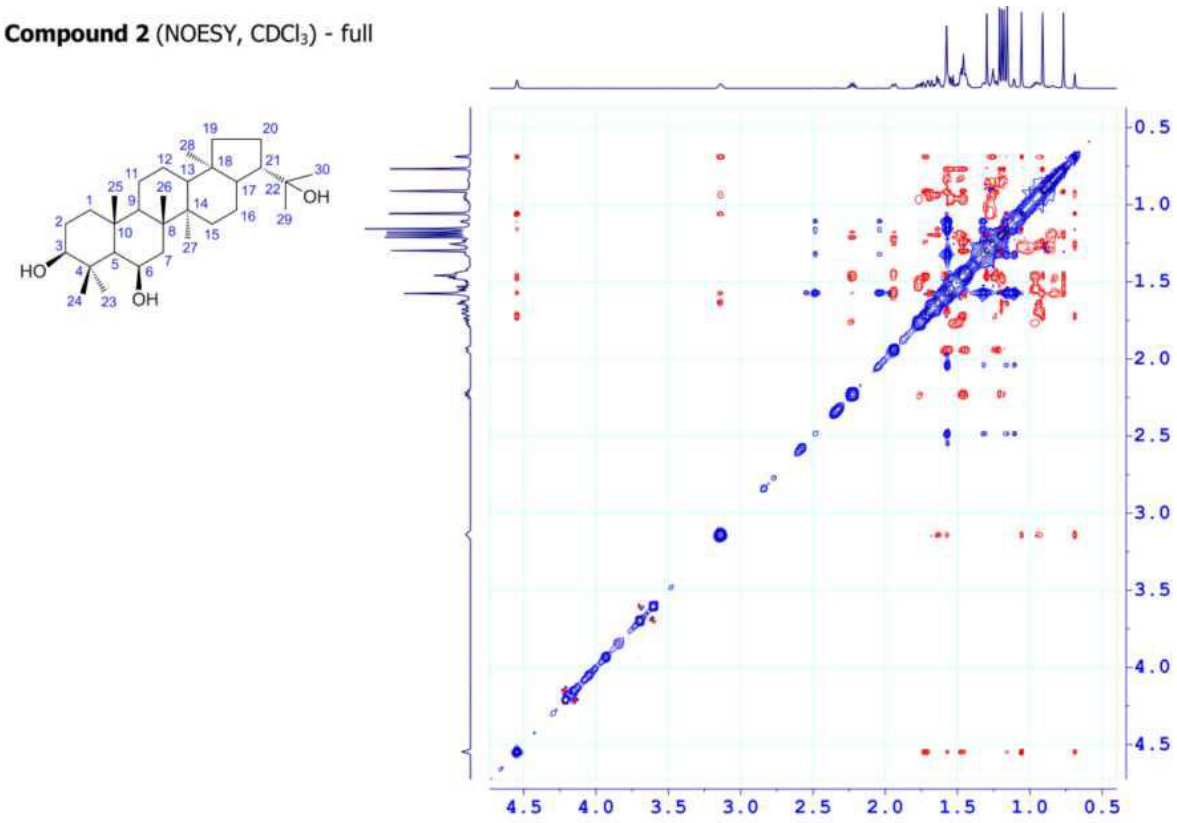

Figure A31: Full NOESY of compound **2**

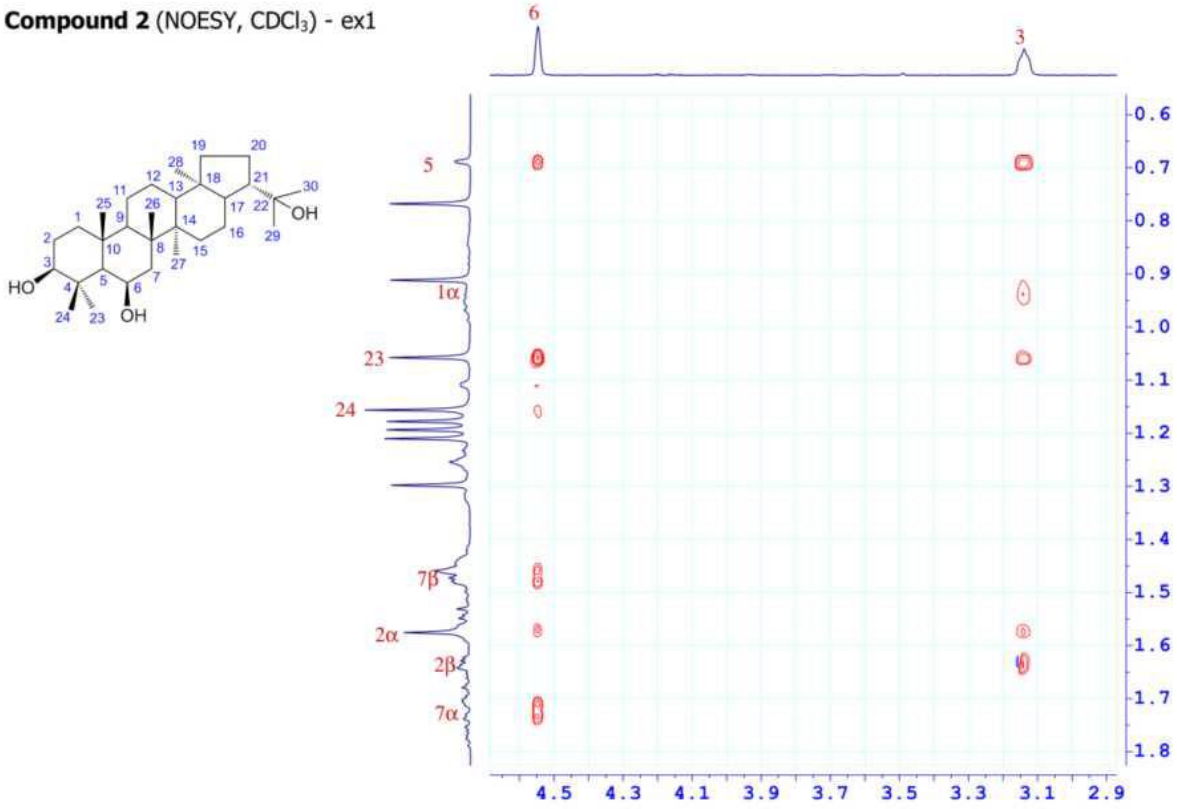

Figure A32: Extended NOESY of compound **2**

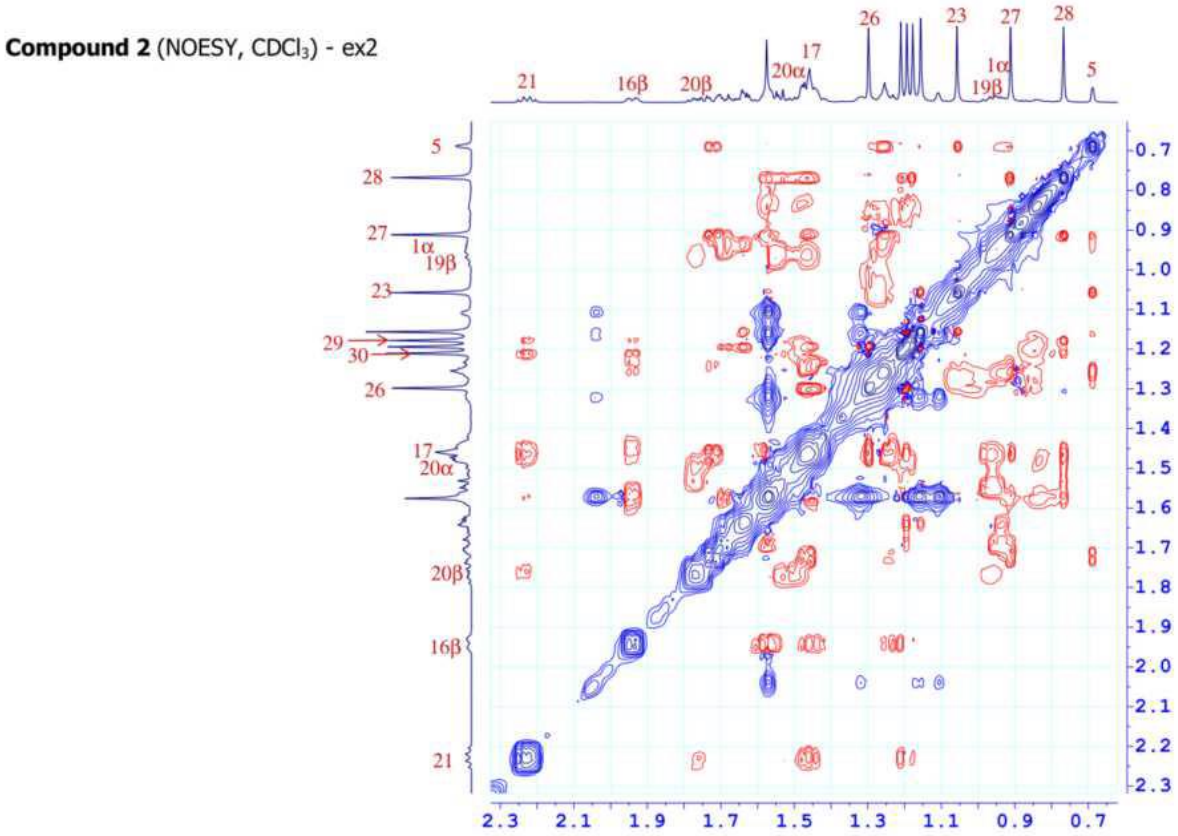

Figure A33: Extended NOESY of compound **2**

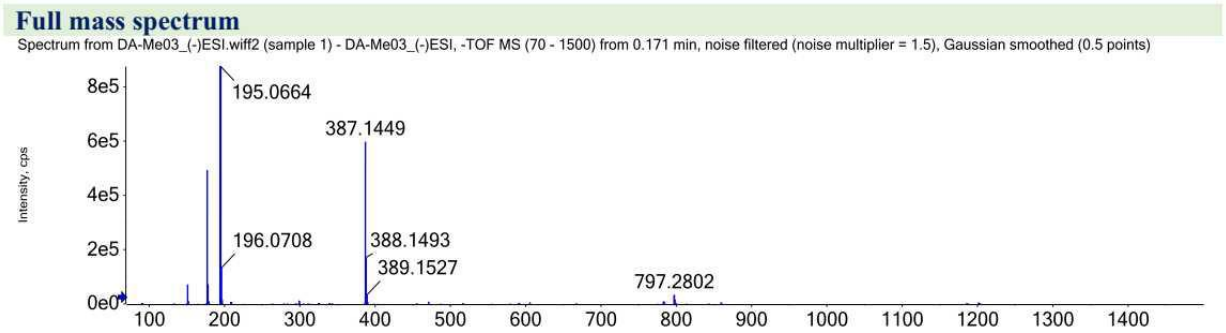

Formula (M)	Ion formula	*m/z*	Calcd *m/z*	Diff (ppm)
$C_{21}H_{24}O_7$	$C_{21}H_{23}O_7^-$	387.1449	387.1449	0

Figure A34. (–)HR-ESI-MS of compound **3**

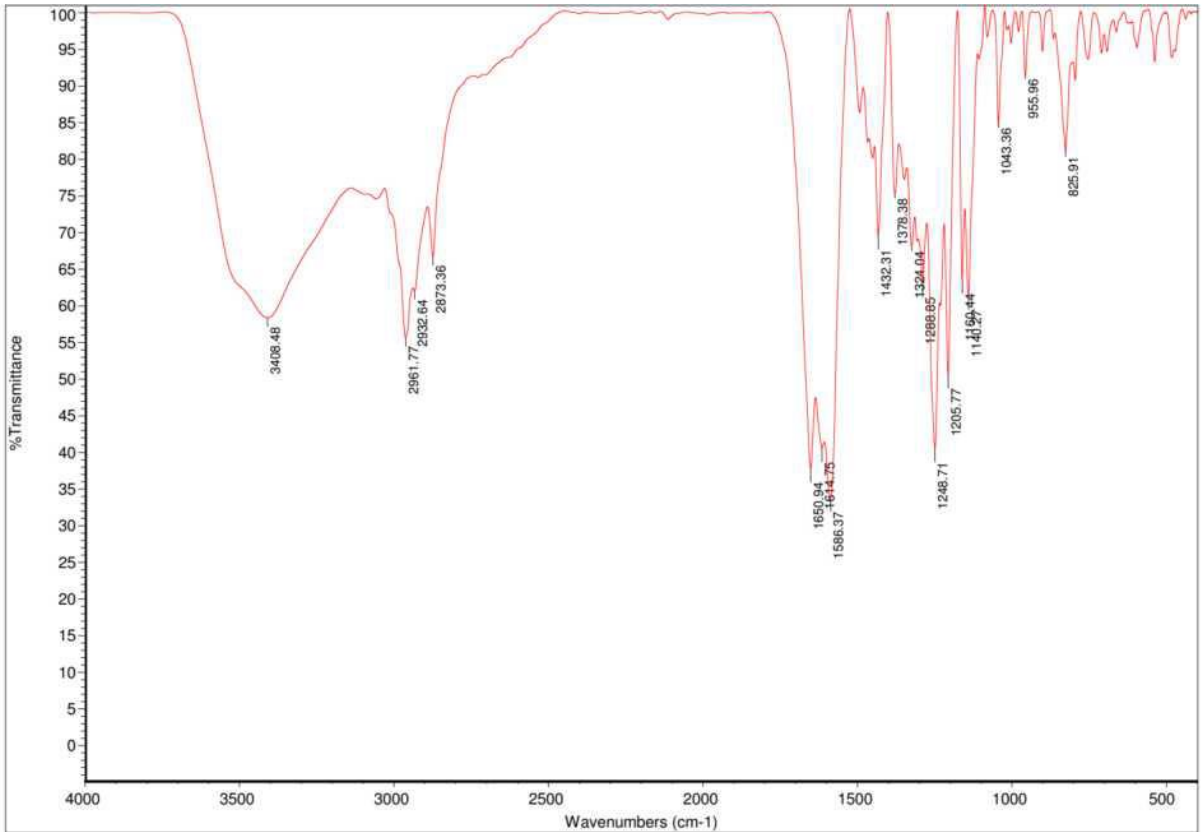

Figure A35: FT-IR of compound **3**

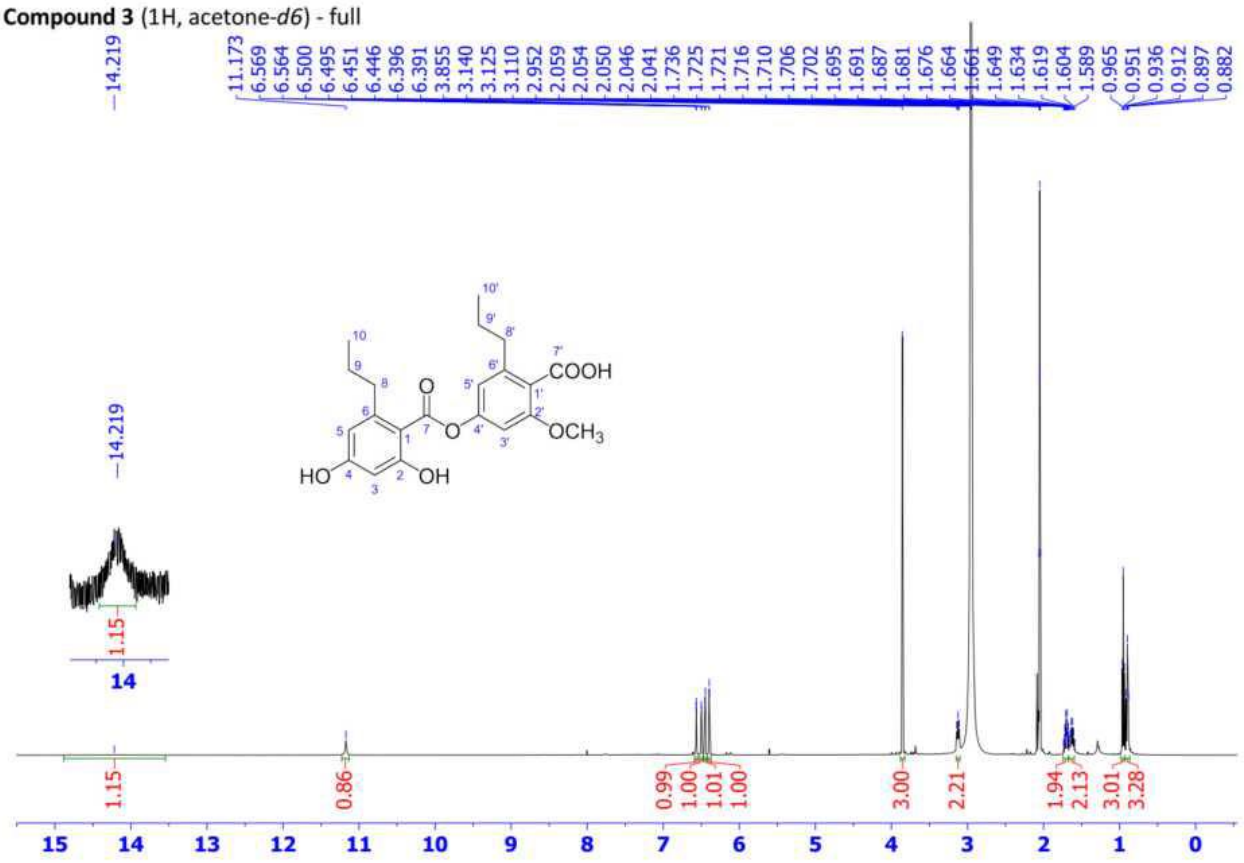

Figure A36: Full [1]H-NMR of compound **3**

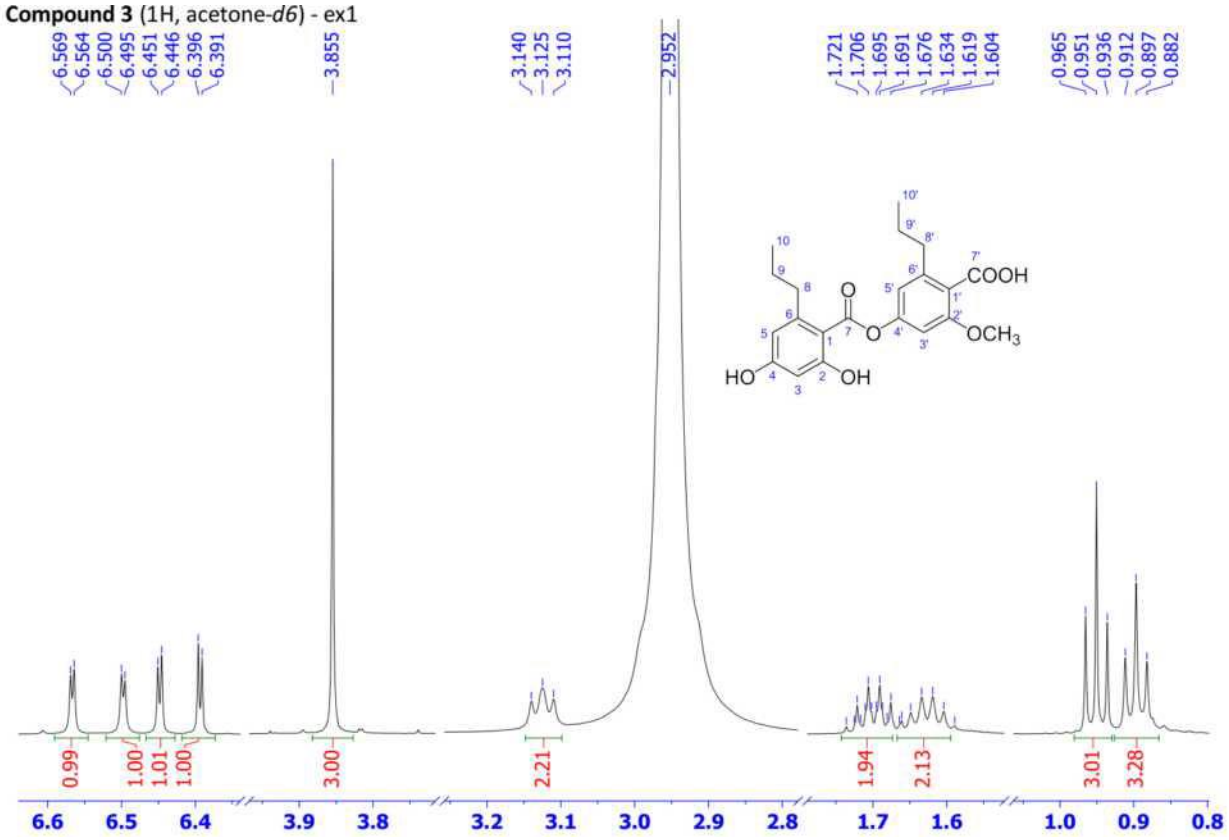

Figure A37: Extended [1]H-NMR of compound **3**

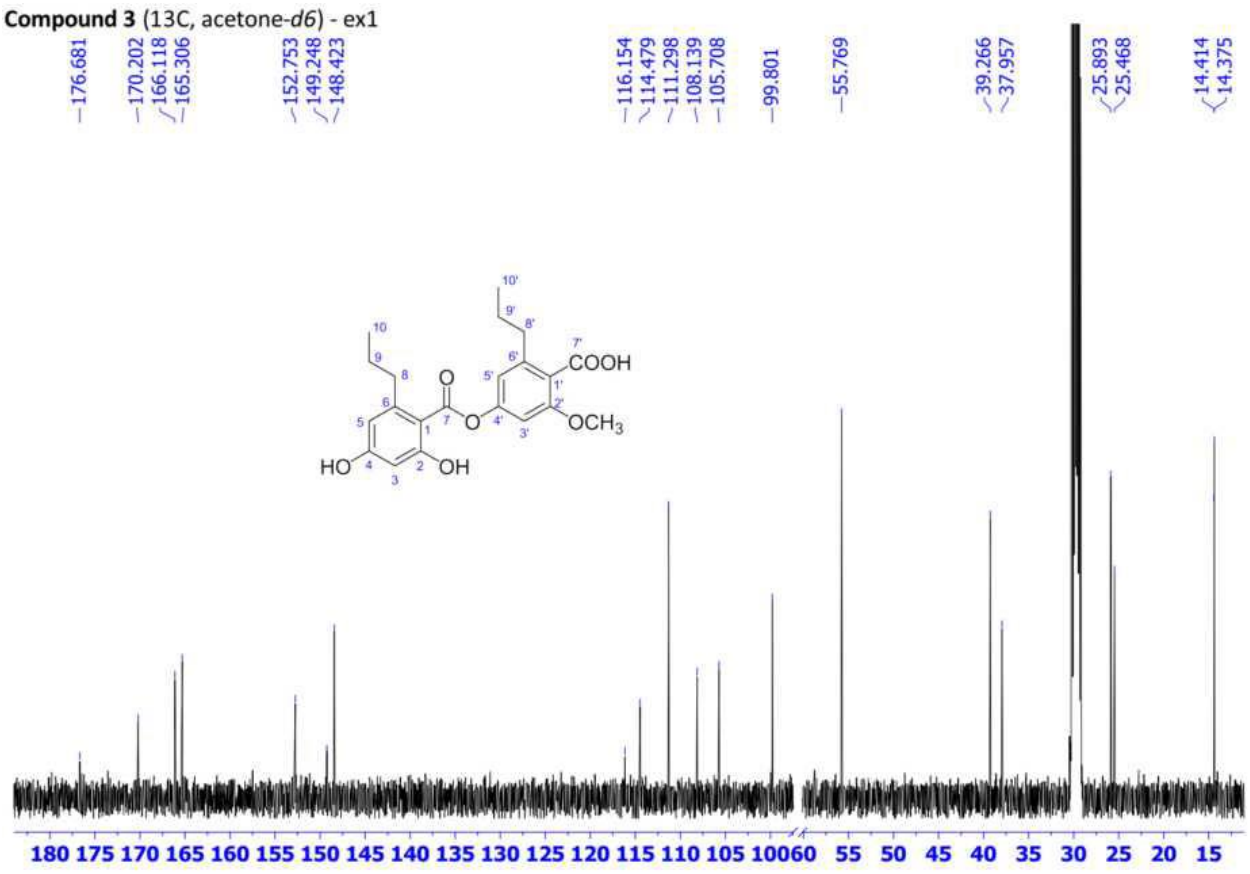

Figure A38: Full ^{13}C-NMR of compound **3**

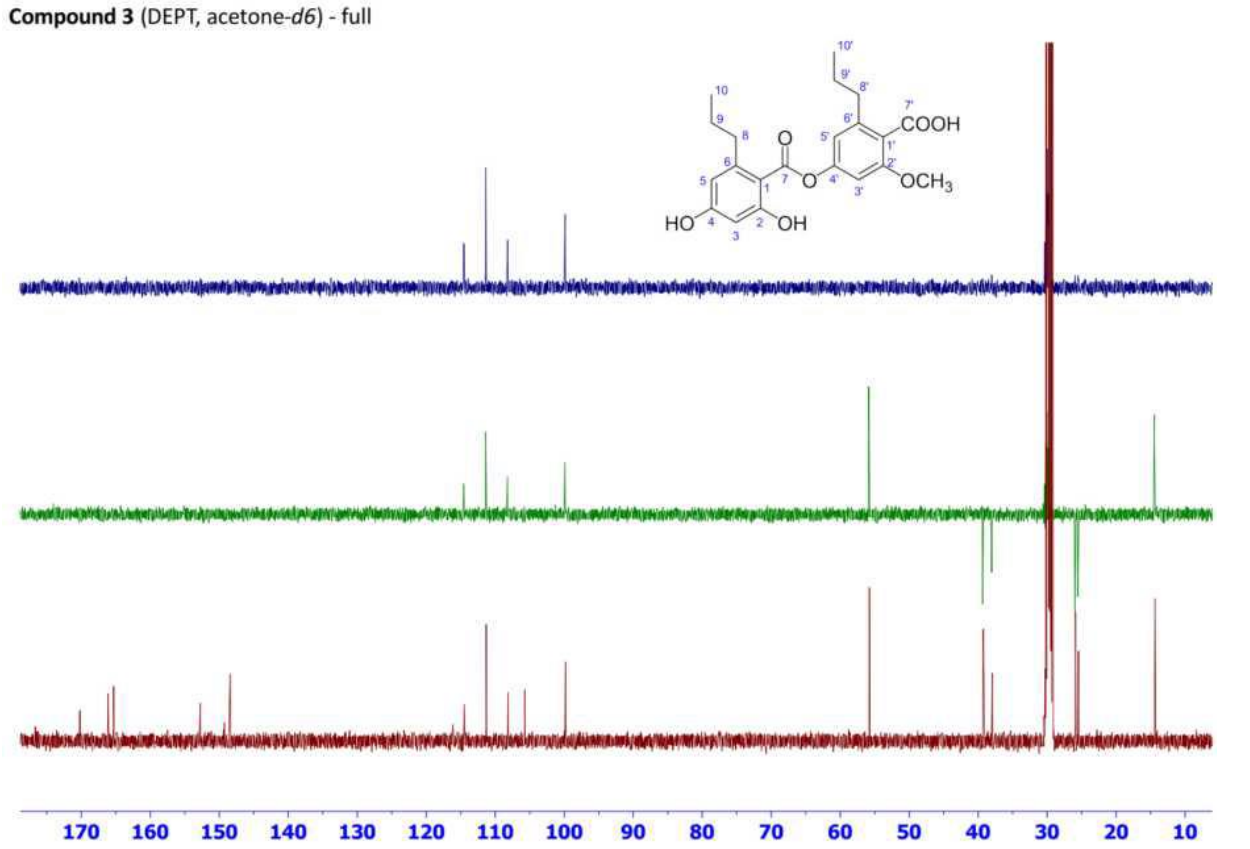

Figure A39: Full DEPT of compound **3**

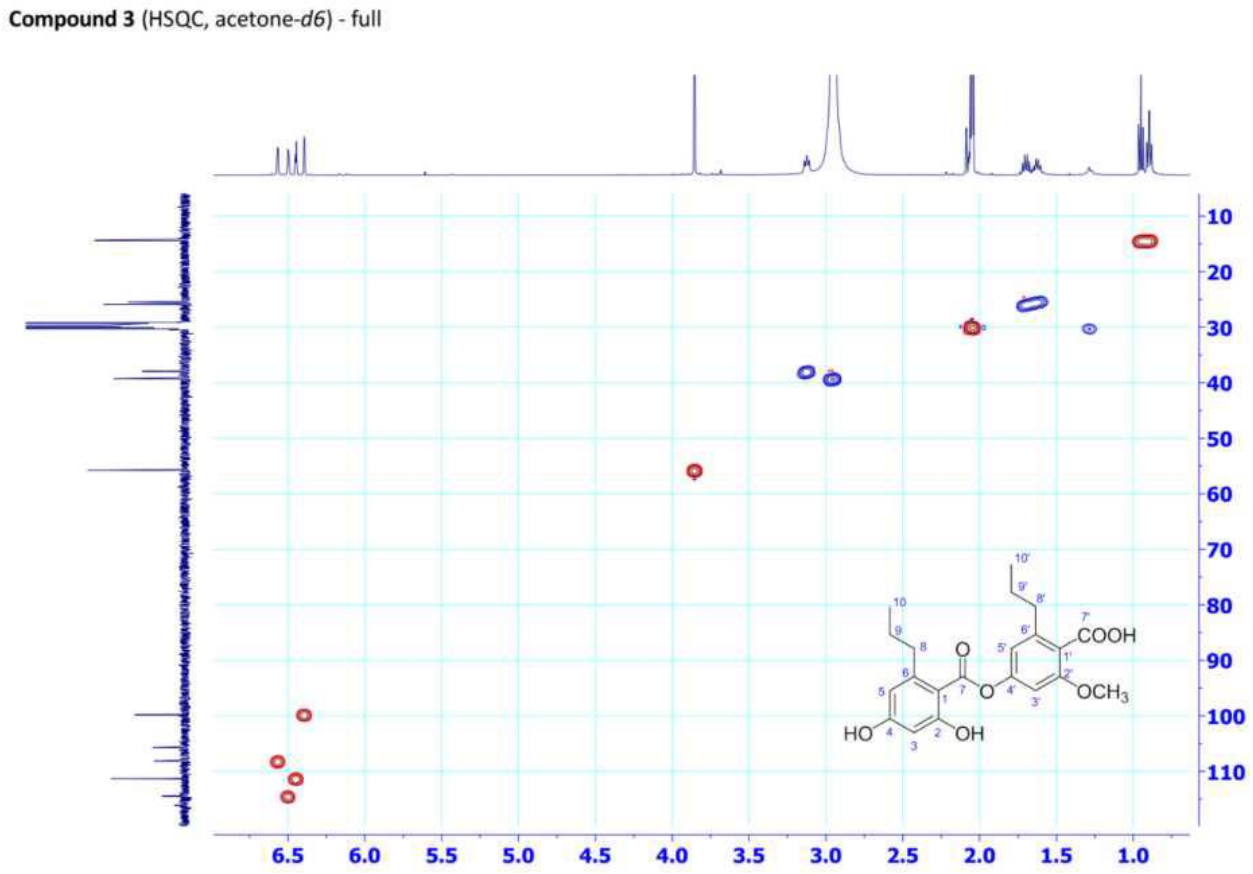

Figure A40: Full HSQC of compound **3**

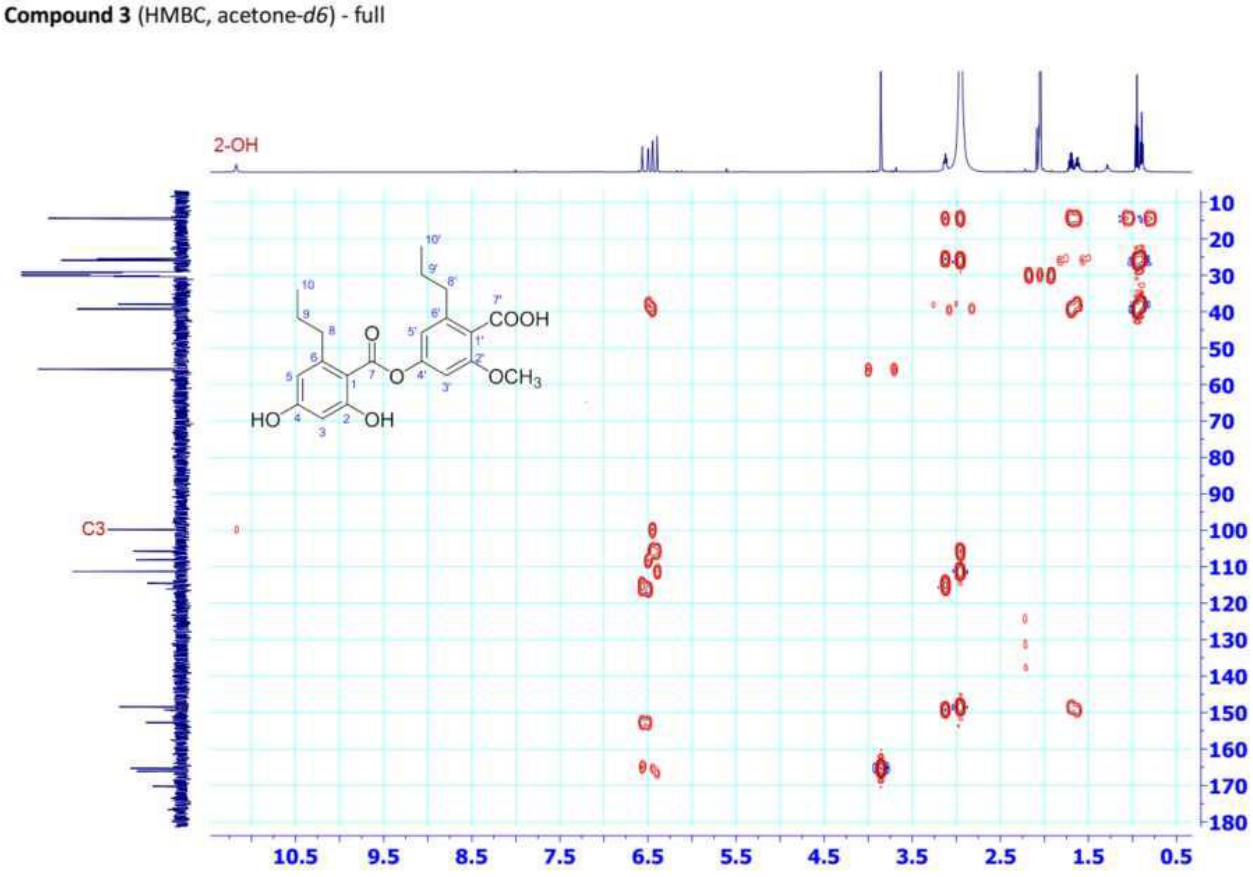

Figure A41: Full HMBC of compound **3**

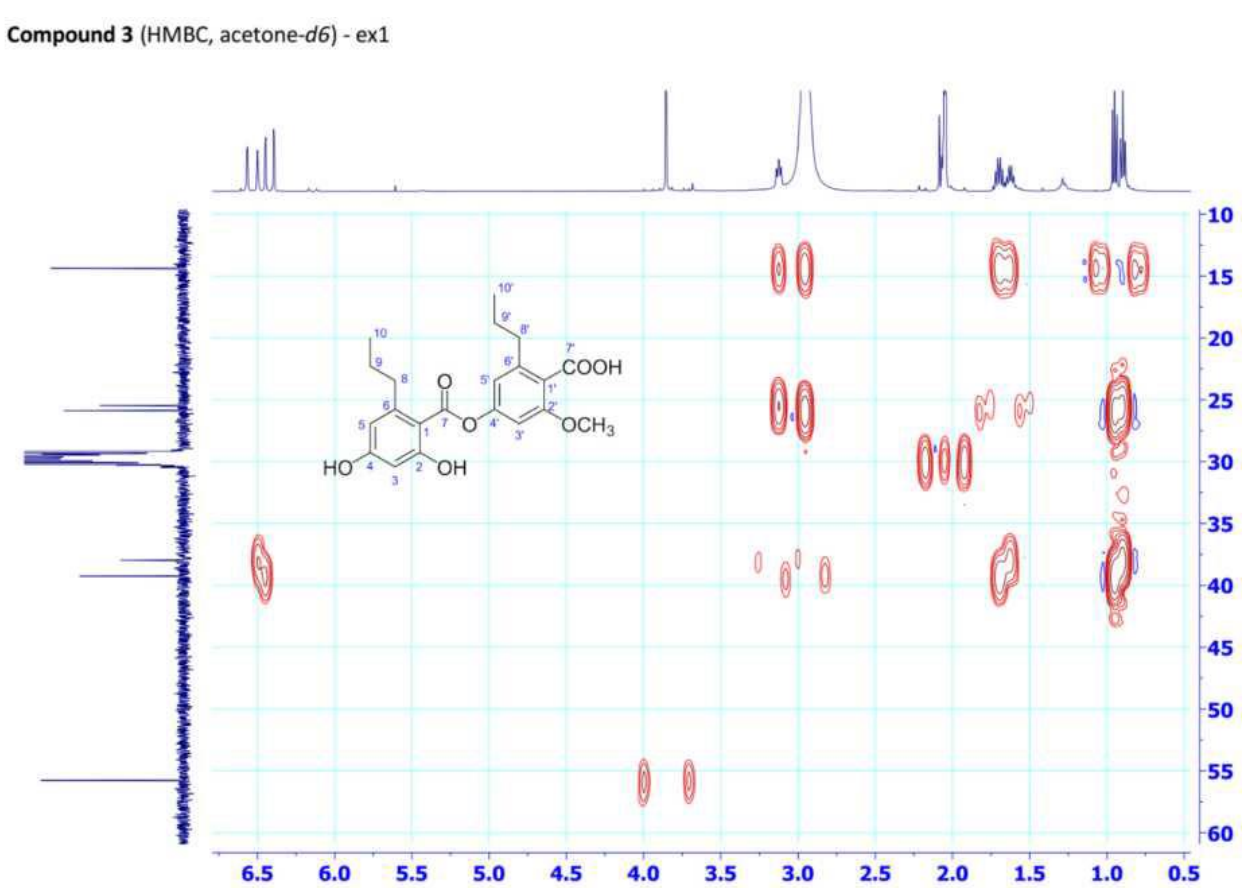

Figure A42: Extended HMBC of compound **3**

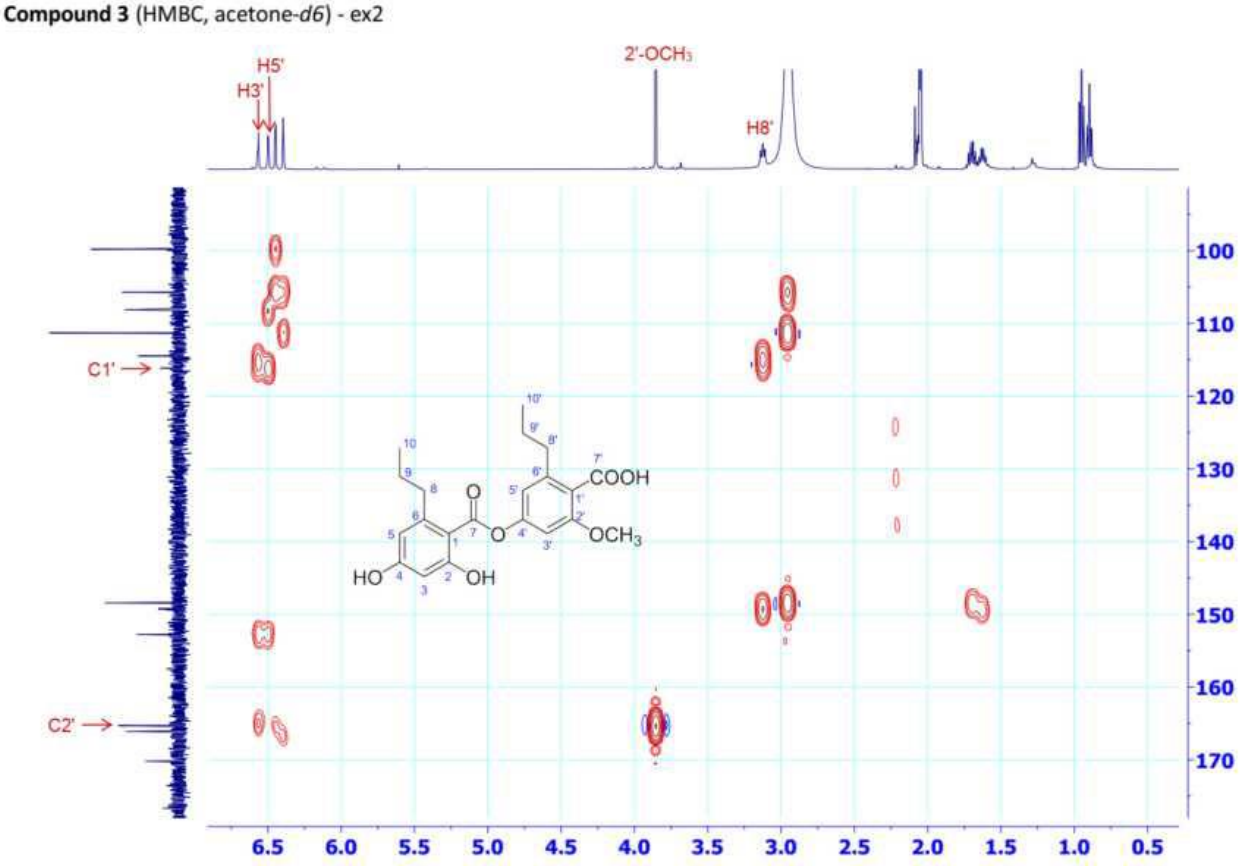

Figure A43: Extended HMBC of compound **3**

Appendix B. List of publications

1. Trong Tuan Nguyen, Thanh Nguyen Quoc Chau, Hieu Mai Van, Toan Phan Quoc, Qui Do Phuoc, The Duy Nguyen, Phuc Dam Nguyen, Tram Nguyen Thi Thu, Tien Dung Le, Trang Dai Thi Xuan, Kamei Kaeko and Kenji Kanaori. A new hopane derivative from the lichen Dirinaria applanata. *Nat. Prod. Res.* **2019**, 1–5.

2. Tuan Nguyen Trong, Mai Van Hieu, Nguyen Quoc Chau Thanh, Loi Huynh Van, Lai Huu Nghia, Tran Thi Tuyet Hoa, Kenji Kanaori. Novel hopanoic acid and depside from the lichen Dirinaria applanata. *Rec. Nat. Prod.* **2020**, *14*, 248–255.

3. Thanh Q. C. Nguyen, Tran Duy Binh, Tuan L. A. Pham, Yen D. H. Nguyen, Dai Thi Xuan Trang, Trong Tuan Nguyen, Kaeko Kamei and Kenji Kanaori. Anti-Inflammatory Effects of Lasia spinosa Leaf Extract in Lipopolysaccharide-Induced RAW 264.7 Macrophages. *Int. J. Mol. Sci.* **2020**, *21*, 1–18.